WAVE ATTENUATION IN MANGROVE FORESTS: AN INVESTIGATION THROUGH FIELD AND THEORETICAL STUDIES

Thesis submitted by
Richard Michael Brinkman BSc (Hons) *Flinders University*
in October 2006

for the degree of Doctor of Philosophy in
the School of Mathematical and Physical Sciences
James Cook University

ELECTRONIC COPY

I, the undersigned, the author of this work, declare that the electronic copy of this thesis provided to the James Cook University Library, is an accurate copy of the print thesis submitted, within the limits of the technology available.

_____ _____

Signature Date

STATEMENT OF ACCESS

I, the undersigned, author of this work, understand that James Cook University will make this thesis available for use within the University Library and, via the Australian Digital Theses network, for use elsewhere.

I understand that, as an unpublished work, a thesis has significant protection under the Copyright Act and I do not wish to place any further restriction on access to this work.

Richard Brinkman
October, 2006

1 ABSTRACT

Mangroves are woody forests that exist at the confluence of the marine and terrestrial environments. These forests are highly biologically productive and play a key role in supporting coastal food chains, and trapping and stabilizing coastal sediments. Mangroves are also known to dissipate significant amounts of wave energy over relatively short distance, which has significance in the area of coastal protection. However, understanding the quantitative effects of mangrove vegetation in reducing surface wave energy has, until now, received very limited research interest. This study presents a field and theoretical investigation of the attenuation of random, wind–induced surface wave energy in mangrove forests. Field observations of wave processes in mangrove forests were undertaken at three study sites with different wave energy regimes. At each site, an array of wave gauges was placed along a transect aligned with the dominant wave direction to measure changes in wave characteristics as waves propagated shoreward through the mangroves. Mean rates of attenuation of total wave energy and significant wave height observed at the three sites averaged 1.5% m^{-1}, and 1.1 % m^{-1} respectively. Attenuation rates are found to be frequency related, with preferred attenuation of shorter period waves. Field data also indicate an increase in the energy transmitted into the forest with increased water depth.

Two theoretical approaches were developed to investigate and model the attenuation of wave energy for waves propagating through mangrove forests: In the first theoretical approach, the water depth in the mangrove forest was assumed constant, and the wave motion was described by a set of amplification factors for individual spectral components. The second approach was developed for a mangrove forest with arbitrary bathymetry, and in this case the wave motion within the forest was determined by solving the mild slope equation with dissipation. Both approaches investigate energy dissipation in the frequency domain by treating the mangrove forest as a random media porous to wave energy, with certain characteristics determined using the geometry of mangrove vegetation. Also, both cases employ modified drag co-efficient to introduce the dependence of the drag coefficient on the spatial density of the vegetation.

Theoretical results from the model with constant water depth show good qualitative agreement with the key wave propagation features identified in the field data, with predicted rates of wave energy attenuation controlled primarily by prescribed vegetation characteristics. Results from the model with arbitrary bathymetry demonstrate that the model was able to reproduce observed rates of wave energy attenuation. Wave energy attenuation was shown to depend strongly on the spatial density of the mangrove vegetation and its structural arrangements, and on the spectral characteristics of the incident waves. Wave energy attenuation was also found to be a function of water depth, with increased energy transmitted into the forest with increased water depth, due to the non-uniform vertical structure typical of mangrove vegetation.

The results of this study demonstrate that it is possible to numerically model the dominant energy dissipation processes and thus predict attenuation of surface wave height within mangrove forests. The ability to predict the attenuation of surface wave energy due mangroves has relevance in the field of costal protection. A model developed in this thesis is applied to assess the theoretical performance of a temporary coastal protection measure using bamboo, and evaluate its cost effectiveness compared to other accepted low-cost measures for attenuating wave energy. The proposed design of a bamboo wave attenuation structure is significantly cheaper than other published designs, for an equivalent level of energy attenuation.

2 ACKNOWLEDGEMENTS

There are many people who have, either directly or indirectly, played a role in the compilation of this thesis. Firstly, I wish to thank my supervisors, Dr Peter Ridd (James Cook University) and Professor Stanisław Massel (Australian Institute of Marine Science), who were both always extremely generous with their time and knowledge, and provided invaluable guidance, counsel and encouragement. In particular, I wish to acknowledge the significant contribution from Professor Massel, whose previous research on wave propagation through porous breakwaters and interest in vegetated coastal zones was the stimulus for work undertaken in this thesis. Many thanks must also go to Mr Keita Furukawa for assistance with the vortex modelling, and for organizing financial support, through the Port and Harbour Research Institute, Japan, for the component of this study undertaken on Iriomote Island. Dr Halmar Halide is gratefully acknowledged for initiating the discussions relating to the coastal engineering applications of this study.

Dr Jamie Bunt, Dr T. Kuwae, Mr E. Kibe and those already mentioned above are thanked for their assistance with the field component of this study.

My professional career and consequently the work presented in this thesis have benefited greatly from interactions with many colleagues at the Australian Institute of Marine Science. I particularly wish to thank Dr Eric Wolanski, who although not directly involved in the research presented here, provided opportunity, advice and mentoring for my professional development during the period of my candidature.

Finally, I am extremely grateful for the continual support and encouragement of my wife [redacted] and the welcome distraction of our children, [redacted] and [redacted]

This study was made possible through the resources offered by the Australian Institute of Marine Science. James Cook University provided financial assistance in the form of a HECS Exemption Scholarship.

3 TABLE OF CONTENTS

4 LIST OF FIGURES

5 LIST OF TABLES

6 STATEMENT OF SOURCES

DECLARATION

I declare that this thesis is my own work and has not been submitted in any form for another degree or diploma at any university or other institution of tertiary education. Information derived from the published or unpublished work of others has been acknowledged in the text and a list of references is given.

Richard Brinkman
October, 2006

1 INTRODUCTION

1.1 Overview

The coastal margin is under increasing pressure from human activity, with approximately 20% of the world's population in 1995 living within 25 km of the coast (Cohen *et al*. 1997), distributed mainly in the subtropics and tropics (Cohen and Small, 1998). Associated with human activity in the coastal strip often comes potentially destructive activities such as land clearing, coastal development and exploitation of the adjacent marine environments. One particular coastal ecosystem that has suffered and remains under increasing pressure from human activity is mangrove forests, with mangroves classified as the most vulnerable of all coastal ecosystems (IPCC, 1995). Mangrove forests are a common feature along many tropical and sub-tropical coastlines throughout the world. They are inter-tidal wetland ecosystems composed primarily of woody halophytes living at the confluence of the marine and terrestrial environments, generally in sheltered coastal and riverine areas with medium to low wave energy climates favorable to the deposition of fine sediment (Alongi, 2002). Mangroves have adapted to this environment of soft, saline, oxygen-deficient soils in a number of unique ways, but of particular relevance to this study is the above-sediment root system exhibited by many mangrove species as a means of increasing their oxygen supply and providing structural stability (see Figure 1.1). The above-sediment components of mangrove root system comprise the roots and pneumatophores, which together with the tree trunk and buttresses form a complex tangled network of woody, rigid vegetation above the forest floor.

The unique structure of mangrove vegetation and their existence in the inter-tidal zone underpins the vital and complex role mangrove forests play in sustaining coastal ecosystems by supporting estuarine and nearshore food-webs through providing essential nutrients, habitats and nursery refuge for many marine and terrestrial organisms amongst the thickly interwoven vegetation. Mangroves are also important as a traditional and commercial resource for fuelwood, charcoal, timber, a

variety of fisheries and the production of tannins for dying and leather production (Qureshi, 1990; Woodroffe, 1992; Siddiqi and Khan, 1990; Bandaranayake, 2002; Glaser, 2003).

Figure 1.1 Mangrove vegetation (*Rhizophora* sp.) on an inter-tidal mudbank in North Queensland, Australia.

As well as providing shelter beds for many organisms, the densely interwoven trunks and roots of mangrove vegetation also influence and modify the local circulation and hydrodynamics processes, and other processes driven by the hydrodynamics. For example, mangrove forests act as an effective buffer between the marine and terrestrial environments by trapping and stabilising nearshore sediment (Furukawa and Wolanski, 1996). Trapping of fine sediments is due to the high turbulence generated by the flow through the vegetation matrix as the forest is inundated, which maintains particles in suspension until the current speeds and turbulence approach zero at high tide slack water. Ebbing tidal current magnitudes are insufficient to re-entrain the sediment due to the high vegetation density. Thus

mangroves active contribute to creation and maintenance of new and existing mud banks.

Mangroves forests that are exposed to significant wave action also act as an energy-reducing buffer by dissipating surface wave energy and reducing the risk of shoreline erosion. The dissipation of wave energy is due primarily to the interaction of the wave motion with the submerged vegetation elements, and the most obvious manifestation of the dissipation is in the reduction of the surface wave height (Mazda *et al*., 1997a). A reduction in wave energy is accompanied by a reduction in the risk of shoreline erosion, which has significance in the area of coastal protection and suggests that, in appropriate circumstances, reforested mangroves could be employed as coastal protection measure (Mazda *et al*., 1997a). Whilst sufficient knowledge for cultivation and reforestation (or restoration) of mangrove areas exists (Das *et al*., 1997; Riley *et al*., 1999), understanding the quantitative effects of mangrove vegetation in reducing surface wave energy has, however, received very limited research interest. With increasing interest in the conservation and rehabilitation of mangrove forests, there is an increased need for understanding the smaller-scale physical processes in mangrove forests. This study builds on the limited understanding of wave processes in mangrove forests, through field and theoretical investigations, resulting in a numerical model capable of replicating and predicting the dissipation of random, wind–induced surface wave energy in mangrove forests.

1.2 Existing data and models of the interaction of waves and vegetation

Knowledge and understanding of the interaction of fluid motion with vegetation has been relatively slow to accumulate. In particular, studies of the interaction of wave motion with submerged and emergent vegetation have focused mainly on seagrass, vegetated salt marshes and kelp, and have generally been confined to temperate latitudes and species endemic to these environments. It has only been in recent decades that studies of hydrodynamic processes within tropical mangrove forests have been undertaken, with the majority of effort directed towards understanding processes that are tidally periodic (Wolanski *et al*., 1980; Mazda *et al*., 1997; Furukawa *et al*., 1997). Unfortunately, at present only a small number of studies of wave processes within mangrove forests have been reported in the literature.

1.2.1 Seagrasses, salt marshes and kelp: poor analogies to mangroves but a place to start.

The majority of existing data and models of wave and vegetation interaction are the results of studies of seagrass, vegetated salt marshes and kelp. Kelp forests are a common feature along coastlines in higher latitudes, such as along the coast of Norway, and along sub-tropical coastlines that experience upwelling, such the Californian Coast. The physical size of the kelp and its relative occupation of the water column are dependent on the particular species. For species endemic to southern California, kelp may grow to a length equal to or greater than the water column, thus forming a surface canopy in depths of between 2 and 30m (Edwards, 1998). By contrast, kelp species found along the Norwegian coast only occupy a fraction of the water column, growing to a length of ~1 to 2m in water depths of 4 to 9 m (Lovas, 2000). Regardless of the physical nature of the species, kelp has been observed to affect the local hydrodynamic processes (Elwany *et al*., 1995; Jackson and Winant, 1983; Lovas, 2000).

Seagrasses are marine flowering plants that grow at and below the intertidal zone, usually on sandy or muddy substrates. Their distribution is dependent on many

factors including exposure to wave action. They depend upon their rhizomes or underground stems for anchorage, which also stabilise the underlying sediment and prevent sediment movement (Kirkman, 1997). Seagrasses occur in a large range of water depths, down to > 50m, but it is when seagrass beds occur in shallow meadows that their influence on wave energy is substantial (Kirkman, 1997; Fonseca and Cahalan, 1992).

Vegetated salt marshes exist at and above the intertidal zone, landward of intertidal sandflats. They are inundated only during spring tides and during storm surges. For European salt marshes, vegetation typically extends up to 50 cm above the substrate (Möller *et al*., 1996). Attenuation of wave energy has been found to be substantial and maximum when the water levels are not elevated above the canopy level (Fonseca and Cahalan, 1992).

Whilst seagrasses, salt marsh vegetation and kelp are biologically, morphologically and environmentally different from mangroves, they are for the purpose of this thesis a rough analogy to mangrove forests in that they occur in wave exposed areas and interact with the wave motion in a way that is manifested as a decrease in wave amplitude across the vegetation field (Möller *et al*., 1996; Brinkman *et al*., 1997; Edwards, 1998; Lovas, 2000). The theoretical techniques that have been developed and employed to investigate the effects of kelp and seagrass type vegetation on wave motion thus provide a starting point for the development of the theory specific for the attenuation of surface wave energy within mangrove forests.

1.2.2 Observational studies of surface wave energy attenuation.

Fonseca and Cahalan (1992) evaluated the wave energy attenuation ability of four species of seagrass though a series of wave tank tests. Leaf lengths of the tested species varied from 17 to 41 cm, and wave tank tests were undertaken for shallow water depth from 6 to 19 cm. Energy attenuation rates (per metre of seagrass) of approximately 40% were observed for water depths similar to vegetation length, but the seagrasses lost their effectiveness in reducing wave energy as the water depth increased above the canopy height.

Knudson *et al*. (1982) reported wave height and energy reduction rates for salt marsh vegetation that extended above the water surface in Chesapeake Bay. An energy reduction rate per metre of vegetation of 26% was found for low incident wave energies.

Möller *et al*. (1996; 1999) presented quantitative evidence for the effectiveness of open coast salt marsh, exposed to significant wave energy, in attenuating incoming waves. Field measurements demonstrated that average wave energy dissipation rates over a 200 m wide salt marsh were 82%, compared with only 29% over an adjacent sand flat of similar width.

Möller and Spencer (2002) presented results from a 10 month long observational study of wave dissipation over macro-tidal salt marshes in eastern England. Observed attenuation rates were highest, at 2.1% per metre, in the first 10 m of salt marsh vegetation. Average attenuation rates were between 0.1% and 0.5% per metre. Attenuation rates showed a seasonal signal apparently linked to the seasonal cycle of vegetation growth.

In one of the few studies in the literature dealing with wave energy attenuation in mangrove forests, wave energy reduction in a reforested area in Vietnam was reported by Mazda *et al*. (1997a). Sea surface elevation and currents were observed at a frequency of 2 Hz along a transect 1.5 km long through a region of replanted mangroves. Whilst this sampling frequency is at the low end of what is optimal for wave sampling, useful data on the incident wave climate were still collected. Estimates of wave height reduction wave reduction of up to 20% per 100 m of vegetation were calculated from the observations along the observational transect. Attenuation due to mangrove vegetation distributed throughout the water column was provisionally calculated as a bottom friction. Observations collected at various stages of the tide allowed the dependence of wave reduction and drag coefficient on water depth to be investigated. The dependence of both the drag coefficient and wave reduction on water depth was shown to be dependent on the vertical structure of the vegetation.

1.2.3 Models of wave damping by vegetation

There have been several attempts to model the attenuation of wave energy due to the interaction waves with vegetation, and a number of the more relevant studies are described below. In each case, the particular approach adopted is tailored to the type of vegetation in question. For example, Möller *et al*. (1999) assumed that increased bottom friction due to the vegetated substrate is the primary reason for the increased wave attenuation over the salt marsh. Such an assumption would not be valid for kelp, for example, where the vegetation is spread relatively uniformly through the water column. For the purpose of this thesis, the key will be to determine from the existing knowledge what approaches and assumptions are suitable and valid for modeling the attenuation of wind-induced random surface waves in mangrove forests.

Jackson (1984) reported observations of internal wave damping due to coastal kelp stands and developed two theoretical approaches to describe the attenuation of wave energy. Both approaches were based on linear wave theory and used a linear coefficient of drag due to the kelp that is uniform through the water column. The solutions were assumed to take the form of an exponential decay of wave amplitude, and using a notation more general than Jackson (1984), such solutions can be expressed as

$$\varsigma(x,t) = a_0 e^{\left[i(kx+\omega t)\right]} \tag{1.1}$$

where ς is the displacement of the free surface due to a progressive wave, a_o is the incident wave amplitude at the origin of the vegetation field ($x = 0$) at time $t = 0$, $k = (k_r + ik_i)$ is the complex wave number and ω is the angular frequency. The amplitude of the decay can be shown to decrease exponentially at a rate determined by the imaginary part of the wave number, k_i, as given by

$$a(x) = a_o e^{-k_i x} \tag{1.2}$$

where a is a real number and denotes the wave amplitude. This relatively simple approach was able to explain well the attenuation of wave amplitude, but it did not

provide a means to asses the attenuation of total wave energy across a spectrum of incident wave energy.

Kobayashi *et al*. (1993) also employed the assumption of an exponential decay in wave height to develop an analytical solution for small amplitude waves propagating over submerged and sub-aerial vegetation, such as seagrass. The fluid domain was modelled as two layers, with the bottom layer occupied by the vegetation. The vegetation was modelled as rigid cylinders and the wave field was assumed to be monochromatic. Inertial forces were neglected, and the effects of vegetation on the flow field was expressed as a drag resistance against the fluid motion given by

$$\begin{aligned} F &= \frac{1}{2}\rho C_d b N u_h \left|u_h\right| \\ &= \rho D u_h \end{aligned} \tag{1.3}$$

where ρ is the fluid density, C_d is the drag coefficient, b is the area per unit height of each vegetation, N is the number of vegetation per unit area, u_h is the horizontal velocity in the vegetation and D is a damping coefficient describing wave energy attenuation due to the drag force F. The introduction of the coefficient D is an attempt to linearise the drag force acting on the vegetation, and the drag coefficient was calibrated against laboratory wave flume studies, and was assumed to be vertically constant.

Asano *et al*. (1992) extended the two–layer model of Kobyashi *et al*. (1993) by including vegetation motion and its interaction with the wave motion. The vegetation motion was modelled as a forced vibration with one degree of freedom, with buoyancy and stiffness of the vegetation being the restoring forces. In order to develop an analytical solution, the drag force on the vegetation was linearised in a similar way to Kobyashi *et al*. (1993) and Jackson (1984), using a procedure that minimized the mean square error introduced when the damping coefficient, D, was introduced as described in Equation (1.3). It was also assumed that the dimensions of the vegetation were constant in the vertical for the bottom layer of the fluid. Viscous shear stresses acting on the interface of layers and the bottom were

neglected as the drag resistance of the vegetation was assumed to be the dominant form of energy dissipation and the drag coefficient was assumed constant through the water column. Also, the vertical component of force acting on the vegetation was ignored. Solutions for motions in each layer were evaluated separately and linked by the linearised damping coefficient, *D*. Model results were compared to laboratory studies of the flow field in the vicinity of artificial seagrass. Dubi and Torum (1994) further developed the two-layer model of Asano *et al*. (1992) by introducing vertical structure into the description of the vegetation to more realistically simulate the frond and stipe of kelp vegetation.

The approach of Kobayashi *et al*. (1993) and subsequent developments by Asano *et al*. (1992) and Dubi and Torum (1994) introduced a number of ideas relevant to the present study, namely the linearization of the drag force term and using a more accurate description of the vertically non-uniform vegetation structure. However, these approaches developed analytical solutions to determine wave forces and damping for monochromatic waves only based on the assumption of an exponential decay in wave amplitude.

The hydrodynamics induced in a vegetation field by wind waves was investigated by Mendez and Losada (1999). Again the modeling approach was based on previous studies of Kobyashi *et al*. (1993) and Dubi and Torum (1994), but the existing solutions were extended to random waves by using an eigen function expansion. Both drag and inertial forces acting on the vegetation were included, and the total force was linearised using the Lorentz hypothesis of equivalent work (Losada *et al*., 1996). As with previous approaches the drag coefficients were assumed to be constant with depth, and the water depth was assumed to be constant in order to simplify computations. However, a significant advance of the Mendez and Losada (1999) model was that the problem was structured in a fluid domain consisting of in front of, within and leeward of the vegetation field, and a solution was found to the momentum equation with dissipation within the region of vegetation interaction in the form of velocity potentials in the three regions of the domain.

1.3 Limitations of the existing knowledge

This review highlights a number of key limitations of existing knowledge relevant to modelling wave propagation through mangrove forests. Most published theoretical approaches and models of the interaction of vegetation and a wave field are developed for a constant water depth, the solution is often assumed to take the form of an exponential decay in wave height and the hydrodynamic drag of the vegetation is often simplistically incorporated as an enhanced bottom friction. Furthermore, almost all theoretical solutions found in the literature are limited to monochromatic incident waves, and coupled with the assumption of exponential decay of wave height, these solutions do not allow investigation of the attenuation of total incident wave energy contained in an arbitrary shaped spectrum of random waves.

The approach of Mendez and Losada (1999) is the exception to the above limitations, in that a solution is found to the problem of flow over kelp for random wind waves. However, like other existing models, their approach assumes constant water depth and uses a drag coefficient of the vegetation that is assumed uniform through the water column. These assumptions do not allow the investigation of changing characteristics of wave attenuation with changing water depth. The physical structure of mangroves is extremely non-uniform in the vertical (as discussed later), and as such, the drag characteristics will vary with the level of inundation. A model of wave propagation within mangroves should capture this vertical non-homogeneity of hydrodynamic drag. Notwithstanding, the theoretical framework developed by Mendez and Losada (1999) provides a good example on which to structure a solution for mangrove forests.

In order to realistically model wave propagation through mangrove forests a number of these limitations must be addressed. Firstly, a suitable formulation of the drag coefficient must be developed to appropriately include dependence on both the vertical structure and spatial density of the vegetation. Due to the close proximity of the trunks and roots of mangrove vegetation, dependence on spatial density is critical, as it can be expected that the disturbance to the flow field caused by the

vegetation will alter the flow field for other vegetation elements nearby, thus altering the force on those elements and in turn altering the effective drag coefficient.

Secondly, a solution is sought for wave propagation through a forest of arbitrary bathymetry. Finally the solution should not be confined to monochromatic waves, but should be developed for a forest exposed to random incident surface waves with an arbitrarily shaped energy spectrum.

In almost all of the studies reviewed above, there have only been partial attempts to verify individual models against field data, with most verification taking the form of qualitative, rather than quantitative assessment of the model performance. This shortcoming has been due not only to the scarcity of appropriate validation data, but also to the generalising assumptions taken to simplify the modelling task (for example, the assumptions of constant water depth and monochromic waves)

This review also highlights the extremely limited number of field observations of wave processes in natural mangrove forests. At the time of writing, there appears to be no quantitative data in the literature on wave processes in natural mangrove forests, apart from what is presented in this thesis.

1.4 Objective and Outline of Thesis

The objective of this thesis is to develop a numerical model of the attenuation of random, wind–induced surface wave energy in mangrove forests and to asses the performance of the model against field data. This thesis reports on observations and analysis of wave processes in mangrove forests at three field sites, and presents the development of a theoretical approach to investigate and model the attenuation of wave energy for waves propagating through a forest with uniform depth. A second, more general theoretical approach is then developed to extend the solution for the more realistic case of a forest with arbitrary bathymetry. Direct comparisons are made between observed and predicted wave energy obtained from the two

theoretical approaches. The application of the more general theoretical approach to the design and evaluation of coastal defense measures is briefly presented.

Some of the work presented in this thesis has also been reported in the following publications:

- **Brinkman, R.**, Massel, S.R., Ridd, P. and Furukawa, K. (1997), Surface wave attenuation in mangrove forest, In: *Pacific Coasts and Ports '97: Proceedings of the 13th Australasian Coastal and Ocean Engineering Conference and the 6th Australasian Port and Harbour Conference*, 7-11 September 1997, Centre for Advanced Engineering, University of Canterbury Christchurch, New Zealand, vol. 2: 941-946

- Massel, S.R., Furukawa, K., **Brinkman, R.** (1999), Surface waves propagation in mangrove forests. *Fluid Dynamics Research*, vol 24:219-249

- **Brinkman, R.**, Massel, S.R. (2003) Wave propagation through mangrove forests with non-horizontal bathymetry. *Fluid Dynamics Research,* (submitted)

- Halide, H., **Brinkman, R.**, Ridd, P. (2004), Designing bamboo wave attenuators for mangrove plantations. *Indian Journal of Marine Science*, vol 33(3): 220-225

2 FIELD STUDIES OF WAVE PROPAGATION THROUGH MANGROVE FORESTS

2.1 Overview

The attenuation of surface gravity waves by mangroves is a complex and little understood problem, and as highlighted by the review of existing data in Chapter 1, studies undertaken to observe this process in the field are scarce. To address this lack of knowledge, field studies were undertaken at three locations with the purpose to measure the attenuation of random wind-induced surface wave energy within natural mangrove forests.

Field experiments were conducted at Cocoa Creek and Oonoonba study sites in Cleveland Bay, near Townsville, Queensland, Australia and at the Nadara River on Iriomote Island, Japan (see locality maps, Figure 2.1 and Figure 2.3).

2.2 Physical settings

2.2.1 Cocoa Creek study site

The Cocoa Creek study site is situated on the eastern shore of Cleveland Bay (19.2°S, 147°E). Cleveland Bay is meso-tidal, with a strong spring-neap signal and a maximum tidal range of *ca.* 3.8 m during spring tides. The Bay is relatively shallow, with the majority of the bay less than 10 m deep. An intertidal tidal mangrove system fringes the southern and eastern sides of the bay, and wide subtidal sandflats exist seawards of the mangrove fringe, with the 2 m isobath located up to 2.5 km offshore.

The regional wind field is dominated by southeasterly trade winds for the dry season months of April to November, producing northward propagating wind waves (Wolanski, 1994). Local diurnal sea breezes are also a persistent feature of the local wind climate in the Bay, with afternoon northeasterly sea breezes with speeds of between 15-25 km/h common throughout the year.

Cleveland Bay is protected from oceanic swell due to the offshore presence of the Great Barrier Reef. However, swell generated by the southeasterly trade winds can propagate into the bay, although refraction around Cape Cleveland results in a reduction of swell wave energy entering the bay. Significant wave heights of swell waves within the Bay are approximately 0.2 m (Larcombe and Ridd, 1994). Wind waves in the bay are thought to be locally generated (Lou and Ridd, 1996) and typically have a short period of 3.6-5.8 s with mean significant wave heights between 0.5-0.6 m, and dominant direction of east-southeast (Department of Environment, 1997). The significant heights of waves incident on the mangrove forests fringing the southern and eastern shores of the bay are presumed to be lower than those observed in the central bay, due to the extensive shallow sandflats immediately seaward of the mangrove fringe.

The Cocoa Creek study site belongs to the marine fringing mangrove forest type, where the mangrove forest lies between the coastline and terrestrial woodlands with only occasional freshwater input from rainfall (Lovelock, 1993). The forest is approximately 280 m wide, and bounded by intertidal mudflats on its seaward extent and by a sandy chenier ridge to landward. Vegetation within the forest is divided into three distinct approximately shore-parallel regions of different mangrove species. *Rhizophora stylosa* are dominant within 180 m from the marine environment, *Aegiceras* species dominate the central section of the forest for approximately 60 m (see Figure 2.2 (a)), and *Ceriops* species are dominant for the landward 60 m of the forest. The site is open directly to Cleveland Bay and receives wind induced surface waves from the west and north. The forest floor is relatively firm, and composed of poorly sorted mud and sand. The Cocoa Creek site was expected to be a low wave energy environment, as indicated by the composition and grain size of the forest floor.

2.2.2 Oonoonba study site

The Oonoonba study site is located on the south western shore of Cleveland Bay (see Figure 2.1). The site is a marine fringing mangrove type forest (Lovelock, 1993) and is open to both swell waves that are refracted around Cape Cleveland and wind waves from the north generated locally by the southeasterly trade winds, and

the afternoon sea-breeze. A large area of intertidal sand flats lies immediately offshore from the study site, and the landward extent of the forest is defined by chenier ridges. The forest at the study site is approximately 130 m wide and the vegetation is dominanted by *Sonneratia* species and *Rhizophora* species. The zonation of the two species is approximately shore parallel, with the *Sonneratia* species dominant in the first 75 m from the seaward extent of the forest (see Figure 2.2 (b)), and *Rhizophora* species dominant in the remainder. The forest floor is composed of firm, well sorted sand, which indicates that site is expected to experience medium wave energy under typical meteorological conditions.

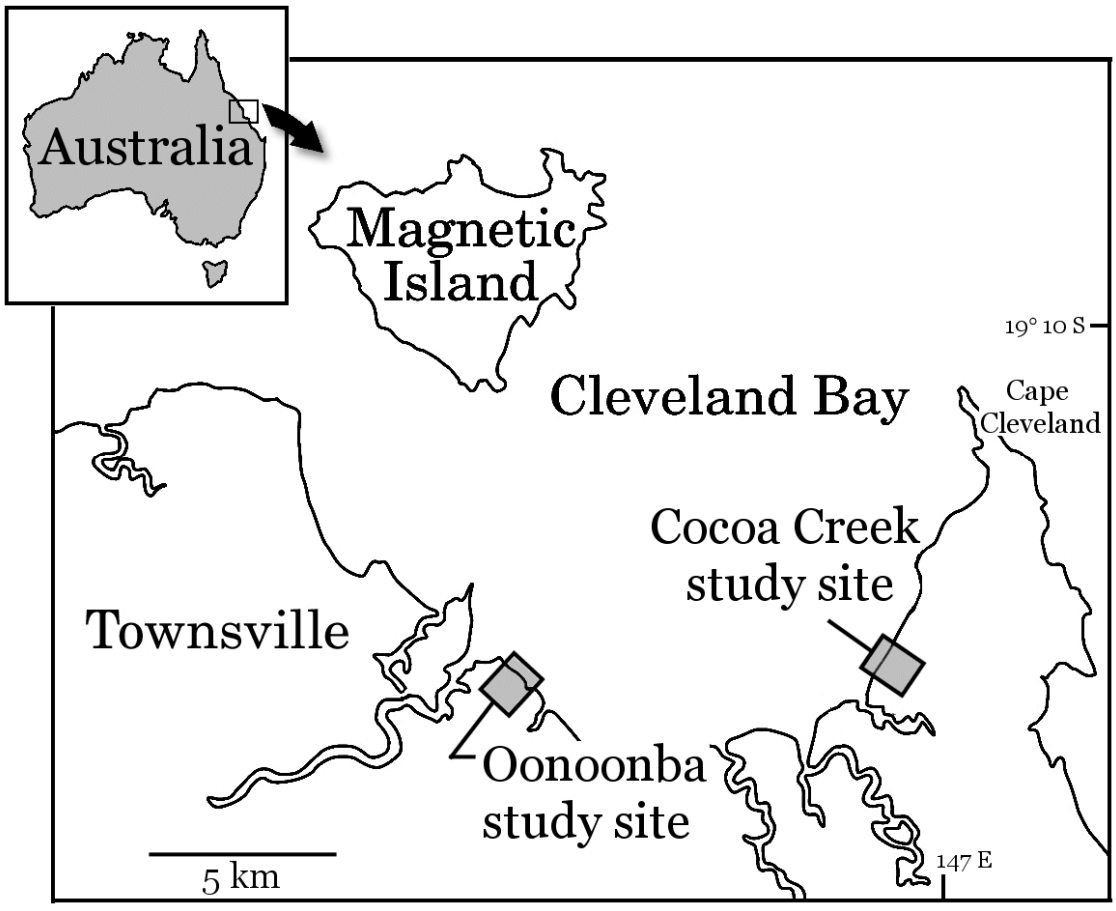

Figure 2.1 Locality map of Cocoa Creek and Oonoonba study sites

Figure 2.2(a) Mangrove vegetation (*Aegiceras* sp.) at Cocoa Creek study site.

Figure 2.2(b) WHISL SeaPac 2100 wave gauge deployed amongst *Rhizophora* sp. at the Oonoonba study site. Note red pencil (length *ca.* 15 cm) for scale.

Figure 2.2(c). *Bruguiera* sp. at Iriomote study site. Note surveying tape (height *ca.* 25 cm) for scale.

2.2.3 Iriomote study site

Iriomote Island lies in the subtropical northwestern Pacific Ocean (24.3°N, 123.7°E). The island is surrounded by coral reefs, and the coastline and river systems host abundant mangroves, the most northerly mangrove forests in the world. The tidal cycle at Iriomote Island is semi- diurnal with a maximum spring tidal range of *ca.* 2.0 m, and a significant spring neap signal. The wind climate on Iriomote is dominated by the Northeast Monsoon during December to March, and the Southwesterly Monsoon between May to October.

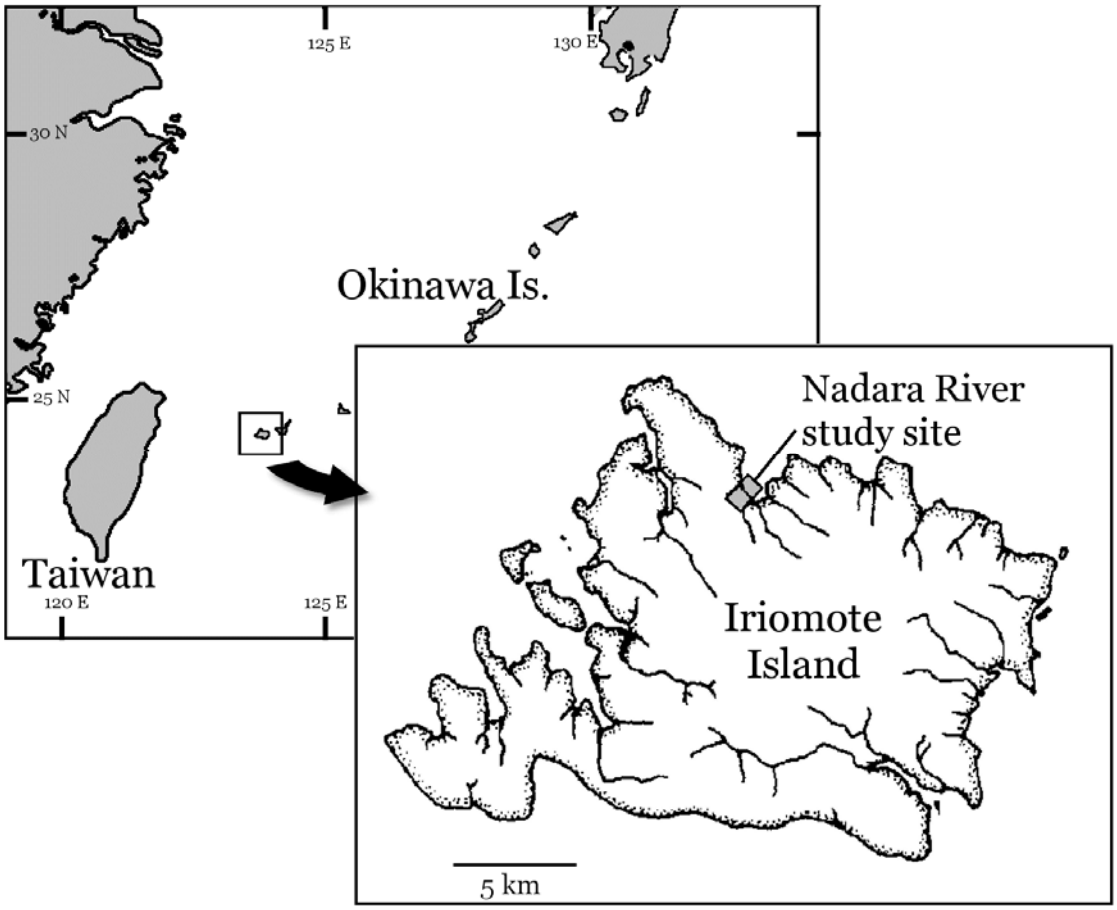

Figure 2.3 Locality map of Iriomote Island study site.

The site chosen on Iriomote Island is near the mouth of the Nadara river (see Figure 2.3). Due to the presence of the off-shore coral reef the site is protected from large wind waves generated offshore, and thus the site was expected to be a low to medium wave energy environment. The site is a riverine forest, with the mangrove forest separating the marine environment from a terrestrial rainforest. However,

during the construction of a road through this forest, a sea wall was erected approximately 50 m from the forest's seaward boundary, effectively isolating the study site from the majority of the mangrove forest up river. At this site the dominant mangrove species is *Bruguiera gymnorrhiza* (see Figure 2.2 (c)).

2.3 Data collection

At each of the three study sites, an instrumented observational array was established along a transect through the mangrove forest. The direction of the transect was aligned with the dominant direction of the incident waves, thus ensuring the observation of wave transformations in the direction of propagation of dominant wave energy. At all three study sites the transect alignment was approximately perpendicular to the seaward boundary of the mangrove forest. The instrumented transect was intended to span the entire width of the forest at each site. Instruments were positioned 0.05 to 0.10 m above the forest floor and became submerged during periods of high water.

Periods of predicted spring tides were chosen for deployment of the observational arrays at each site. Instruments were left in place and operational for all stages of the tide. This approach enabled the collection of wave information at a range of water depths, from the onset of tidal inundation to maximum inundation at times of high water, followed by receding water depths on the ebbing tides.

Observations of the structure and spatial density of the vegetation were also undertaken. At a number of representative locations within the forest at each site, the number of roots and trunks per square metre, and their diameters at elevations of 0.0 m, 0.5 m, 1.0 m and 1.5 m above the forest floor were recorded.

At the Cocoa Creek and Oonoonba study sites, field surveys were undertaken to determine the bathymetry profile of the forest floor. However at Iriomote, the slope of the seabed was estimated from simultaneous observations of the mean water depth at the instrument locations. Due to the remoteness of each study site, bathymetry surveys were referenced to an arbitrary local datum, which for the Cocoa Creek and Oonoonba sites, was set as the base of the local chenier ridge.

Cocoa Creek study site

The instrumented transect established at the Cocoa Creek site consisted of three Woods Hole Instrument System Limited (WHISL) SeaPac 2100 wave gauges and two differential pressure sensors logging data to JCU Atom loggers (hereafter referred to as differential pressure sensors). All instruments recorded data digitally. The WHISL wave gauges sampled at a frequency of 4 Hz in a burst sampling mode. The differential pressure sensors recorded continuously at a frequency of 4 Hz. Both the WHISL wave gauge and differential pressure sensors determined instantaneous sea surface elevation from observations of the instantaneous pressure head, using the hydrostatic assumption. The array was operational for the period 8-10 January 1997 and during this period three high tides completely inundated the forest. A schematic diagram showing the study site bathymetry and instrument locations is presented in Figure 2.4 (a).

Oonoonba study site

The observational array deployed at the Oonoonba site consisted of two WHISL SeaPac 2100 wave gauges and two differential pressure sensors. Unfortunately the most seaward instrument in this array, one of the two WHISL wave gauges, failed to record wave data due to an electronics malfunction. Thus the most seaward instrument was located 70 m in from the front of the forest, and the array was reduced to only span the most landward 80 m of the forest. Instrument sampling frequencies were consistent with those used at Cocoa Creek. The array was inundated on 3 occasions during its operational deployment for the period 14-16 April 1999. A schematic diagram of the study site bathymetry and instrument locations is shown in Figure 2.4 (b).

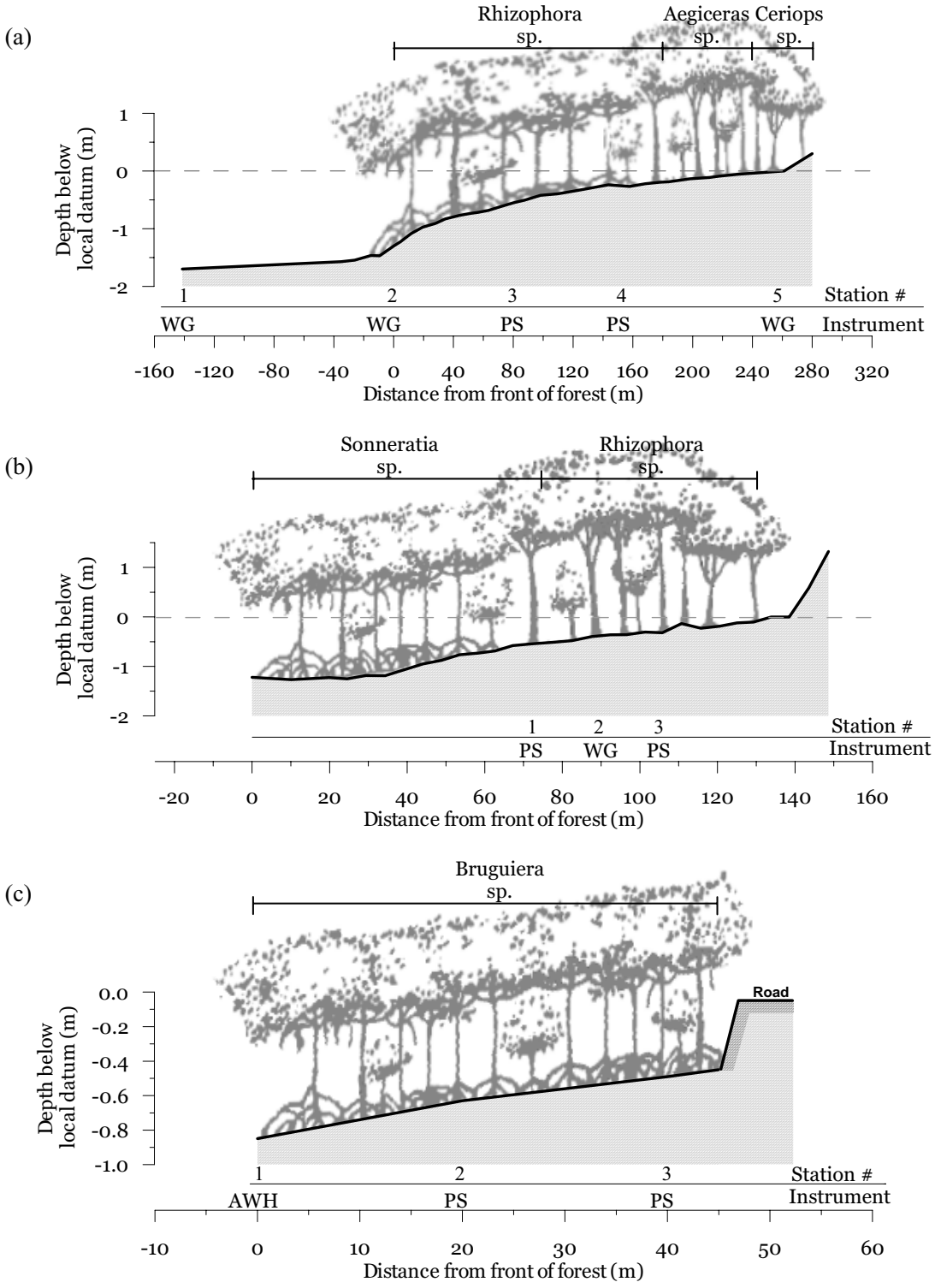

Figure 2.4 Schematic representation of (a) Cocoa Creek, (b) Oonoonba and (c) Iriomote Island study sites. Forest bathymetry profile along instrumented transect is shown as the solid black line. Dominant mangrove species are indicated across the top of each profile. Instrument stations are shown below each profile relative to distance from the seaward edge of the forest at each site, with WG = WHISL SeaPac 2100 wave gauge, PS = differential pressure sensors, AWH = Alec wave

gauge. Drawn vegetation is not indicative of the actual vegetation structure but is included only to highlight extent of forest at each site.

Iriomote study site

Due to the relatively small width (*ca.* 50 m) of the study site at Iriomote, a reduced number of instruments were deployed at this site. The observational array consisted of one ALEC Instruments AWH-16M wave gauge, with a sampling frequency of 5 Hz and two differential pressure sensors sampling as at 4 Hz. The instrument array was operational for 3 days between February 8-10, 1997, capturing 4 high tides. Figure 2.4 (c) presents a schematic diagram of the study site and instrument locations.

2.4 Data reduction and processing procedures

Water level observations at each site were reduced to the corresponding arbitrary datum established at each site from the field surveys (Cocoa Creek and Oonoonba) or bathymetry estimation (Iriomote).

To facilitate consistent analysis of sea surface elevation records from all wave-recording instruments, data from the differential pressure sensors and ALEC AWH wave gauge were sub-sampled into wave burst time series to be concurrent with the data produced from the WHISL wave gauge. Data were sub-sampled such that there were 4096 data points per burst, and the interval between bursts was 20 minutes. Burst sampling details are presented in Table 2.1.

Table 2.1 Summary of wave instrumentation sampling details

Instrument Type	Sampling frequency (Hz)	Burst length (min:sec)	Burst Interval (min)	Data points per burst	Sites deployed *C*=Cocoa Creek *O*=Oonoonba *I*=Iriomote
WHISL SeaPac 2100	4.0	17:04.0	20	4096	*C,O*
Differential pressure sensors	4.0	17:04.0	20	4096	*C,O,I*
ALEC	5.0	13:39.2	20	4096	*I*

AWH wave gauge					

For each study site, data from the most seaward instrument in the observational array was analysed to identify two inundation events with the highest incident wave energy. Data recorded by each instrument during these events were then selected for analysis. Wave burst time series of water surface elevation were analysed for basic statistical and spectral quantities. Wave energy density spectra were estimated by using a Fast Fourier Transform (FFT) procedure, optimized for computational efficiency for the wave burst time series of 4096 data points. A frequency-dependent correction, based on linear wave theory, was applied to the raw depth fluctuations determined from the observed pressure fluctuations to offset the attenuation of the higher frequencies of the wave energy spectrum with depth. Whilst linear wave theory is not strictly applicable to shallow water conditions, Möller *et al*. (1996) demonstrated, through comparison of concurrent corrected water depth fluctuations and high frequency video footage of the sea surface, that the recovery of surface wave information from subsurface pressure measurements, as done here, satisfactorily approximated actual sea surface fluctuations.

In addition to the mean water depth and wave energy density spectra, the following wave parameters were calculated for each wave burst:

Parameter	*Units*	
▪ Significant wave height, H_s	(m)	determined from statistics of wave burst time series of water surface elevation
▪ Maximum wave height, H_{max}	(m)	
▪ Mean wave period, T_m	(s)	
▪ Mean wave length, L_m	(m)	
▪ Total wave energy contained in the wave spectrum (E_{tot})	(J m^{-2})	estimated from wave spectra

The field data collected, and parameters determined from this data will enable the description of wave processes within the mangrove forests at the three study sites at a reasonable spatial resolution. The data are used in Chapter 5 both to describe the key effects of mangrove vegetation on the propagation of random wind-induced

gravity waves through mangroves, and to test theoretical models developed in the following Chapters.

3 MODELLING THE INTERACTION OF MANGROVES WITH WAVE MOTION

3.1 Overview

The purpose of this Chapter is to develop and describe appropriate equations of wave motion in the vicinity of a mangrove forest, and use them to construct a theoretical approach to modelling the attenuation of wave energy within mangrove forests. Interactions between wave motion and mangrove vegetation is thought to be the dominant energy dissipation mechanism for waves propagating through mangrove forests. Bottom shoaling is also thought to contribute, to a lesser degree, to the dissipation of wave energy.

In the early stages of this thesis it was decided for simplicity to develop the initial theory based on the assumption of uniform horizontal bathymetry within the forest. This theoretical approach is developed and presented in the remainder of this Chapter. The approach adopted is based on the work of Massel and Butowski (1980) who investigated the propogation of random wind waves through a porous rubble-mound type of break water. Their approach is similar to the work of Mendez and Losada (1999) in that the fluid domain is divided into three regions (in front, within and behind the breakwater/seagrass) and within each fluid region a solution was found to the momentum equation with dissipation in the form of a velocity potential. An approach following this paradigm was used as it allowed the wave motion to be described in terms of spectral qualities by a defining set of amplification factors in front of, within and behind the forest. The amplification factors describe spectral components propagating in positive and negative direction and account for energy transmission, reflection and attenuation. The method presented in this Chapter differs from Massel and Butowski (1980) and Mendez and Losada (1999) in that the effect of the vegetation is included as a vertically variable drag force, which is modified based on the spatial distribution of the vegetation within a control volume. The modification of the drag coefficient is determined by the use of a discreet vortex method, following the approach Furukawa and Hosokawa (1996).

As the course of this study progressed, a second theoretical approach was developed for the case of wave propagation through a forest with an arbitrary bathymetry profile. In this case the wave motion in the vicinity of the forest is described by a complex wave amplitude that is a solution to the mild-slope equation (Berkhoff, 1972) which incorporates effects of both the vegetation and non-uniform bathymetry. In contrast to the first theoretical approach, non-propagating evanescent modes are neglected and only progressive waves are taken into account. This second approach, presented in Chapter 4, effectively supercedes the initial theoretical approach that neglected variations in bathymetry. However the two approaches converge for the case of a uniform bathymetry profile and comparison for this case is presented in Chapter 5.

3.2 Definitions and assumptions

In order to adequately define the problem, certain definitions and assumptions regarding the wave motion and characteristics of the fluid are required.

Consider the wave motion and co-ordinate system presented in Figure 3.1. The co-ordinate system is defined such that the x-coordinate is horizontal, the z-coordinate is vertical and directed upwards, and the origin O(x,z) lies at the mean free surface of the fluid. A mangrove forest exists in the region $0 < x < l$, and is uniform in the y direction. The substrate is assumed to be impermeable. Water depths in front of and behind the forest are assumed to be constant and equal to h_1 and h_3, respectively. Within the forest the water depth defined by the bathymetry profile, $h_2(x)$ is arbitrary.

It is assumed that unidirectional waves with height, H, approach the mangrove forest from a direction normal to the forest/sea boundary. Waves crests are assumed to be perpendicular to the direction of travel, and thus the wave motion becomes two dimensional in the plane $0,x,z$. Further, the wave height, H, relative to the water depth, h, is assumed to be small as is the wave steepness defined as the ratio of the wave height, H, to the wavelength, L, allowing the solution to exploit simplifications introduced through small amplitude wave theory. The assumption of small amplitude waves implies the that displacement of the sea surface from the undisturbed water level, $\zeta(x,t)$, will always be small.

The fluid under consideration is assumed to be homogeneous, incompressible and inviscid. At the spatial and temporal scales of the processes under consideration, Corriolis acceleration and fluid density stratification can be neglected, and thus the fluid motion can be justifiably assumed irrotational. Further, the effect of viscosity is negligible compared to frictional, drag and inertial forces experienced within a mangrove forest, and can thus be ignored. The assumption of irrotationality allows the wave motion to be described in terms of a velocity potential, $\Phi(x, y, z, t)$. The function Φ has dimension [L^2 T^{-1}] and other wave parameters such as the horizontal

and vertical components of orbital velocity, wave induced pressure and sea surface displacement can be expressed in terms of spatial or temporal gradients of Φ.

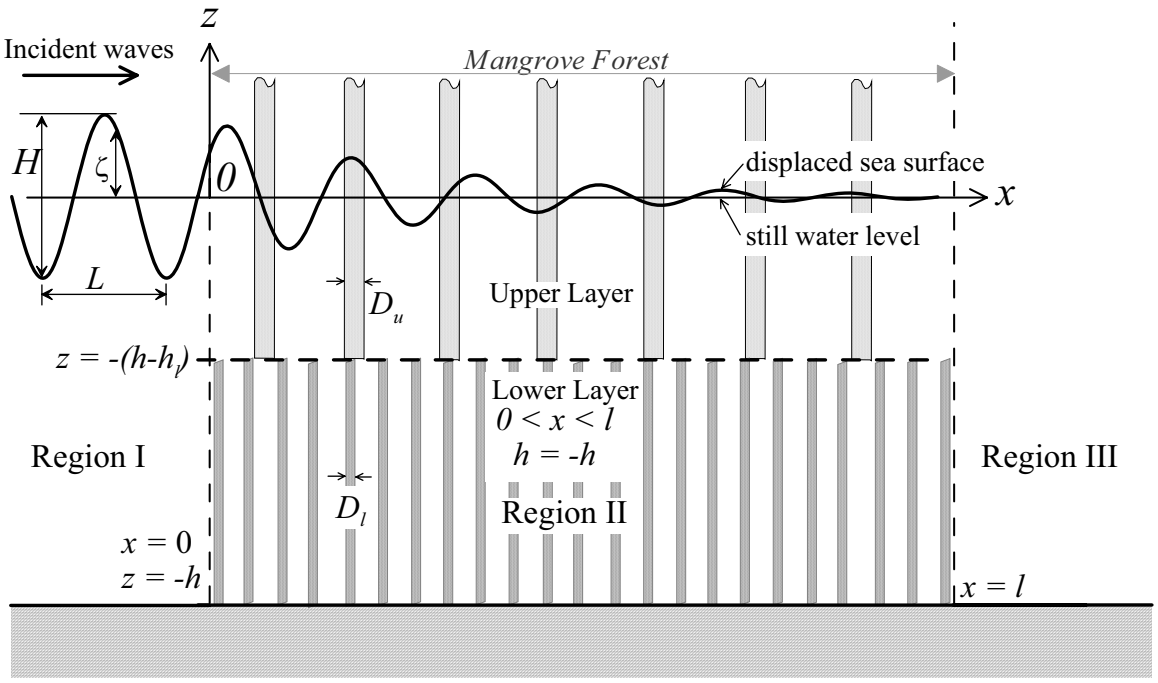

Figure 3.1 Idealised mangrove vegetation, model co-ordinate system and definition sketch for horizontal bathymetry profile.

3.3 Theory: uniform horizontal bathymetry

3.3.1 Governing Equations

Consider the case of a forest with uniform horizontal bathymetry, $h_2(x) = h_2 = \text{constant}$. It is convenient to separate the fluid domain into three distinct regions: Region *I* is defined as the area immediately seaward of the mangrove forest ($-\infty < x < 0$), Region *II* is defined as the area of the mangrove forest ($0 < x < l$), and Region *III* is the area immediately behind the mangroves ($l < x < \infty$). A potential, Φ_i, will be found which is a solution to a boundary value problem posed for each region (*i*=*I*, *II*, *III*), of the fluid domain.

3.3.1.1 Region I:

For two-dimensional motion, the equation of mass conservation reduces to:

$$\frac{\partial u_1}{\partial x} + \frac{\partial w_1}{\partial z} = 0 \tag{3.1}$$

where u_1 and w_1 are horizontal and vertical components of the wave orbital velocity. As the wave motion is irrotational, u_1 and w_1 can be expressed as spatial derivatives of Φ_1,

$$\begin{aligned} u_1 &= \frac{\partial \Phi_1}{\partial x} \\ w_1 &= \frac{\partial \Phi_1}{\partial z} \end{aligned} \tag{3.2}$$

and the velocity potential satisfies the Laplace equation:

$$\frac{\partial^2 \Phi_1}{\partial x^2} + \frac{\partial^2 \Phi_1}{\partial z^2} = \nabla^2 \Phi_1 = 0 \tag{3.3}$$

The boundary value problem can now be posed by the formulation of appropriate boundary conditions for wave potential Φ_1 at the sea surface and the sea floor.

At the sea surface, $z = \zeta_1$, there is no transfer of mass across the air/fluid interface. Therefore a point on the surface moves in a direction normal to the surface with a velocity equal to the normal component of the velocity of the surface. This is known as the kinematic boundary condition. For small amplitude waves, with small steepness, this condition can be simplified and expressed as (Massel, 1996):

$$\frac{\partial \zeta_1}{\partial t} = \frac{\partial \Phi_1}{\partial z} \quad \text{at} \quad z = 0 \tag{3.4}$$

Note that due to the assumption of low wave steepness, the kinematic condition is now applied on the plane $z = 0$ and not on the surface $z = \zeta_1$.

Also at the sea surface, there must exist a dynamic balance between the air and water pressures along the air/fluid interface. This balance can be expressed using the Bernoulli equation, which for wave motion with potential Φ_1 is expressed as (Massel, 1996):

$$\frac{\partial \Phi_1}{\partial t} + \frac{1}{2}\left[\left(\frac{\partial \Phi_1}{\partial x}\right)^2 + \left(\frac{\partial \Phi_1}{\partial z}\right)^2\right] + \frac{p - p_a}{\rho_w} + gz = 0 \quad \text{at} \quad z = \zeta_1 \tag{3.5}$$

where p_a is the atmospheric pressure and ρ_w is the water density. Assuming that at the sea surface, the atmospheric pressure is constant and equal to p, Equation (3.5) can be written in the form of the dynamic boundary condition (Massel, 1996):

$$\frac{1}{2}\left(\frac{\partial \Phi_1}{\partial x}\right)^2 + \frac{1}{2}\left(\frac{\partial \Phi_1}{\partial z}\right)^2 + \frac{\partial \Phi_1}{\partial t} + gz = 0 \quad \text{at} \quad z = \zeta_1 \tag{3.6}$$

By using the assumptions of small wave amplitude and steepness, we can both apply this condition at $z = 0$, and neglect squares of velocity, after which the dynamic boundary condition can be expressed as:

$$\frac{\partial \Phi_1}{\partial t} + g\zeta_1 = 0 \quad \text{at} \quad z = 0 \tag{3.7}$$

or

$$\frac{\partial^2 \Phi_1}{\partial t^2} + g\frac{\partial \zeta_1}{\partial t} = 0 \quad \text{at} \quad z = 0 \tag{3.8}$$

Now using the kinematic boundary condition (Equation (3.4)) yields

$$\frac{\partial^2 \Phi_1}{\partial t^2} + g\frac{\partial \Phi_1}{\partial z} = 0 \quad \text{at} \quad z = 0 \tag{3.9}$$

At the seabed (z = -h), the substratum is assumed to be impermeable, and therefore there is no motion through the boundary at z = -h. It then follows that the velocity normal to the boundary must be zero:

$$w_1 = \frac{\partial \Phi_1}{\partial z} = 0 \text{ at } z = -h$$

or, for the more general case of non-uniform bottom topography, where $\frac{\partial h}{\partial x} \neq 0$:

$$\frac{\partial \Phi_1}{\partial z} + \frac{\partial \Phi_1}{\partial x}\frac{\partial h}{\partial x} = 0 \quad \text{at } z = -h \tag{3.10}$$

Equations (3.3), (3.7), (3.9) and (3.10) represent a boundary value problem for small wave motion in the Region I of the fluid, which has a solution in the form of a velocity potential $\Phi_1(x,z,t)$.

The wave field within Region I is composed not only of the incident wave field, but also includes waves reflected from the forest boundary. With this in mind, the potential $\Phi_1(x,z,t)$ is represented in the Fourier-Stjeltjes integral as follows (Massel, 1996):

$$\Phi_1(x,z,t) = \Re \int_0^\infty \left(\frac{-ig}{\omega} \right) \exp(-i\omega t) \times \left\{ \left[\exp(ik_1 x) - \exp(-ik_1 x) \right] \frac{\cosh k_1(z+h_1)}{\cosh k_1 h_1} + \sum_\alpha M_\alpha \exp(\alpha x) \frac{\cos \alpha(z+h_1)}{\cos \alpha h_1} \right\} dA_i(\omega) \tag{3.11}$$

where $\Re$ denotes the real part of the complex function, and M_α are amplification factors of the particular spectral components. The first term in the parenthesis on the right-hand side represents the progressive waves and part of the reflected waves. The remaining part of the reflected waves is given by the first term in the

summation against M_α, i.e. when the complex wave number $\alpha = -ik$. The wave number, α, has to satisfy the following dispersion relation

$$\frac{\omega^2}{g} + \alpha \tan(\alpha h_1) = 0 \tag{3.12}$$

where ω is the angular frequency. This dispersion relation has an infinite discrete set of real roots α_n and one imaginary root $\alpha = -ik_1$, such as:

$$\frac{\omega^2}{g} - k_1 \cdot \tanh(k_1 h_1) = 0 \tag{3.13}$$

The wave number $\alpha = -ik$ represents the progressive wave while the modes with $\alpha \neq ik$ correspond to non-propagating evanescent wave modes.

Increments of the spectral amplitudes $dA_i(\omega)$ are related to the frequency spectrum as follows (Massel, 1996):

$$\frac{\mathrm{E}[dA_i(\omega) \cdot dA_i^*(\omega')]}{d\omega\, d\omega'} = S_i(\omega)\delta(\omega - \omega') \tag{3.14}$$

where $S_i(\omega)$ is the incident frequency spectrum, E denotes averaging in the stochastic sense, and δ( ) is the delta function.

3.3.1.2 Region II:

Region *II* is the area in the fluid domain that encompasses the mangrove forest. The complex and random nature of mangrove vegetation makes it extremely difficult to represent this vegetation exactly in a theoretical model. Therefore the vegetation must be parameterized in some way based on representative characteristics. The physical structure of many mangrove species, particularly the *Rhisophora and Bruguiera* species, changes dramatically with distance above the forest substrate (Wolanski *et al*., 1980; Lovelock, 1993; Mazda *et al*., 1997b). In general, dense trunks and randomly oriented roots are present immediately above the substrate, but

this density tapers in cross section as roots converge towards a single trunk some distance above the substrate (Figure 3.2). Atop the trunks sits the leaf canopy. Dispersed between trunks and roots are pneumatophores which are knee –like root structures that extend from the substrate but do not intersect a trunk. The cross-sectional shape of trunks and roots is quite random, but in general approximate a circle. During tidal inundation, the sea surface elevation rarely increases to the level of the canopy.

Figure 3.2 Cross-section of mangrove vegetation and obstruction to flow *vs* elevation. Adapted from Wolanski *et al.* 1980

This structure is represented in the model by an idealized mangrove structure of two layers of vertical cylindrical elements with different diameters and number of elements in each layer, as displayed in Figure 3.1. The bottom layer and top layers are representative of the root and trunk dominant sections of the mangrove structure, respectively. Consider now a small control volume of the idealized mangrove forest vegetation of size $\Delta x \times \Delta y \times h$. The volume is selected such that it is sufficiently large to accommodate representative numbers of trunks and roots, but also sufficiently small in order to neglect both the variation of wave velocity and the exact location of each trunk or root within the volume. The special sampling of

$\Delta x = \Delta y = 1m$ is taken as a reasonable compromise given the above-mentioned constraints. Within the control volume, a bottom layer containing a high spatial density of roots extends a thickness h_l above the substrate. Within this layer there are N_l trunks, each of the mean diameter $\overline{D}_l$. Above the bottom layer, beginning at $z = -(h-h_l)$ and extending up to and beyond the sea surface at $z = 0$, there are N_u trunks, each of the mean diameter $\overline{D}_u$. The canopy is not represented in the idealized structure. Estimates of vegetation density, and thus representative values of N_l, N_u, $\overline{D}_l$, $\overline{D}_u$ and h_l, are available from field data, and in general, $N_u > 1$ and $N_l \gg 1$, and h_l is of order 0.3 m - 1.0 m.

Interactions between wave motion and mangrove vegetation is the dominant energy dissipation mechanisms for waves propagating through Region *II*. Therefore it is assumed that dissipation due to vegetation dominates and bottom friction can be neglected (Petryk and Bosmajian, 1975; Asano *et al*., 1992; Mazda *et al*., 1997a).

With this assumption, the momentum equation with dissipation can be expressed as

$$\frac{\partial \vec{u}_2}{\partial t} = -\frac{1}{\rho_w}\nabla(p_2 + \rho_w g z) - \frac{1}{\rho_w}\vec{F} \tag{3.15}$$

where $\vec{u}_2 = (u_2, w_2)$ is the wave-induced velocity vector in Region *II*, p_2 is the corresponding dynamic pressure, and $\vec{F}$ is a force vector (per unit volume).

3.3.1.2.1 Consideration of drag due to mangrove vegetation

The total force imposed on an object in a moving flow is the vectorial sum of drag, lift and inertial forces. Drag force is caused by pressure differences around the perimeter of the object, and is directed in the direction of the velocity. The force due to pressure difference in the direction normal to the direction of flow is known as lift. Inertial force results from accelerations of the fluid relative to the object. Accelerations cause changes in kinetic energy of the fluid, and thus work on the object. The force on each cylindrical component of the idealized mangrove structure can be examined to reveal the relative importance of drag, lift and inertial forces. At

this stage the lift force can be neglected, because by definition it operates normal to the velocity direction and thus only affects motion in the *y*-dimension, which is ignored for this theoretical development. Therefore it is left to determine the relative importance of only drag and inertial forces. The ratio of drag and inertial forces can be represented as (Morison *et al*., 1950)

$$\frac{\Delta F_i}{\Delta F_d} = \frac{\rho_w C_m V \partial u / \partial t}{\frac{1}{2}\rho_w C_d A u |u|} \tag{3.16}$$

in which ΔF_i and ΔF_d are the inertial and drag forces, per unit length of pile, V is the cylinder volume per unit length, A is the projected area per unit length, C_m and C_d are the inertia and drag coefficients, and u is a wave induced velocity.

Evaluation of the ratio above at $(z = 0)$ yields:

$$\frac{(\Delta F_i)_{z=0}}{(\Delta F_d)_{z=0}} = \frac{C_m \pi D}{C_d H} \tanh kh \tag{3.17}$$

where D is the diameter of the cylinder, H is the wave height. For very shallow water $\tanh kh \to kh$ and thus the ratio reduces to

$$\frac{(\Delta F_i)_{z=0}}{(\Delta F_d)_{z=0}} = \frac{C_m \pi D}{C_d H} kh \tag{3.18}$$

Using values of D = 0.02 to 0.05 m and H ~ 0.5 m, which are typical of the mangrove forests at the three field sites (see Chapter 2), the ratio further reduces to

$$\frac{(\Delta F_i)_{z=0}}{(\Delta F_d)_{z=0}} \approx (0.05 \text{ to } 0.10)\frac{C_m}{C_d} \tag{3.19}$$

The inertia and drag coefficients are both functions of Reynolds number, *Re*. For wave induced flows in mangrove areas, *Re* lies in the range 200<*Re*<25000 and

within this range the corresponding value of the ratio $\frac{C_m}{C_d} \approx 1$ (SPM, 1984). Therefore, the ratio of inertial to drag force becomes

$$\left(\Delta F_i\right)_{z=0} = (0.05 \text{ to } 0.10) \times \left(\Delta F_d\right)_{z=0} \tag{3.20}$$

which indicates that the drag forces dominate, and inertial forces can be neglected. Focusing now only on drag forces, the total force, $\vec{F}$, per unit volume, for the upper and lower layers, respectively, can be expressed as

$$\vec{F}_u(x,z) = \frac{1}{2}\rho_w \bar{D}_u \sum_{j=1}^{j=N_u} C_d^{(m)}(Re)\vec{u}_{n,j}(x,z)\left|\vec{u}_{n,j}(x,z)\right| \quad \text{for } -(h-h_l) < z < 0 \tag{3.21}$$

and

$$\vec{F}_l(x,z) = \frac{1}{2}\rho_w \bar{D}_l \sum_{j=1}^{j=N_l} C_d^{(m)}(Re)\vec{u}_{n,j}(x,z)\left|\vec{u}_{n,j}(x,z)\right| \quad \text{for } -h < z < -(h-h_l) \tag{3.22}$$

The vector $\vec{u}_{n,j}(x,z)$ is water velocity, normal to the longitudinal axis of the particular trunk j induced by wave orbital velocity $\vec{u}(x,z) = [u(x,z), w(x,z)]$. $C_d^{(m)}$ denotes a modified drag coefficient, introduced to parameterize the interaction between fluid motion and roots and trunks, and the effect of this on the drag coefficient C_d. The modified drag coefficient $C_d^{(m)}$ takes the form

$$C_d^{(m)}(Re,x,z) = K(N,Re)\ C_d(Re,x,z) \tag{3.23}$$

where $K(N,Re)$ is a modification factor controlled by mangrove density (given by N trunks per unit volume) and the Reynolds number. Determination of the drag coefficient modification factor K is described in Section 3.4. It should be noted now that it is appropriate to introduce notation indicating the that drag coefficient, C_d, is a function of both the x and z-coordinates, due to its dependence on the wave orbital velocity $\vec{u}(x,z)$. The Reynolds number can be calculated from

the wave orbital velocity, the diameter of the particular trunk, *D*, and the kinematic viscosity, *v*, as follows:

$$Re = \frac{|\vec{u}(x,z)|D}{v} \tag{3.24}$$

The unmodified drag coefficient, C_d, is dependent on the Reynolds number as follows (SPM, 1984):

$$C_d(Re,x,z) = \begin{cases} 1.2 & \text{for } Re \le 2\times10^5 \\ 1.2 - 0.5\left(\frac{\mathrm{Re}}{3\times10^5} - \frac{2}{3}\right) & \text{for } 2\times10^5 \le Re \le 5\times10^5 \\ 0.7 & \text{for } Re > 5\times10^5 \end{cases} \tag{3.25}$$

3.3.1.2.2 Linearising drag terms

Expressions for the total force vectors, $\vec{F}_l$ and $\vec{F}_u$ in Equations (3.21) and (3.22), respectively, are non-linear due to the terms involving the local orbital velocity and its absolute value. Thus the momentum equations for wave motion in the upper and lower layers are also non-linear and cannot be solved exactly. To overcome this problem a linearisation procedure is employed, which seeks to substitute a linear term for the non-linear term, under the constraint that the mean error, $\bar{\varepsilon}$, due to the substitution is minimized. Such a procedure is widely used in ocean engineering for the determination of forces on off-shore structures (Gudmestad and Connor, 1983). The substitution takes the form

$$\frac{1}{\rho_w}\vec{F}(x,z) \approx f_e \omega_p \vec{u}_2(x,z) \tag{3.26}$$

The error, ε, of this approximation is defined as

$$\varepsilon(x,z) = \frac{1}{\rho_w}\vec{F}(x,z) - f_e \omega_p \vec{u}_2(x,z) \rightarrow \text{minimum} \tag{3.27}$$

where ω_p is the peak frequency, and f_e is the unknown linearisation coefficient.

The linearisation procedure employed is based on the concept of minimizing, in the stochastic sense, the error of the linear approximation. The minimization can be represented as

$$\int_{-h}^{0}\int_{0}^{l} E\left[\varepsilon^2\right] dxdz = minimum \tag{3.28}$$

where $E[\ ]$ denotes averaging in stochastic sense. A detailed description of the linearisation procedure and determination of the coefficient f_e will be given in Section 3.5. It is, however, now practical to briefly describe the linearisation coefficient, f_e, as a function of the statistical characteristics of wave-induced orbital velocities in the forest. These velocities are unknown at the commencement of the linearisation procedure, and an initial value of the coefficient is needed. Using this initial value, a new estimate of the orbital velocity field is calculated, and a new estimate of f_e is obtained. The calculation of the wave field, and f_e is therefore done in a recursive manner until f_e converges to a single value.

From a physical perspective, the linearisation approximation simplifies the problem of defining the energy dissipation of a complicated and spatially variable network of trunks and roots by assuming that the energy dissipation within the forest is determinable and characterized by term $f_e\omega_p\vec{u}_2(x,z)$.

Following the linearisation procedure, the momentum equation in Region *II* becomes:

$$\frac{\partial \vec{u}_2}{\partial t} + \frac{1}{\rho_w}\nabla(p_2 + \rho_w g z) + f_e\omega_p\vec{u}_2 = 0 \tag{3.29}$$

Orbital velocity, $\vec{u}_2$, is a wave-induced property, and thus temporally periodic in nature. As such, it can be represented as

$$\vec{u}_2 = |\vec{u}_2| \exp(-i\omega t) \tag{3.30}$$

After appropriate differentiation and substitution into Equation (3.29), the momentum equation becomes

$$\omega(i - f_e \frac{\omega_p}{\omega})\vec{u}_2 = \frac{1}{\rho_w} \nabla(p_2 + \rho_w g z) \tag{3.31}$$

Taking the curl of Equation (3.31) yields

$$\omega(i - f_e \frac{\omega_p}{\omega}) \nabla \times \vec{u}_2 = \frac{1}{\rho_w} \nabla \times \nabla(p_2 + \rho_w g z) = 0 \tag{3.32}$$

It then follows $\nabla \times \vec{u}_2 = 0$ and thus there exists a velocity potential in Region *II* such that

$$\vec{u}_2 = \nabla \Phi_2 \tag{3.33}$$

which on substitution into the momentum equation yields:

$$\frac{\partial \Phi_2}{\partial t} + \frac{1}{\rho_w}(p_2 + \rho_w g z) + f_e \omega_p \, \Phi_2 = 0 \tag{3.34}$$

A boundary value problem is now constructed for Region *II* using the potential Φ_2.
At the air/sea interface ($z \approx \varsigma$ and $p \approx 0$) Equation (3.34) can be approximated as

$$\frac{\partial \Phi_2}{\partial t} + g\varsigma + f_e \omega_p \, \Phi_2 = 0 \tag{3.35}$$

The periodicity of wave motion implies that

$$\Phi = |\Phi| \exp(-i\omega t), \ \frac{\partial \Phi}{\partial t} = -i\omega \Phi \ \text{ and } \ \frac{\partial^2 \Phi}{\partial t^2} = -\omega^2 \Phi \tag{3.36}$$

By utilizing this periodicity and invoking the kinematic boundary condition at the sea surface (Equation (3.4)), the surface boundary condition becomes

$$g\frac{\partial \Phi_2}{\partial z} - \omega^2(1 + i f_e \frac{\omega_p}{\omega})\Phi_2 = 0, \quad \text{at } z = \zeta \approx 0 \tag{3.37}$$

At the sea bottom, the substratum is impermeable, and there is no motion through the boundary at $z = -h$. It follows that the velocity normal to the boundary must be zero, and for the general case of non-uniform bottom topography, the boundary condition is:

$$\frac{\partial \Phi_2}{\partial z} + \frac{\partial \Phi_2}{\partial x}\frac{\partial h_2}{\partial x} = \frac{\partial \Phi_2}{\partial z} = 0 \text{ at } z = -h \tag{3.38}$$

Equations (3.33), (3.37) and (3.38) formulate the boundary value problem for potential Φ_2 in Region *II*.

The wave field in Region *II* is composed of progressive waves, waves reflected from the mangrove boundary at $x = l$, and a set of disturbances due to the reflection from the boundaries at $x = 0$ and $x = l$. These disturbances attenuate quickly with distance from the corresponding boundaries. The velocity potential, Φ_2, can thus be represented as:

$$\begin{aligned}\Phi_2(x,z,t) = \Re \int_{-\infty}^{\infty} \left(\frac{-ig}{\omega}\right) \exp(-i\omega t) \\ \times \sum_{\psi} \left\{ \left[P_\psi \exp(-\psi x) + Q_\psi \exp(\psi x) \right] \frac{\cos\psi(z+h)}{\cos\psi h} \right\} dA_i(\omega)\end{aligned} \tag{3.39}$$

where P_ψ and Q_ψ are the amplification factors of the spectral components propagating in positive and negative x direction, respectively. Wave number ψ has to satisfy the following dispersion relation

$$\omega^2\left(1+if_e\frac{\omega_p}{\omega}\right)+g\psi\tan(\psi h)=0. \tag{3.40}$$

In general, the wave number ψ is a complex function, i.e. $\psi=\psi_r+i\psi_i$. The real part, ψ_r, controls the attenuation of wave amplitude within the mangrove region while the imaginary part, ψ_i, provides the phase of the wave. When there is no energy dissipation (i.e. $f_e=0$), wave number $\psi\to\alpha$, with the condition that Equation (3.12) is satisfied.

3.3.1.3 Region III:

In the absence of mangroves, the boundary value problem for Region *III* is equivalent to the boundary value problem for Region *I*. Therefore, Equations (3.3), (3.7), (3.9) and (3.10) represent a boundary value problem for small wave motion in the Region *III* of the fluid. This problem has a solution in the form of a velocity potential $\Phi_3(x,z,t)$. In Region *III*, only progressive waves exist, propagating in the positive *x*-direction out of the mangrove forest. Therefore, the potential Φ_3 takes the form:

$$\begin{aligned}\Phi_3(x,z,t)=\Re\int_{-\infty}^{\infty}\left(\frac{-ig}{\omega}\right)\exp(-i\omega t)\\ \times\sum_{\alpha}T_\alpha\exp\left[\alpha(l-x)\right]\frac{\cos\alpha(z+h)}{\cos\alpha h}dA_i(\omega)\end{aligned} \tag{3.41}$$

in which T_α are the amplification factors of the particular spectral components and wave numbers α satisfy Equation (3.12).

3.3.2 Boundary Conditions at the interfaces of Regions I, II and III:

The potentials $\Phi_1(x,z,t)$, $\Phi_2(x,z,t)$ and $\Phi_3(x,z,t)$ must satisfy the matching conditions which provide continuity of pressure and horizontal velocity at the

interfaces of Regions *I* and *II* and Regions *II* and *III*, corresponding to $x = 0$ and $x = l$.

At $x = 0$, equality of dynamic pressure requires that

$$p_1(0,z,t) = p_2(0,z,t) \tag{3.42}$$

Evaluating the dynamic pressures from the corresponding velocity potential yields

$$p_1(0,z,t) = -\rho_w \frac{\partial \Phi_1}{\partial t} = \Re \int_{-\infty}^{\infty} \rho_w g \exp(-i\omega t)\Theta_1(z) dA_i(\omega) \tag{3.43}$$

and

$$p_2(0,z,t) = \Re \int_{-\infty}^{\infty} \rho_w g \exp(-i\omega t)\Theta_{12}(z) dA_i(\omega) \tag{3.44}$$

where

$$\Theta_1 = \sum_{\alpha} M_\alpha \frac{\cos\alpha(z+h)}{\cos\alpha h} = \sum_{\alpha} \left(M_\alpha \frac{B_\alpha}{\cos\alpha h} \right) \frac{\cos\alpha(z+h)}{B_\alpha} \tag{3.45}$$

and

$$\begin{aligned} \Theta_{12} &= \sum_{\psi} \left(1 + if_e \frac{\omega_p}{\omega} \right) (P_\psi + Q_\psi) \frac{\cos\psi(z+h)}{\cos\psi h} \\ &= \sum_{\psi} \left\{ \left(1 + if_e \frac{\omega_p}{\omega} \right) (P_\psi + Q_\psi) \frac{B_\psi}{\cos\psi h} \right\} \frac{\cos\psi(z+h)}{B_\psi} \end{aligned} \tag{3.46}$$

The functions B_α^2 and B_ψ^2 are defined, respectively, as

$$B_\alpha^2 = \left\{ \frac{h}{2} \left[\frac{\sin(2\alpha h)}{2\alpha h} + 1 \right] \right\} \tag{3.47}$$

and

$$B_\psi^2 = \left\{ \frac{h}{2}\left[\frac{\sin 2\psi h}{2\psi h} + 1 \right] \right\} \tag{3.48}$$

To evaluate the boundary conditions it is convenient to invoke the orthogonality of functions $\frac{\cos\alpha(z+h)}{B_\alpha}$ and $\frac{\cos\psi(z+h)}{B_\psi}$ in the domain $(-h,0)$. Therefore from Equations (3.45) and (3.46) we obtain

$$M_\alpha = \frac{\cos\alpha h}{B_\alpha} \cdot \int_{-h}^{0} \Theta_1 \frac{\cos\alpha(z+h)}{B_\alpha} dz \tag{3.49}$$

and

$$\left(1 + if_e \frac{\omega_p}{\omega}\right)\left(P_\psi + Q_\psi\right) = \frac{\cos\psi h}{B_\psi} \int_{-h}^{0} \Theta_{12} \frac{\cos\psi(z+h)}{B_\psi} dz \tag{3.50}$$

Returning to the condition of pressure continuity, $p_1(0,z,t) = p_2(0,z,t)$ requires that

$$\Theta_1 = \Theta_{12} \tag{3.51}$$

Therefore

$$P_\psi + Q_\psi = \sum_\alpha L_{\alpha\psi} M_\alpha \tag{3.52}$$

where $L_{\alpha\psi}$ is defined as

$$L_{\alpha\psi} = \frac{\cos(\psi h)}{B_\psi^2\left(1 + if_e \frac{\omega_p}{\omega}\right)\cos(\alpha h)} \int_{-h}^{0} \cos\alpha(z+h)\cos\psi(z+h) dz \tag{3.53}$$

In a similar way, for boundary $x = l$, the equality of pressure determines that

$$P_\psi \exp(-\psi l) + Q_\psi \exp(\psi l) = \sum_\alpha L_{\alpha\psi} T_\alpha \tag{3.54}$$

Equations (3.52) and (3.54) form a system of equations for P_ψ and Q_ψ. Solution of the system yields

$$P_\psi = \frac{1}{2\sinh(\psi l)} \sum_\alpha L_{\alpha\psi} \left[\exp(\psi l) M_\alpha - T_\alpha \right] \tag{3.55}$$

and

$$Q_\psi = \frac{1}{2\sinh(\psi l)} \sum_\alpha L_{\alpha\psi} \left[T_\alpha - \exp(-\psi l) M_\alpha \right] \tag{3.56}$$

The condition of horizontal velocity continuity $x = 0$ requires that

$$\frac{\partial \Phi_1}{\partial x} = n_p \frac{\partial \Phi_2}{\partial x} \tag{3.57}$$

where n_p is the 'surface porosity' of the mangroves at $x = 0$. Conceptually, it is a projection of the mangrove vegetation on the plane x = 0, z. From a physical point of view, an obvious analogy is the volume porosity n_v, defined as

$$n_v = 1.0 - \frac{V_t}{V_0}, \tag{3.58}$$

where V_t is the volume of vegetation and V_0 is a total control volume. It should be noted here that $n_p = 1$ represents absence of vegetation and $n_p = 0$ is a fully reflective wall.

Differentiating appropriate expressions for Φ_1 and Φ_2 and substituting into (3.57) yields, for $x = 0$

$$2ikl\frac{\cosh k(z+h)}{\cosh kh}+\sum_{\alpha l}(\alpha l)M_\alpha\frac{\cos\alpha(z+h)}{\cos\alpha h}=n_p\sum_{\psi}(\psi l)\left(-P_\psi+Q_\psi\right)\frac{\cos\psi(z+h)}{\cos\psi h} \tag{3.59}$$

In the same way, the continuity of the horizontal component of velocity at $x=l$ gives

$$\sum_{\alpha}(\alpha l)T_\alpha\frac{\cos\alpha(z+h)}{\cos\alpha h}=n_p\sum_{\psi}(\psi l)\left[-P_\psi\exp\left(-\psi l\right)+Q_\psi\exp(\psi l)\right]\frac{\cos\psi(z+h)}{\cos\psi h} \tag{3.60}$$

Substituting for P_ψ and Q_ψ (Equations (3.55) and (3.56)) results in a system of equations for amplification factors M_α and T_α

$$\begin{aligned}P_1\frac{\cosh(z+h)}{\cosh kh}=-\sum_{\alpha}\left\{P_2\frac{\cos\alpha(z+h)}{\cos\alpha h}+\sum_{\psi}\frac{P_3(P_4+P_5)}{2\sinh(\psi l)}L_{\alpha\psi}\frac{\cos\psi(z+h)}{\cos\psi h}\right\}M_\alpha\\+\sum_{\alpha}\left\{\sum_{\psi}\frac{2P_3}{2\sinh(\psi l)}L_{\alpha\psi}\frac{\cos\psi(z+h)}{\cos\psi h}\right\}T_\alpha\end{aligned} \tag{3.61}$$

and

$$\begin{aligned}0=\sum_{\alpha}\left\{\sum_{\psi}\frac{2P_3}{2\sinh(\psi l)}L_{\alpha\psi}\frac{\cos\psi(z+h)}{\cos\psi h}\right\}M_\alpha\\-\sum_{\alpha}\left\{P_2\frac{\cos\alpha(z+h)}{\cos\alpha h}+\sum_{\psi}\frac{P_3(P_4+P_5)}{2\sinh(\psi l)}L_{\alpha\psi}\frac{\cos\psi(z+h)}{\cos\psi h}\right\}\end{aligned} \tag{3.62}$$

where

$$\begin{aligned}&P_1=2ikl;\quad P_2=\alpha l;\quad P_3=n_p\psi l\\&P_4=\exp(\psi l);\quad P_5=\exp(-\psi l)\end{aligned} \tag{3.63}$$

3.3.3 Solving for amplification factors M_α and T_α :

Determination of amplification factors M_α and T_α requires appropriate manipulation of Equations (3.61) and (3.62). Introducing the multiplier $\frac{\cos\gamma(z+h)}{\cos\gamma h}$, where wave number γ satisfies the dispersion relation (Equation (3.12)) and integrating in the domain $z=(-h,0)$ yields

$$\begin{aligned} -\sum_\alpha \Pi_1 M_\alpha + \sum_\alpha \Pi_2 T_\alpha &= \Pi_3 \\ \sum_\alpha \Pi_2 M_\alpha - \sum_\alpha \Pi_1 T_\alpha &= 0 \end{aligned} \tag{3.64}$$

where functions Π_1, Π_2 and Π_3 are given by

$$\begin{aligned} \Pi_1 &= P_2\Lambda_{\alpha\gamma} + \sum_\psi \frac{P_3(P_4+P_5)}{2\sinh(\psi l)} L_{\alpha\psi}\Lambda_{\gamma\psi} \\ \Pi_2 &= \sum_\psi \frac{2P_3}{2\sinh(\psi l)} L_{\alpha\psi}\Lambda_{\gamma\psi} \\ \Pi_3 &= P_1\Lambda_{k\gamma} \end{aligned} \tag{3.65}$$

and

$$\begin{aligned} \Lambda_{\alpha\gamma} &= \int_{-h}^{0} \frac{\cos\alpha(z+h)}{\cos\alpha h}\frac{\cos\gamma(z+h)}{\cos\gamma h}dz \\ \Lambda_{\gamma\psi} &= \int_{-h}^{0} \frac{\cos\gamma(z+h)}{\cos\gamma h}\frac{\cos\psi(z+h)}{\cos\psi h}dz \\ \Lambda_{k\gamma} &= \int_{-h}^{0} \frac{\cos k(z+h)}{\cos k h}\frac{\cos\gamma(z+h)}{\cos\gamma h}dz \end{aligned} \tag{3.66}$$

Equation (3.64) represents a linear system of equations of the infinite modes of the amplification factors M_α and T_α. The accuracy of the solution is determined by the number of modes evaluated. If the number of modes is limited to a finite, relatively small number *N*, then the system of equations can be presented in the more compact form

$$A_{ij} X_j = B_i \tag{3.67}$$

where matrix A and vectors X_j and B_i are defined as

$$A_{ij} = \begin{cases} -\Pi_1 & \text{for } 1 \le i \le N, 1 \le j \le N \\ \Pi_2 & \text{for } 1 \le i \le N, N+1 \le j \le 2N \\ \Pi_2 & \text{for } N+1 \le i \le 2N,\ 1 \le j \le N \\ -\Pi_1 & \text{for } N+1 \le i \le 2N, N+1 \le j \le 2N \end{cases}$$

$$X_j = \begin{cases} M_\alpha & \text{for } 1 \le j \le N \\ T_\alpha & \text{for } N+1 \le j \le 2N \end{cases} \tag{3.68}$$

$$B_i = \begin{cases} \Pi_3 & \text{for } i = 1 \\ 0 & \text{for } i > 1 \end{cases}$$

Equation set (3.67) can be solved using the standard procedure of matrix A decomposition with subsequent back substitution (Press *et al*., 1986).

When amplification factors M_α, T_α, P_ψ and Q_ψ are known, the frequency spectra of various physical quantities, such as sea surface displacement ζ, and wave-induced velocities u and w can be determined from the corresponding potentials. Of particular interest for this investigation are the frequency spectra of the velocities and surface displacement in Region *II*. As will be described in Section 3.5, various parameters associated with the frequency spectra of the horizontal velocity component are fundamental to the linearisation procedure. The frequency spectra of the horizontal velocity is

$$u_2 = \Re \int_{-\infty}^{\infty} \tilde{U}_2(\omega) \exp(-i\omega t) dA_i(\omega) \tag{3.69}$$

where

$$\tilde{U}_2(\omega) = \left(\frac{-in_p g}{\omega} \right) \sum_\psi \psi \left[-P_\psi \exp(-\psi x) + Q_\psi \exp(\psi x) \right] \frac{\cos \psi (z+h)}{\cos \psi h} \tag{3.70}$$

and the corresponding standard deviation squared, also known as the variance, is

$$\sigma_{u_2}^2 = \int_0^\infty \left\{ \left[\Re \tilde{U}_2(\omega) \right]^2 + \left[\Im \tilde{U}_2(\omega) \right]^2 \right\} S_i(\omega) d\omega \tag{3.71}$$

in which $\Re$ and $\Im$ denote the real and imaginary parts of the complex value, respectively.

In Region *II*, the surface displacement $\zeta_2(x,t)$ can be found from Equation (3.39) as follows

$$\begin{aligned} \zeta_2(x,t) &= -\frac{1}{g}\left(\frac{\partial \Phi_2}{\partial t} + f_e \omega_p \Phi_2 \right)_{z=0} \\ &= \Re \int_{-\infty}^{\infty} \exp(-i\omega t) \cdot \Upsilon(\omega, x) dA_i(\omega) \end{aligned} \tag{3.72}$$

in which

$$\Upsilon(\omega, x) = \left(1 + i f_e \frac{\omega_p}{\omega} \right) \sum_{\psi} \left[P_\psi \exp(-\psi x) + Q_\psi \exp(\psi x) \right] \tag{3.73}$$

Therefore, the frequency spectrum of the sea surface displacement in Region *II* will be

$$S_2(\omega; x) = \left| \Upsilon(\omega, x) \right|^2 S_i(\omega) \tag{3.74}$$

Computation of the solution of the Equation set (3.67) and the determination of amplification factors M_α, T_α, P_ψ and Q_ψ, and corresponding frequency spectra was enabled through the development of a computational model written in FORTRAN programming language. At the commencement of computations, the wave field in the mangrove forest is unknown. Therefore, to enable an initial solution, an initial value of the linearisation coefficient, f_e, is set. Using this initial

value, an estimate of the orbital velocity field is calculated, and a new estimate of f_e is obtained. The calculation of the wave field, and f_e is therefore done in a recursive manner until f_e converges to a single value. This recursive procedure is outlined in Figure 3.3. The computational model was employed to investigate the propagation of surface waves and the attenuation of wave energy for various scenarios of vegetation structure and spatial density. Results from the model and their comparison with field observations are presented in Chapter 5.

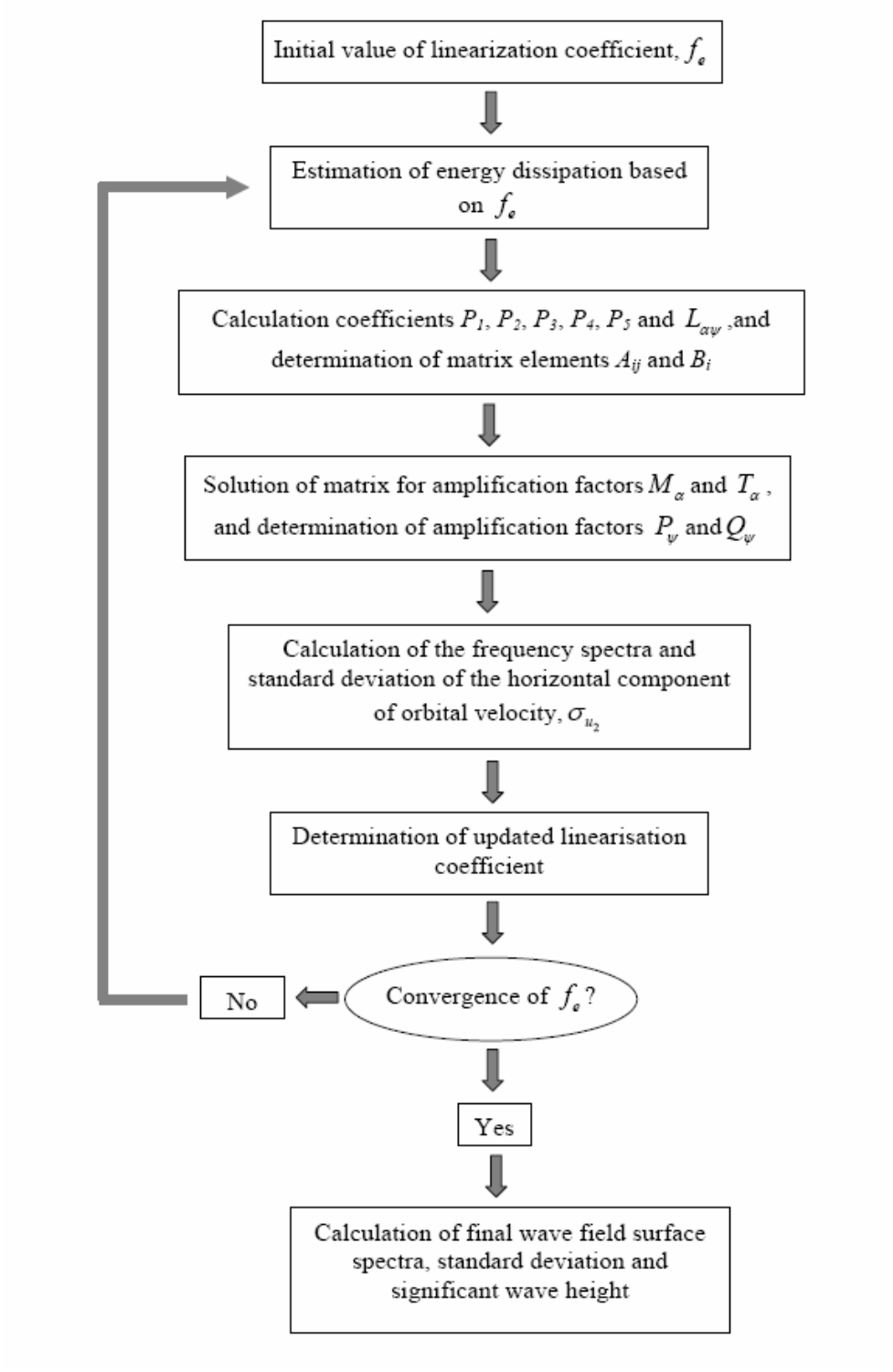

Figure 3.3 Flow chart of numerical computations for model with horizontal bathymetry.

3.4 Effects of root density on drag coefficient

As reported in Chapter 3.2.1, a modified drag coefficient $C_d^{(m)}$ is used to parameterize the modification of the drag coefficient C_d due to the interactions of the vegetation with the wave motion. Interactions which affect the drag coefficient take place at the scale of the vegetation elements, and take the form of vortices that form on the downstream side of the obstacle. Vortices trailing from the obstacle form a wake which intercepts with obstacles downstream (Furukawa *et al*., 1997). The Reynolds number, together with the intensity and length-scale of the turbulence present in the incident flow control the size, nature and persistence of the vortices and wake formation, and for the case of a matrix of obstacles, the scale of the turbulence is also dependent on the proximity of other obstacles (Furukawa and Wolanski, 1996; Furukawa *et al*., 1997). The intensity of the turbulence and its diffusion control the drag forces on the obstacle induced by the flow.

An analogy to wave motion through a matrix of mangrove vegetation can be found in the studies reported by Laird (1962) and Laird and Warren (1963) who investigated wave-induced hydrodynamic forces on groups of emergent vertical cylinders. Experimental results indicated that the modification of the drag coefficient was dependent on the orientation of the cylinder groups to the incident waves and the relative spacing (*S/D*) of the cylinders, where *D* is the cylinder diameter and *S* is the distance between the cylinder axis (Chakrabarti, 1991). For arrays of 3 and 5 cylinders orientated normal to the flow, the drag coefficient was found to increase as the *S/D* approached 1.1, but remained relatively constant for *S/D* > 2.0. However, for the case where the array was aligned in the direction of wave propagation, there was an observed decrease in the drag coefficient as the spacing was reduced, due to shielding of the downstream cylinders by the upstream cylinder. These results are not directly applicable to random mangrove vegetation, but provide evidence that in areas where there are obstructions to the flow, the drag coefficient is dependent on the geometry and spatial density of these obstructions, and this dependence cannot be neglected.

The modification of the drag coefficient is due mainly to the interaction of vortices with downstream vegetation, and thus it is appropriate to use the discrete vortex method of Furukawa and Hosokawa (1996) to investigate the effects of vegetation density. The discrete vortex method is based on a two dimensional Navier-Stokes equation, which, after taking rotation of the equation, is transformed to a vorticity transport equation as follows

$$\frac{\partial \boldsymbol{\omega}}{\partial t} + \boldsymbol{U} \cdot \nabla \boldsymbol{\omega} = K_h \nabla^2 \boldsymbol{\omega} \tag{3.75}$$

where, $\boldsymbol{U}$ is depth averaged velocity vector ($\boldsymbol{U}$=(U,V)), t is time, K_h is horizontal eddy viscosity, and $\boldsymbol{\omega}$ is the vorticity defined as $\frac{\partial V}{\partial x} - \frac{\partial U}{\partial y}$. Vorticity has a continuous distribution over the calculated domain, and in order to produce a discrete vorticity distribution, the circulation, Γ, is introduced by the integration of vorticity over a small domain as:

$$\boldsymbol{\omega} = \frac{\Gamma}{\pi \boldsymbol{\varepsilon}^2} \exp\left(-\frac{r^2}{\boldsymbol{\varepsilon}^2} \right) \tag{3.76}$$

where r is the distance from the center of the structure, and $\boldsymbol{\varepsilon}$ is the core radius (Chorin, 1973, Leonard, 1980, Furukawa and Hosokawa, 1996). Equation (3.76) describes the discrete vorticity induced by circulation Γ at a distance r from the centre of the structure.

Solid boundaries such as trunks and roots are expressed by boundary element vortices, and conservation of circulation and no-slip conditions are applied along solid boundaries. Circulation is explicitly introduced in the flow by separation from the boundary layer on the trunks (Kawahara, 1978), and the intensity of the circulation is calculated by a simplified boundary layer model. All circulation in the model domain is introduced explicitly.

Summation of the velocity induced by all circulation and the potential flow gives a detailed flow field around individual mangrove trunks. The resulting drag force, F, acting on a trunk is

$$F = \oint_A p\,\mathbf{n}\,ds \tag{3.77}$$

where, p is surface pressure, $\mathbf{n}$ is the vector normal to the surface, and A is surface path around the trunk. Surface pressure, p, around each root is calculated from the Bernoulli theorem for a known velocity field, and the drag force is then calculated as

$$C_d = F\frac{2}{\rho_w A \boldsymbol{U}^2} \tag{3.78}$$

where A is the projected area of the root to the approaching flow.

3.4.1 Application of a discrete vortex model

The discrete vortex method was employed for four scenarios to investigate the modification of the drag coefficient due to various spatial densities of vegetation. Scenario 1 with only 1 root is presented only for comparison. The mangrove roots were assumed to be vertical, cylindrical and distributed in a regular quadratic matrix form over an area of 1 m ×1 m. The range of flow velocity, $\boldsymbol{U}$, used in the simulations, covers all wave-induced velocities encountered in tropical mangrove forests. Vegetation and ambient flow details for the four scenarios are presented in Table 3.1.

Snapshots of the predicted flow field in the vicinity of the mangrove vegetation are shown in Figure 3.4 for scenarios 3 and 4. For the scenario with a single root, there is clear vortex generation and the formation of a wake of vortices downstream of the root. The wake displays the typical pattern of a von Karman vortex trail. With an increase in spatial density of the root matrix, there is strong and complex interaction of the downstream roots with the vortices wakes generated upstream.

Table 3.1 Vortex modelling scenarios

Scenario	Number of Roots	Root diameter (cm)	Flow velocity (cm/s)
1	9	2	1, 5, 10, 20, 50, 100
2	25	2	5, 10, 50
3	1	8	1, 5, 10, 20, 50, 100
4	9	8	1, 5, 10, 20, 50

A summary of the calculated values of the drag coefficient, C_d, for the four scenarios of root diameter and spatial density is shown in Figure 3.5. Regression analysis of the dependence of the drag coefficients computed via the vortex model on the Reynolds number of the incident flow indicated that for the Reynolds numbers from the range $200 < Re < 80000$, the drag coefficient C_d could be expressed as

$$C_d(Re) = 1.07 Re^{-0.01} \quad \text{for a single root } (N=1) \tag{3.79}$$

and

$$C_d(Re) = 1.72 Re^{-0.10} \quad \text{for nine and twenty five roots } (N=9,25) \tag{3.80}$$

It is clear that Equation (3.80) describes drag coefficients of a lower magnitude than those calculated by Equation (3.79), due to the wake interaction effects.

Retuning now to the modified drag coefficient, $C_d^{(m)}$, as described by Equation (3.23), the modification factor of the drag coefficient in the mangrove forest when compared with the case of a single trunk can be expressed as

$$K(N) = 1.61 Re^{-0.09} \tag{3.81}$$

The modified drag coefficient as described by Equations (3.23) and (3.81) was used for all cases of the wave propagation model.

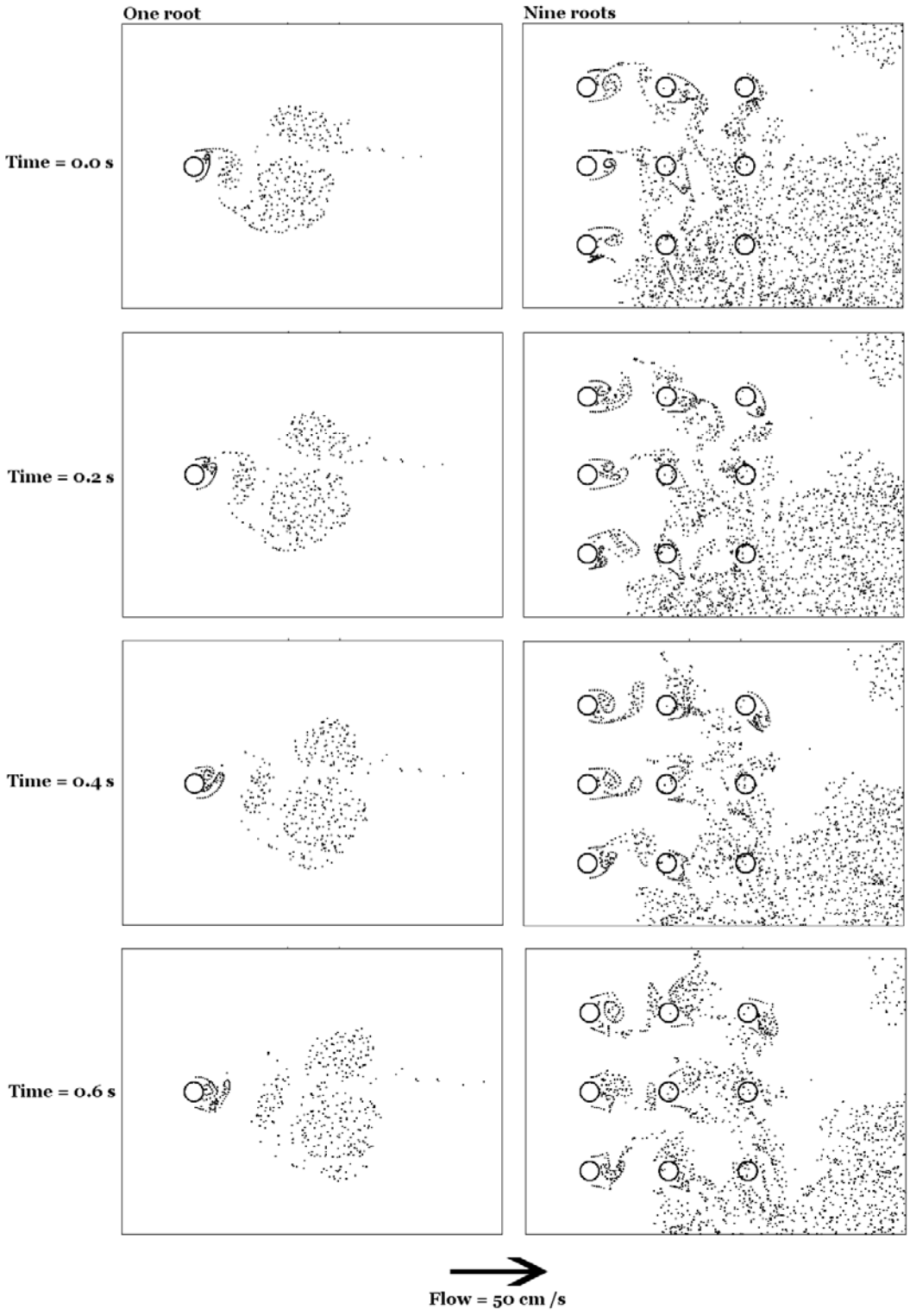

Figure 3.4 Time sequence of the distribution of discrete vortices. Time step is 0.2 s. Ambient flow is 50 cm/s from left to right, and root diameter is 0.08m. Left and right columns show one nine roots, respectively, and represent scenarios 3 and 4 of Table 3.1. Dots represent particles released into the flow field at separation points.

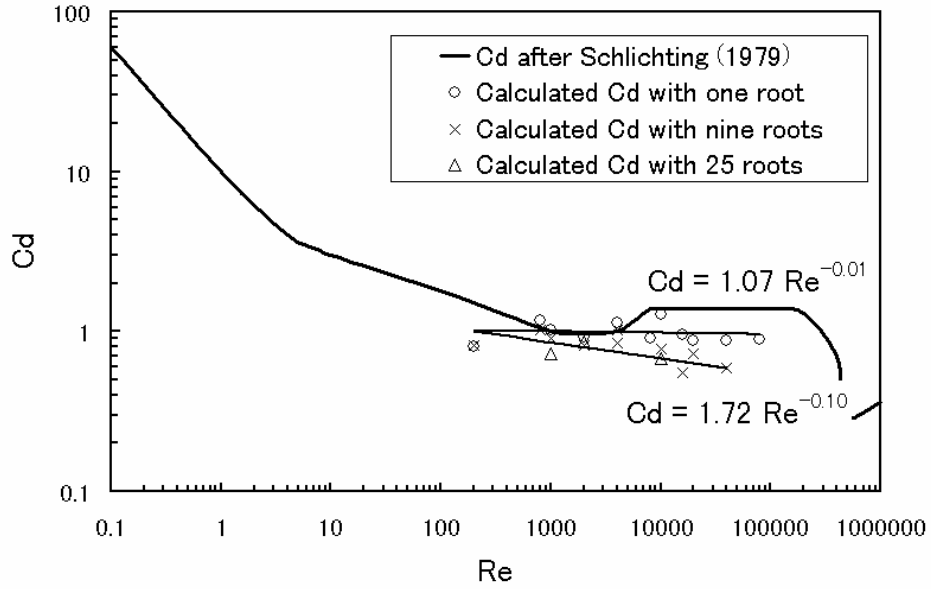

Figure 3.5 Summarized C_d value obtained by calculations.

3.5 Linearisation procedure

As mentioned in Section 3.3.1, a linearisation procedure was employed to facilitate the solution for wave motion within the mangrove forest. The linearisation procedure is based on the minimization, in the stochastic sense, of the mean error $\varepsilon(x,z)$ that is introduced by substituting linear for non-linear terms. The error can be expressed as (see Equation (3.27))

$$\varepsilon(x,z) = \frac{1}{\rho_w}\vec{F}(x,z) - f_e \omega_p \vec{u}_2(x,z) \tag{3.82}$$

with the minimization taking the form

$$\int_{-h}^{0}\int_{0}^{d} E\left[\varepsilon^2\right] dxdz = min \tag{3.83}$$

Therefore, finding the minimum can be expressed as a rate of change of the error with respect to the linearisation coefficient

$$\int_{-h}^{0}\int_{0}^{l}\frac{\partial}{\partial f_e}\left\{E\left[\varepsilon^2\right]\right\}dxdz=0 \tag{3.84}$$

where $E[\ ]$ denoted averaging in stochastic sense. Equation (3.84) expands to

$$\int_{-h}^{0}\int_{0}^{l}E\left[\varepsilon\frac{\partial\varepsilon}{\partial f_e}\right]dxdz=0 \tag{3.85}$$

which on substitution of Equation (3.82) results in

$$\int_{-h}^{0}\int_{0}^{l}E\left[\frac{1}{\rho_w}\vec{F}(x,z)\vec{u}_2(x,z)-f_e\omega_p\vec{u}_2^2(x,z)\right]dxdz=0 \tag{3.86}$$

or

$$f_e=\frac{1}{\omega_p}\frac{\int_{-h}^{0}\int_{0}^{l}E\left[\frac{1}{\rho_w}\vec{F}(x,z)\vec{u}_2(x,z)\right]dx\,dz}{\int_{-h}^{0}\int_{0}^{l}E\left[\vec{u}_2^2\right]dxdz} \tag{3.87}$$

Using the expressions for drag forces in the upper and lower layers of the mangrove forest in Equation (3.87), results in

$$\begin{aligned}f_e=&\frac{\int_{-h}^{-(h-h_l)}\int_{0}^{l}\bar{D}_l\sum_{j=1}^{j=N_l}C_d^{(m)}(Re,x,z)E\left[\vec{u}_2(x,z)\vec{u}_{n,j}(x,z)\left|\vec{u}_{n,j}(x,z)\right|\right]dx\,dz}{2\omega_p\int_{-h}^{0}\int_{0}^{l}E\left[\vec{u}_2^2\right]dxdz}\\&+\frac{\int_{-(h-h_l)}^{0}\int_{0}^{l}\bar{D}_u\sum_{j=1}^{j=N_u}C_d^{(m)}(Re,x,z)E\left[\vec{u}_2(x,z)\vec{u}_{n,j}(x,z)\left|\vec{u}_{n,j}(x,z)\right|\right]dx\,dz}{2\omega_p\int_{-h}^{0}\int_{0}^{l}E\left[\vec{u}_2^2\right]dxdz}\end{aligned} \tag{3.88}$$

where again $\vec{u}_{n,j}(x,z)$ denotes the water velocity, normal to the longitudinal axis of the particular trunk j induced by wave orbital velocity $\vec{u}(x,z)=[u(x,z),w(x,z)]$. It can be seen that the linearisation coefficient, f_e, depends on the second and third moments of the water velocity in the mangrove region. To determine these

moments, the probability density of the water velocity is required within Region *II*. However, the exact probability density of wave velocity within mangrove forest is not known. In general, in a water body subjected to wave motion, both components of velocity $\vec{u}_2(x,z)$ have probability densities very close to normal distributions, with zero mean values and different standard deviations σ_{u2} and σ_{w2}. It is assumed that this general rule is applicable within Region II, and thus the probability densities can be expressed in terms of their standard deviations as

$$f(u_2) = \frac{1}{\sqrt{2\pi}\sigma_{u_2}} \exp\left[-\frac{1}{2} \frac{u_2^2}{\sigma_{u_2}^2} \right] \tag{3.89}$$

$$f(w_2) = \frac{1}{\sqrt{2\pi}\sigma_{w_2}} \exp\left[-\frac{1}{2} \frac{w_2^2}{\sigma_{w_2}^2} \right] \tag{3.90}$$

It should be noted that the standard deviations σ_{u_2} and σ_{w_2} are functions of both *x*- and *z*-coordinates. Also it is usually assumed that both components are statistically independent, i.e. $E[u_2 \cdot w_2] = 0$.

Let us now determine the probability density function for $\vec{u}_2^2$. Let us define variable U as

$$U = |\vec{u}_2| = \sqrt{u_2^2 + w_2^2} \tag{3.91}$$

where

$$\vec{u}_2 = u_2 \cdot \vec{i} + w_2 \cdot \vec{j} \tag{3.92}$$

It can be shown that (Massel and Butowski, 1980)

$$f_1\left(|\vec{u}_2|\right) = f_1(U) = \frac{U}{\sigma_{u_2}\ \sigma_{w_2}} I_0\left(m_1\ U^2\right) \exp\left(-m_2\ U^2\right) \text{ at } U \geq 0 \tag{3.93}$$

where

$$m_1 = \frac{1}{4}\frac{\sigma_{u_2}^2 - \sigma_{w_2}^2}{\sigma_{u_2}^2 \sigma_{w_2}^2} \qquad m_2 = \frac{1}{4}\frac{\sigma_{u_2}^2 + \sigma_{w_2}^2}{\sigma_{u_2}^2 \sigma_{w_2}^2} \tag{3.94}$$

and function $I_0(\ )$ is a modified Bessel function of the zero order (Abramowitz and Stegun, 1968).

For very small water depths, $w_2 \to 0$, $\sigma_{w2} \to 0$ and $\frac{w_2}{u_2} \ll 1$, and Equation (3.93) can be approximated as (Massel & Butowski 1980)

$$f_1(U) = f_1\left(|\vec{u}_2|\right) = \frac{2}{\sqrt{2\pi}\,\sigma_{u_2}} \exp\left(-\frac{1}{2}\frac{U^2}{\sigma_{u2}^2}\right) \tag{3.95}$$

Using Equation (3.93), the required variable $\vec{u}_2^2 = u_2^2 + w_2^2 = U_2$ can be found by a transformation of variables as follows

$$f_2(U_2) = f_2\left(|\vec{u}_2|^2\right) = \frac{1}{2\sigma_{u_2}\,\sigma_{w_2}} I_0(m_1 U_2) \exp\left(-m_2 U_2\right) \tag{3.96}$$

Hence, the mean value $E\left[\vec{u}_2^2\right]$ becomes

$$E\left[\vec{u}_2^2\right] = E\left[U_2\right] = \int_0^\infty U_2 f_2(U_2)\, dU_2 = \sigma_{u_2}^2 + \sigma_{w_2}^2 \tag{3.97}$$

For the very small water depth when $\sigma_{w_2} \approx 0$

$$f_2(U_2) = \frac{1}{\sqrt{2\pi}\,\sigma_{u_2}\sqrt{U_2}} \exp\left(-\frac{1}{2}\frac{U_2}{\sigma_{u_2}^2}\right) \tag{3.98}$$

and respectively

$$E\left[\vec{u}_2^2\right] = \sigma_{u_2}^2 \tag{3.99}$$

Let us now determine the mean value of $E\left[\vec{u}_2(x,z)\vec{u}_{n,j}(x,z)\left|\vec{u}_{n,j}(x,z)\right|\right]$. Recall that one of the simplifying assumptions was that all trunks and roots would be treated as vertical cylinders. Therefore, for vertical trunks and roots i.e. when $\vec{u}_{n,j}(x,z) = u_2(x,z)$, the only drag forces are those induced by the horizontal component u_2 of the orbital velocity, and it follows that the linearisation coefficient f_e can be simplified as

$$\begin{aligned} f_e = & \frac{\int_{-h}^{-(h-h_l)} \int_0^l \bar{D}_l N_l C_d^{(m)}(Re,x,z) E\left[u_2^2(x,z)\left|u_2(x,z)\right|\right] dxdz}{2\omega_p \int_{-h}^{0} \int_0^l \sigma_{u_2}^2 dxdz} \\ & + \frac{\int_{-(h-h_l)}^{0} \int_0^l \bar{D}_u N_u C_d^{(m)}(Re,x,z) E\left[u_2^2(x,z)\left|u_2(x,z)\right|\right] dxdz}{2\omega_p \int_{-h}^{0} \int_0^l \sigma_{u_2}^2 dxdz} \end{aligned} \tag{3.100}$$

For vertical trunks from Eq. (3.91) it follows that

$$u_2^2(x,z)\left|u_2(x,z)\right| = U^2 U = U^3 = U_3 \tag{3.101}$$

in which $U = u_2(x,z)$. Change of the variables in Equation (3.95) gives

$$f_3(U_3) = \frac{2}{3\sqrt{2\pi}\sigma_{u_2} U_3^{\,2/3}} \exp\left(-\frac{1}{2}\frac{U_3^{2/3}}{\sigma_{u_2}^2}\right) \tag{3.102}$$

and the mean value $E\left[u_2^2(x,z)\left|u_2(x,z)\right|\right]$ becomes

$$E\left[u_2^2(x,z)\left|u_2(x,z)\right|\right] = \left(\frac{8}{\pi}\right)^{1/2} \sigma_{u_2}^3 \tag{3.103}$$

After substitution of Equations (3.99) and (3.103) into Equation (3.100) the linearisation coefficient is obtained as

$$f_e = \frac{1}{\omega_p}\sqrt{\frac{2}{\pi}}\left\{ \frac{\int_{-h}^{-(h-h_l)}\int_0^l \bar{D}_l N_l C_d^{(m)}(Re,x,z)\sigma_{u_2}^3\,dxdz}{\int_{-h}^{0}\int_0^l \sigma_{u_2}^2\,dxdz} + \frac{\int_{-(h-h_l)}^{0}\int_0^l \bar{D}_u N_u C_d^{(m)}(Re,x,z)\sigma_{u_2}^3\,dxdz}{\int_{-h}^{0}\int_0^l \sigma_{u_2}^2\,dxdz} \right\} \tag{3.104}$$

The standard deviations of orbital velocities are needed for the calculation of the linearisation coefficient. However, these are not known *a priori*. Therefore, the calculations have to be done in a recursive manner, i.e. for some initial value of f_e, the boundary value problem is solved and the standard deviations are determined from the corresponding frequency spectra, as described in Chapter 3.3.

4 MODELLING THE INTERACTION OF MANGROVES WITH WAVE MOTION – ARBITRARY WATER DEPTH

4.1 Theory

In this chapter the theory will be developed for wave motion in a mangrove forest with arbitrary bathymetry. The solution differs from that presented in Chapter 3 in that the wave motion in the vicinity of the forest is not described by a set of amplification factors but is instead described by a complex wave amplitude which is a solution to the mild-slope equation. Thus the complex wave amplitude will incorporate the effects of both the vegetation and changes in water depth. Also, in contrast to the approach presented in Chapter 3, only progressive waves are taken into account and non-propagating evanescent modes are neglected.

4.1.1 Governing Equations:

Using the same notation introduced in Chapter 3 to describe the three regions of the idealized mangrove forest, consider now the case of a forest with an arbitrary bathymetry profile in Region *II*, and hence water depth, $h_2 = h_2(x) \neq \text{constant}$ (see Figure 4.1). However, at $x = 0$, $h_2(0) = h_1$ and at $x = l$, $h_2(l) = h_3$. Again a potential, Φ_i, will be found which is a solution to a boundary value problem posed for each region (i=*I*, *II*, *III*) of the fluid domain.

Region I:

The boundary value problem posed for Region *I* is, as expected, the same as for the case of a horizontal bottom in Section 3.2.2 and represented by Equations (3.3), (3.7), (3.9) and (3.10). The potential in Region *I* can be represented using the Fourier-Stjeltjes integral as follows (Massel, 1996):

$$\Phi_1(x,z,t) = \Re \int_{-\infty}^{\infty} \left(\frac{-ig}{\omega}\right) \exp(-i\omega t)[\exp(ik_1 x) + K_R \exp(-ik_1 x)] \cdot \frac{\cosh k_1(z+h_1)}{\cosh k_1 h_1} dA_i(\omega) \tag{4.1}$$

where K_R is the coefficient of reflection of waves off the ocean\mangrove boundary at $x = 0$ and k_1 is the wave number which satisfies the dispersion relation given by Equation (3.13). The first term in the square parenthesis on the right-hand side of Equation (4.1) represents the progressive waves propagating towards the mangrove forest, while the second term represents waves reflected from the ocean/mangrove boundary. In contrast to the solution presented in Chapter 3, in this representation non-propagating evanescent modes are neglected and only progressive waves are taken into account. Increments of the spectral amplitudes $dA_i(\omega)$ are as described by Equation (3.14).

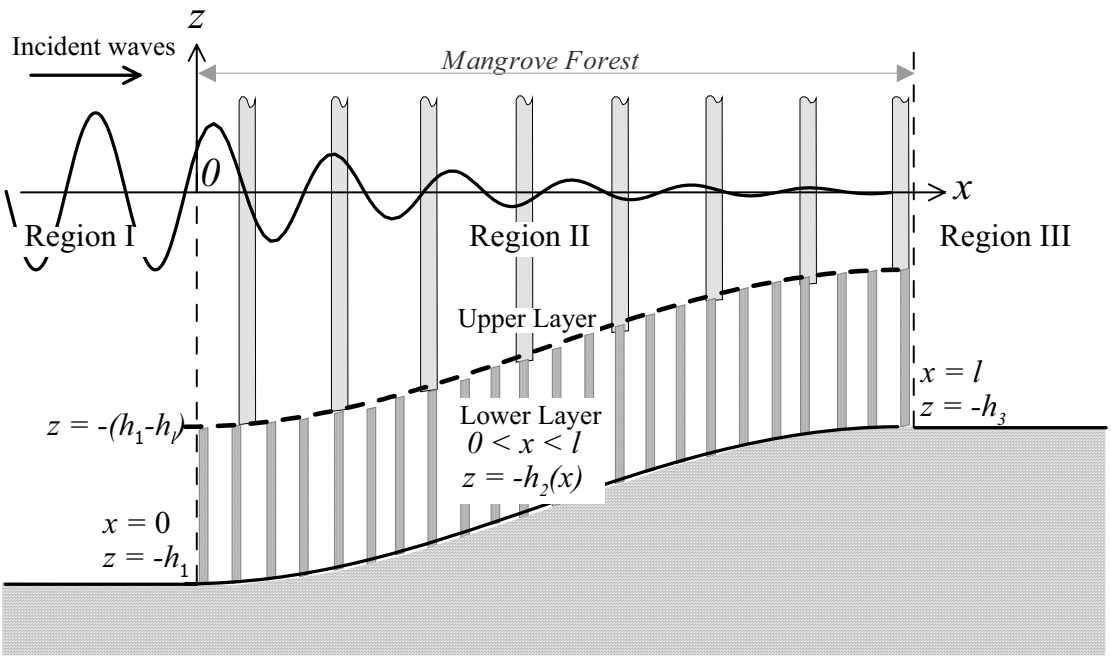

Figure 4.1 Model co-ordinate system and definition sketch for arbitrary bathymetry profile

Region II:

The solution for wave motion in Region *II* for arbitrary bathymetry will differ from the solution presented in Section 3.2, due to the effect of the bathymetry on the wave field. Again, the boundary value problem formulated is similar to that posed for a horizontal bottom, with the exception of the boundary condition at the sea floor ($z = -h_2(x)$). For the current case this condition is

$$\frac{\partial \Phi_2}{\partial z} + \frac{\partial \Phi_2}{\partial x}\frac{\partial h_2}{\partial x} = 0 \text{ at } z = -h_2(x) \tag{4.2}$$

Equations (3.33), (3.37) and (4.2) formulate the boundary value problem for potential Φ_2 in Region *II*. The velocity potential within Region *II* can be represented as

$$\Phi_2(x,z,t) = \Re \int_{-\infty}^{\infty} \left(\frac{-ig}{\omega}\right) \exp(-i\omega t)\varphi(x,\omega)\frac{\cosh k_2(x)(z+h_2(x))}{\cosh k_2(x)h_2(x)} dA_i(\omega) \tag{4.3}$$

where $\varphi(x,\omega)$ is a complex wave amplitude and $k_2(x)$ is the local wave number satisfying the dispersion relation of the form shown in Equation (3.13).

The amplitude of surface waves propagating over an arbitrary, gradually varying bathymetry can be described by the 'mild-slope' equation, so-called due to an inherent assumption that the slope of the bathymetry must be small (Berkhoff, 1972)

$$\frac{\partial}{\partial x}\left(CC_g\frac{\partial \varphi}{\partial x}\right) + \frac{\partial}{\partial y}\left(CC_g\frac{\partial \varphi}{\partial y}\right) + k_2^2 CC_g\varphi = 0 \tag{4.4}$$

where C is the phase velocity, C_g is the group velocity and k is the wave number.

For two-dimensional (x,z) wave motion and including the effects of dissipation as described by Massel (1996), the extended mild-slope equation takes the form

$$\frac{d^2\varphi}{dx^2} + CC_g^{-1}\frac{dCC_g}{dx}\frac{d\varphi}{dx} + \left[k_2^2(1+\psi) + i\gamma k_2\right]\varphi = 0 \tag{4.5}$$

where γ is a dissipation factor due to the interactions of the flow with the mangrove vegetation, and ψ s defined as (Massel, 1996)

$$\psi = \varepsilon_1(k_2h_2)\left(\frac{dh_2}{dx}\right)^2 + \varepsilon_2(k_2h_2)\frac{d^2h_2}{dx^2} \tag{4.6}$$

Functions $\varepsilon_1(k_2h_2)$ and $\varepsilon_2(k_2h_2)$ are dependent on the local wave number, $k_2(x)$, and bottom slope. A complete description of these functions is not necessary for this thesis and can be found in Massel (1996). In mangrove forests, the bathymetry, although arbitrary, is typically close to horizontal and varies gradually. It thus follows that $\left(\frac{dh_2}{dx}\right)^2 \to 0$, $\frac{d^2h_2}{dx^2} \to 0$ and therefore $\psi \to 0$. Accordingly, Equation (4.6) can be approximated as

$$\frac{d^2\varphi}{dx^2} + CC_g^{-1}\frac{dCC_g}{dx}\frac{d\varphi}{dx} + \left[k_2^2 + i\gamma k_2\right]\varphi = 0 \tag{4.7}$$

Dissipation of wave energy in shallow water was investigated by Dingemans (1985) for the case of dissipation due to non-linear bottom friction. In this case the momentum equation for wave motion in shallow water can be represented as

$$\frac{\partial \vec{u}}{\partial t} + g\nabla\varsigma + W\vec{u} = 0 \tag{4.8}$$

where $\vec{u}$ is the horizontal velocity, ς is the sea surface elevation and $W\vec{u}$ is a linear term describing non-linear bottom friction. By comparison of Equation (4.8) and the momentum equation with dissipation in Region *II*, given by Equation (3.29), it is apparent that

$$W = f_e\omega_p \tag{4.9}$$

Continuing to follow the approach and notation of Dingemans (1985), the mild slope equation with dissipation can be presented as

$$\frac{d^2\varphi}{dx^2} + CC_g^{-1}\frac{dCC_g}{dx}\frac{d\varphi}{dx} + \left[k_2^2 + \frac{ik_2W}{\sqrt{CC_g}}\right]\varphi = 0 \tag{4.10}$$

Comparison of Equations (4.7) and (4.10) and knowing that for shallow water $CC_g = gh_2$, yields

$$\gamma = \frac{W}{\sqrt{gh_2}} = \frac{f_e \omega_p}{\sqrt{gh_2}} \tag{4.11}$$

Substitution into Equation (4.7) results in

$$\frac{d^2\varphi}{dx^2} + D(x)\frac{d\varphi}{dx} + E(x)\varphi = 0 \tag{4.12}$$

where $E(x) = k_2^2 + i\frac{f_e \omega_p}{\sqrt{gh_2}} k_2$ and (Dingemans, 1985; Massel, 1996)

$$D(x) = CC_g^{-1}\frac{dCC_g}{dx} = \frac{G(k_2h_2)}{h_2}\frac{dh_2}{dx} \tag{4.13}$$

The function $G(k_2h_2)$, which describes variations of wave number k_2 due to variations in water depth h_2 as described the extended refraction-diffraction equation (Massel, 1996), takes the form

$$G\left(k_2h_2\right) = \frac{k_2h_2}{T + k_2h_2\left(1-T\right)^2}\left[1 - 3T^2 + \frac{2T}{T + k_2h_2\left(1-T\right)^2}\right] \tag{4.14}$$

where $T = \tanh\left(k_2h_2\right)$

Thus Equation (4.12) describes the complex wave amplitude of surface waves propagating through Region *II*.

Region III:

The wave field in Region *III* is composed exclusively of waves transmitted through the mangrove forest. In this case the velocity potential Φ_3 takes the form:

$$\Phi_3(x,z,t) = \Re \int_{-\infty}^{\infty} \left(\frac{-ig}{\omega}\right) \exp(-i\omega t) \cdot K_T \exp(ik_3 x) \cdot \frac{\cosh k_3(z+h_3)}{\cosh k_3 h_3} dA_i(\omega) \tag{4.15}$$

where K_T is the coefficient of transmission of wave energy through the mangrove forest and k_3 is a wave number satisfying the dispersion relation of the form shown in Equation (3.13).

4.1.2 Boundary conditions at the interfaces of Regions I, II and III:

The potentials $\Phi_1(x,z,t)$, $\Phi_2(x,z,t)$ and $\Phi_2(x,z,t)$ must again satisfy conditions which provide continuity of pressure and horizontal velocity at the boundaries of Regions *I*, *II* and *III*. In particular at $x = 0$, the continuity of dynamic pressure in Regions *I* and *II* requires that

$$p_1(0,z,t) = p_2(0,z,t) \tag{4.16}$$

in which

$$p_1(0,z,t) = \Re \int_{-\infty}^{\infty} \rho_w g \exp(-i\omega t)[1+K_R] \frac{\cosh k_1(z+h_1)}{\cosh k_1 h_1} dA_i(\omega) \tag{4.17}$$

and

$$p_2(0,z,t) = \Re \int_{-\infty}^{\infty} \rho_w g \exp(-i\omega t)\varphi(0,\omega) \frac{\cosh k_2(z+h_2)}{\cosh k_2 h_2} dA_i(\omega) \tag{4.18}$$

At x=0, h_1=h_2(0) and it follows that k_1=k_2 which yields

$$1+K_R = \varphi(0,\omega) \tag{4.19}$$

Continuity of horizontal velocity at x=0 requires that:

$$\frac{\partial \Phi_1(0,z,t)}{\partial x} = n_p \frac{\partial \Phi_2(0,z,t)}{\partial x} \tag{4.20}$$

where n_p is the surface porosity of the mangroves at $x = 0$

Differentiating Equations (4.1) and (4.3), and substituting into Equation (4.20) yields

$$ik_1(1-K_R) = n_p \frac{\partial \varphi(0,\omega)}{\partial x} \tag{4.21}$$

Combining Equations (4.21) and (4.19) yields the boundary condition for the solution to the mild slope equation (Equation (4.5)) at $x = 0$

$$\frac{\partial \varphi(0,\omega)}{\partial x} = \frac{ik_1}{n_p}(2-\varphi(0,\omega)) \tag{4.22}$$

Similarly, at $x=l$, the continuity of dynamic pressure requires that

$$p_2(l,z,t) = p_3(l,z,t) \tag{4.23}$$

and for the continuity of horizontal velocity

$$n_p \frac{\partial \Phi_2(l,z,t)}{\partial x} = \frac{\partial \Phi_3(l,z,t)}{\partial x} \tag{4.24}$$

Appropriate differentiation of Equations (4.1) and (4.3), and subsequent substitution into Equations (4.23) and (4.24) yields

$$\frac{\partial \varphi(l,\omega)}{\partial x} = \frac{ik_3}{n_p}\varphi(l,\omega) \quad \text{at } x=l \tag{4.25}$$

4.1.3 Solving for complex wave amplitude φ :

Having defined the mild slope equation within the forest and formulated the boundary conditions, the governing equations must now be presented in a form that enables solution using some numerical technique. A finite difference scheme is used and the spatial co-ordinate x is discretized as follows:

$$x_i = i\Delta x,\ (i = 1, 2...N)\ ,\ \text{ie at } x=0,\ i=1,\ \text{and } i=N \text{ at } x=l. \tag{4.26}$$

Using this notation, and taking appropriate differences, we can represent Equation (4.12) as

$$(2 - \Delta x D_i)\varphi_{i-1} + (-4 + 2\Delta x^2 E_i)\varphi_i + (2 + \Delta x D_i)\varphi_{i+1} = 0 \tag{4.27}$$

The boundary conditions at $x=0$ ($i=1$), given by Equation (4.22) can be represented in finite difference form as

$$\varphi_{i-1} = \varphi_{i+1} - 2ik_1\Delta x(2 - \varphi_i) \tag{4.28}$$

which on substitution into Equation (4.27) for $i=1$ yields

$$\left[ik_1\Delta x(2 - \Delta x D_1) + \Delta x^2 E_1\right]\varphi_1 + 2\varphi_2 = 2ik_1\Delta x(2 - \Delta x D_1) \tag{4.29}$$

Similarly, using Equation (4.25) at $x=l$ ($i=N$) yields

$$2\varphi_{N-1} + \left[ik_3\Delta x(2 + \Delta x D_N) + \Delta x^2 E_N - 2\right]\varphi_N = 0 \tag{4.30}$$

Equations (4.27), (4.29) and (4.30) result in a finite set of equations:

$$
\begin{array}{lllllll}
b_1\varphi_1 & + & c_1\varphi_2 & & & & = r_1 \\
a_2\varphi_1 & + & b_2\varphi_2 & + & c_2\varphi_3 & & = r_2 \\
 & & a_3\varphi_2 & + & b_3\varphi_3 & + \quad c_3\varphi_4 & = r_3 \\
 & & & & \vdots & \vdots \quad \vdots & \vdots \\
 & & & & a_{N-1}\varphi_{N-2} & + \quad b_{N-1}\varphi_{N-1} & + c_{N-1}\varphi_N = r_{N-1} \\
 & & & & & a_N\varphi_{N-1} & + \; b_N\varphi_N = r_N
\end{array}
$$

which can be expressed in matrix form as:

$$
\begin{bmatrix}
b_1 & c_1 & 0 & 0 & \cdots & & & \\
a_2 & b_2 & c_2 & 0 & \cdots & & & \\
0 & a_3 & b_3 & c_3 & \cdots & & & \\
 & & & & \cdots & & & \\
 & & & & \cdots & a_{N-1} & b_{N-1} & c_{N-1} \\
 & & & & \cdots & 0 & a_N & b_N
\end{bmatrix}
\cdot
\begin{bmatrix} \varphi_1 \\ \varphi_2 \\ \varphi_3 \\ \cdots \\ \varphi_{N-1} \\ \varphi_N \end{bmatrix}
=
\begin{bmatrix} r_1 \\ r_2 \\ r_3 \\ \cdots \\ r_{N-1} \\ r_N \end{bmatrix}
\tag{4.31}
$$

Coefficients a_i, b_i and c_i, (i=1,N) are determined from Eq.(4.27) with utilization of corresponding boundary conditions. Equation set (4.31) represents a finite set of equations that describe the complex wave amplitude within the forest, and can be solved using the standard procedure for a tri-diagonal system of linear equations (Press *et al*., 1986).

Having determined the velocity potential, $\Phi_2(x,z,t)$, within Region *II*, it is possible to determine the frequency spectra of orbital velocity and sea surface displacement. Frequency spectra of the orbital velocities are needed to determine the standard deviations of the orbital velocities for the linearisation procedure. The horizontal component of the orbital velocity within Region *II* is:

$$
u_2(x,z,t) = \Re \int_{-\infty}^{\infty} \tilde{U}_2(\omega) \exp(-i\omega t)\; dA_i(\omega) \tag{4.32}
$$

where

$$\tilde{U}_2(\omega, x, z) = -\frac{ig}{\omega}\frac{\partial\varphi}{\partial x}\frac{\cosh k_2(z+h_2(x))}{\cosh k_2 h_2(x)} \tag{4.33}$$

The corresponding variance (standard deviation squared) is therefore

$$\sigma_{u_2}^2 = \int_0^\infty \left\{ \left[\Re\tilde{U}_2(\omega)\right]^2 + \left[\Im\tilde{U}_2(\omega)\right]^2 \right\} S_i(\omega) d\omega \tag{4.34}$$

where $\Im$ denotes the imaginary part of the complex function, $\tilde{U}_2$.

Frequency spectra of the sea surface displacement are also of interest. In Region *II*, the surface displacement is given by

$$\begin{aligned} \varsigma_2(x,t) &= -\frac{1}{g}\left(\frac{\partial\Phi_2}{\partial t}\right)_{z=0} \\ &= \Re\int_{-\infty}^{\infty} \exp(-i\omega t)\,\varphi(x,\omega)\,dA_i(\omega) \end{aligned} \tag{4.35}$$

The frequency spectra of the sea surface displacement is thus found through the standard procedure (Massel, 1996)

$$S(\omega, x) = \left|\varphi(x,\omega)\right|^2 S_i(\omega) \tag{4.36}$$

A computational model was developed to solve the finite set of equations constructed from Equations (4.27), (4.29) and (4.30) to enable calculation of the velocity potential, $\Phi_2(x,z,t)$. Again the progression towards a solution is done in a recursive manner, starting from an initial prescribed value of the linearisation coefficient, f_e, as outlined in Figure 4.2. The computational model was employed to investigate the propagation of surface waves and the attenuation of wave energy for various scenarios of vegetation structure and spatial density. Results from this model, and their direct comparison with both results from the model with uniform bathymetry and field observations are presented in Chapter 5.

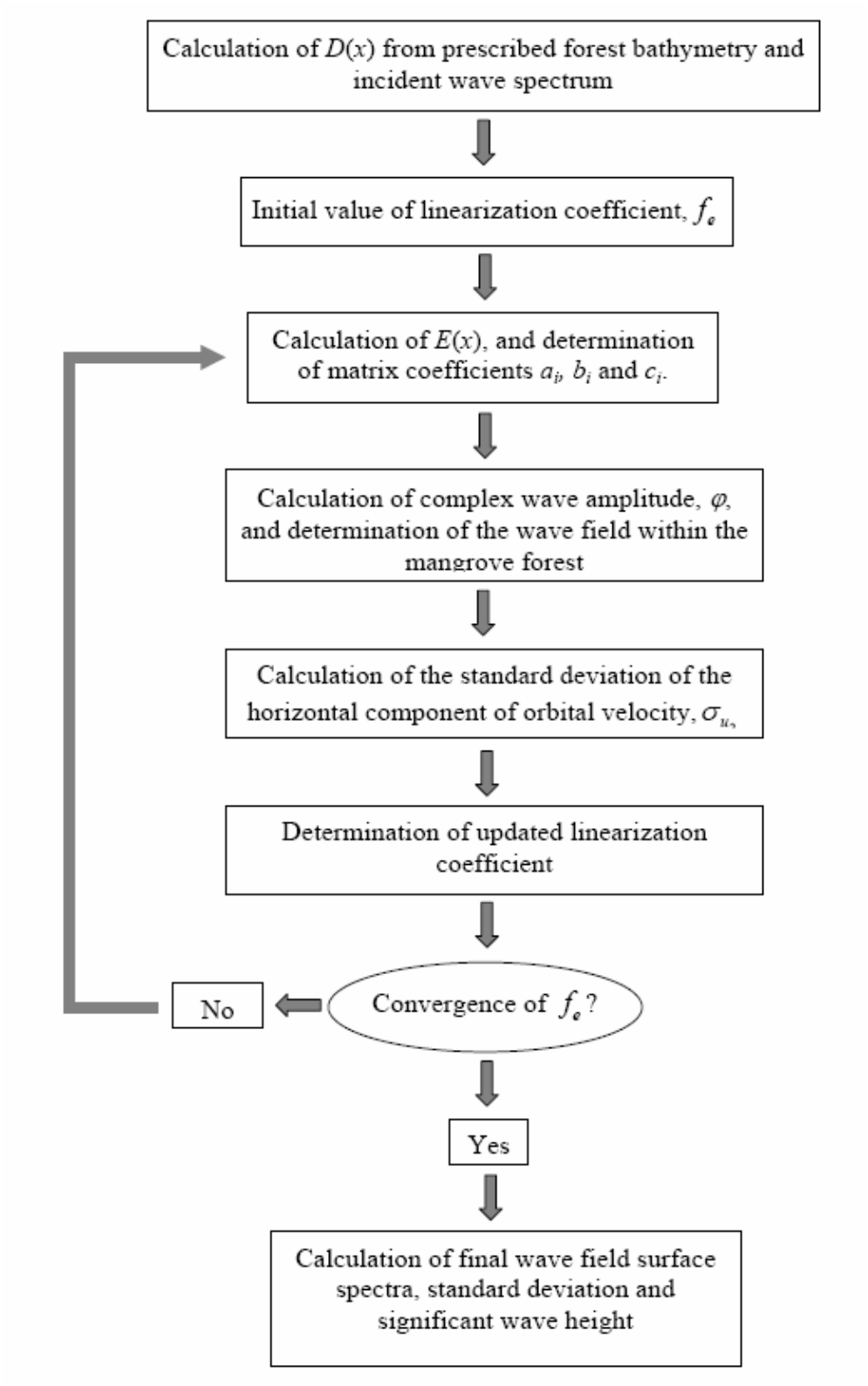

Figure 4.2 Flow chart of numerical computations for model with arbitrary bathymetry

5 RESULTS

5.1 Overview

This Chapter documents results from the field observations and the modelling undertaken using the two theoretical approaches developed in Chapters 3 and 4. The key features of the field data are explored and used to describe the dominant effects of mangrove vegetation on the propagation of random wind-induced gravity waves through mangroves. Results from the numerical models developed in Chapters 3 and 4 are presented and inter-compared, and qualitatively assessed against the key features observed in the field data. A quantitative assessment of the performance of the more general model is then made based on direct comparison of the model results with field data.

5.2 Field Results

The observational arrays deployed at the Cocoa Creek, Oonoonba and Iriomote study sites were operational for a total of 9 days and captured data for 11 tidal inundation events. For each study site, data from the most seaward instrument in the observational array was analysed to identify two inundation events with the highest incident wave energy. These events were then selected for complete analysis of all bursts of wave data from each observational instrument.

5.2.1 General patterns of wave attenuation

Figure 5.1 through to Figure 5.6 present contrasts in the wave energy spectra at times before, near and after the time of high tide during each of two periods of inundation, at each of the study sites. These data show a number of characteristics common to the majority of the computed wave spectra. Firstly, there is a sharp reduction in both the total energy and the energy of the dominant wave period across the instrumented width of the forests at each site. Secondly, there is a general 'flattening' of wave spectra as waves propagate through the vegetation, with a subtle indication of preferred attenuation of shorter period waves. Thirdly, there is

an increase in the energy transmitted into the forest with increased water depth. This observation is also apparent in the analysis of the variation of total wave energy with water depth, presented in Figure 5.7.

The wave energy spectra also show that at each of the study sites, the incident wave field was composed primarily of wind-generated waves, with periods less than 15 s, although the slight indication of double peaks (at periods of 2.5 and 7.0 seconds) in the spectra at Oonoonba on April 15th, 1999 suggests that the wave field was composed of locally generated short period wind-waves (period < 6s s) and swell (period > 6 s). This observation of is consistent with historic observations of the wave field in Cleveland Bay (Larcombe, *et al.*, 1995). The configuration of the observational arrays and subsequent analysis of observed wave data did not allow investigation of the directionality of the wave field at each site. However, visual confirmation of the alignment of the instrumented transect with the dominant direction of the incident waves ensured observation of wave transformations in the direction of propagation of dominant wave energy

The wave spectra at Oonoonba span a broader frequency range, and are more energetic than the spectra observed at both the Iriomote and Cocoa Creek Study sites. Analysis of the total spectral wave energy at each study site, presented in Figure 5.7 indicated that the Oonoonba site represented the most energetic wave environment of the three study sites, followed by Iriomote, then the Cocoa Creek study site. It is appropriate to recall that the most seaward instrument in the Oonoonba array was in fact 70 m landward from the front of the forest and thus is likely to provide an underestimate of the actual wave energy incident on the forest at this site. For comparison, the maximum total wave energy recorded at Oonoonba was 34 Jm^{-2}, compared to 6.9 Jm^{-2} at Iriomote and 0.7 Jm^{-2} at Cocoa Creek. In order to put this amount of total wave energy in context with other studies of the interaction of vegetation with wave energy on exposed coasts, by contrast, the maximum total wave energy recorded at the seaward margin of a salt marsh exposed to high energy from wind generated waves at Norfolk on the English east coast was 196 Jm^{-2} (Möller *et al.*, 1999), indicating that, as expected, our study sites ranged from medium to low wave energy environments.

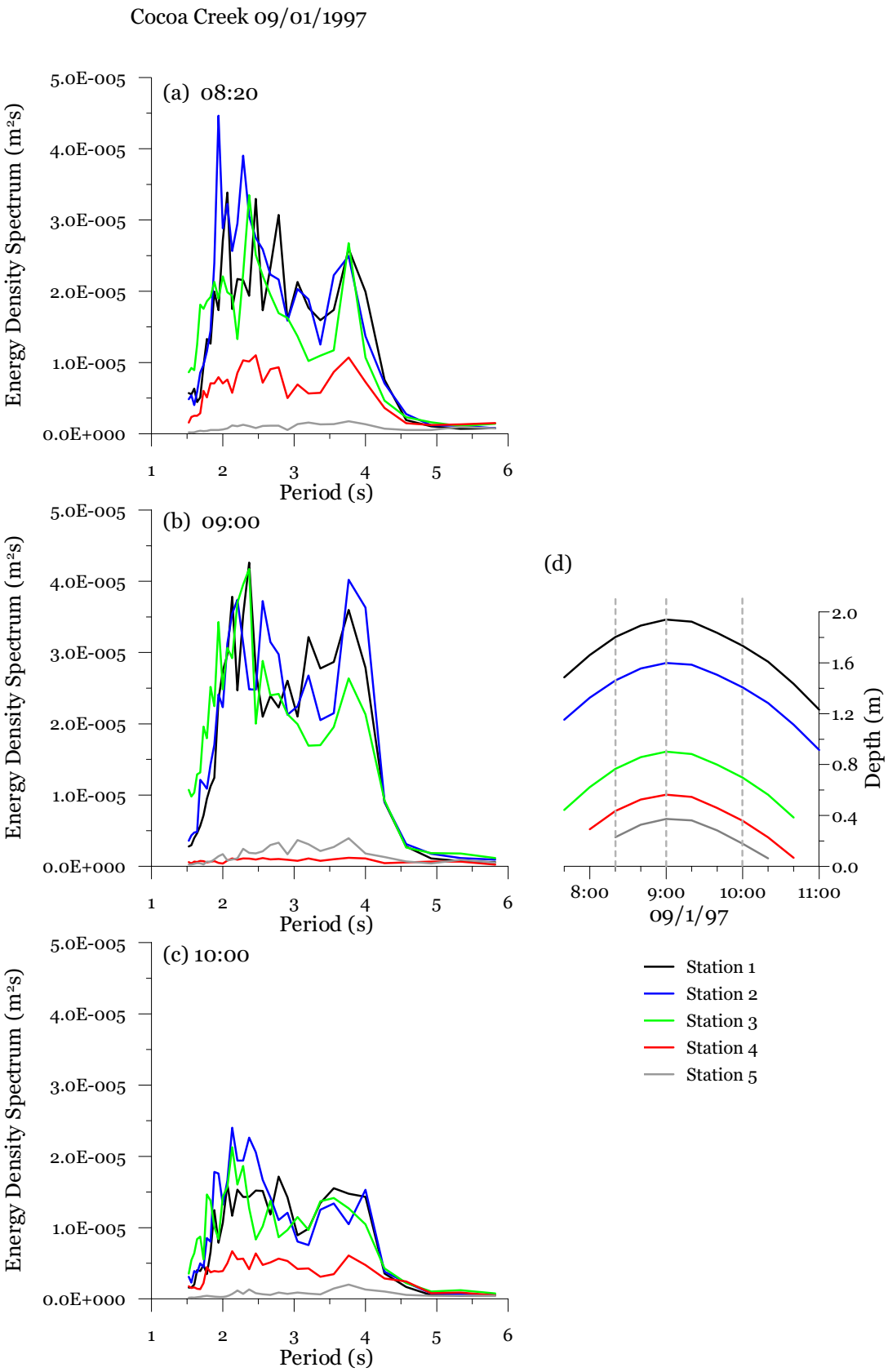
Cocoa Creek 09/01/1997
(a) 08:20
(b) 09:00
(c) 10:00
(d)
Energy Density Spectrum (m²s)
Period (s)
Depth (m)
09/1/97
Station 1
Station 2
Station 3
Station 4
Station 5

Figure 5.1 Wave energy density spectra at Cocoa Creek on January 9, 1997: (a).08:20, (b) 09:00 and (c) 10:00. Observed water depth is shown in (d), and vertical lines indicate the times of spectra shown in (a) – (c).

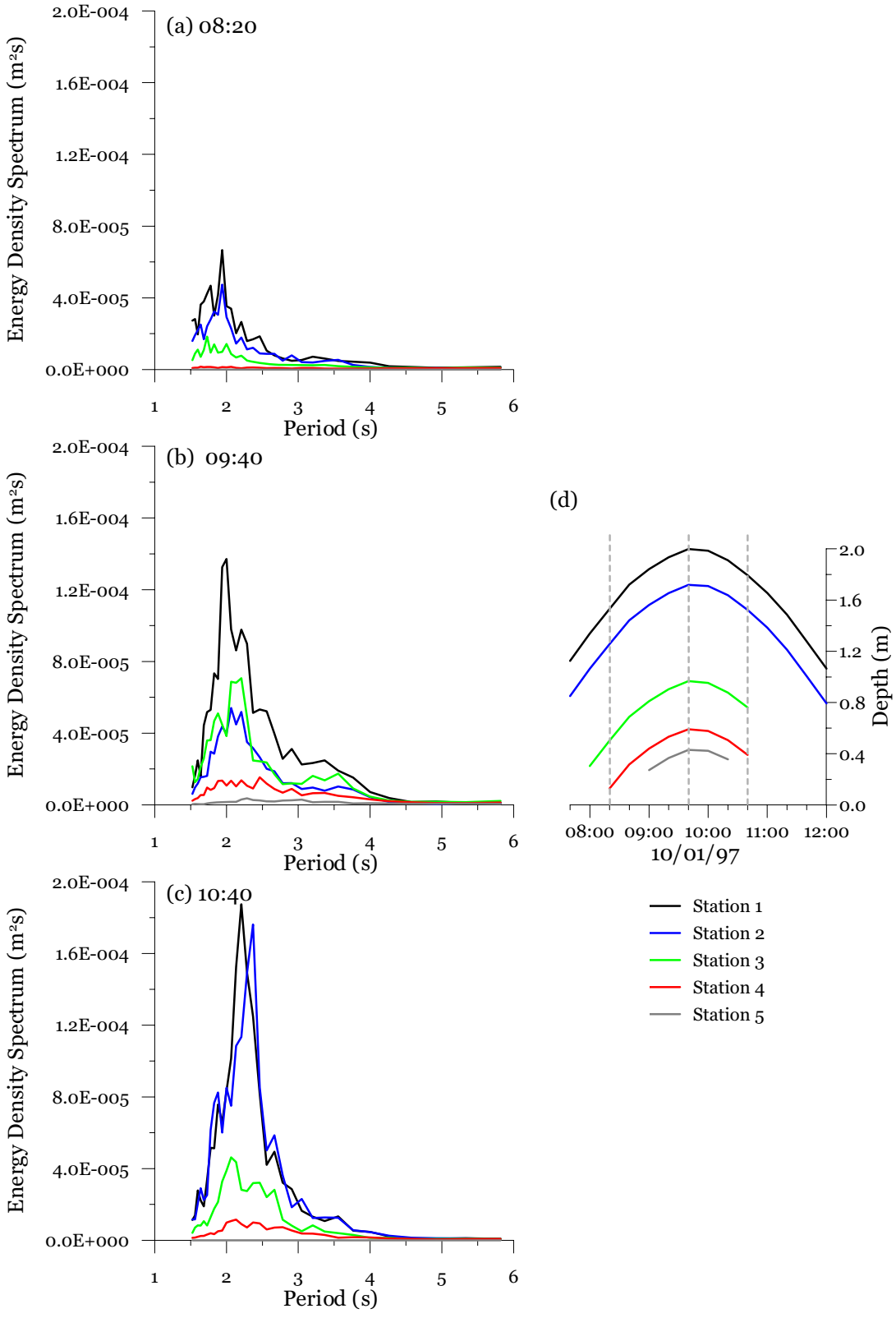

Figure 5.2 Wave energy density spectra at Cocoa Creek on January 10, 1997: (a).08:20, (b) 09:40 and (c) 10:40. Observed water depth is shown in (d), and vertical lines indicate the times of spectra shown in (a) – (c).

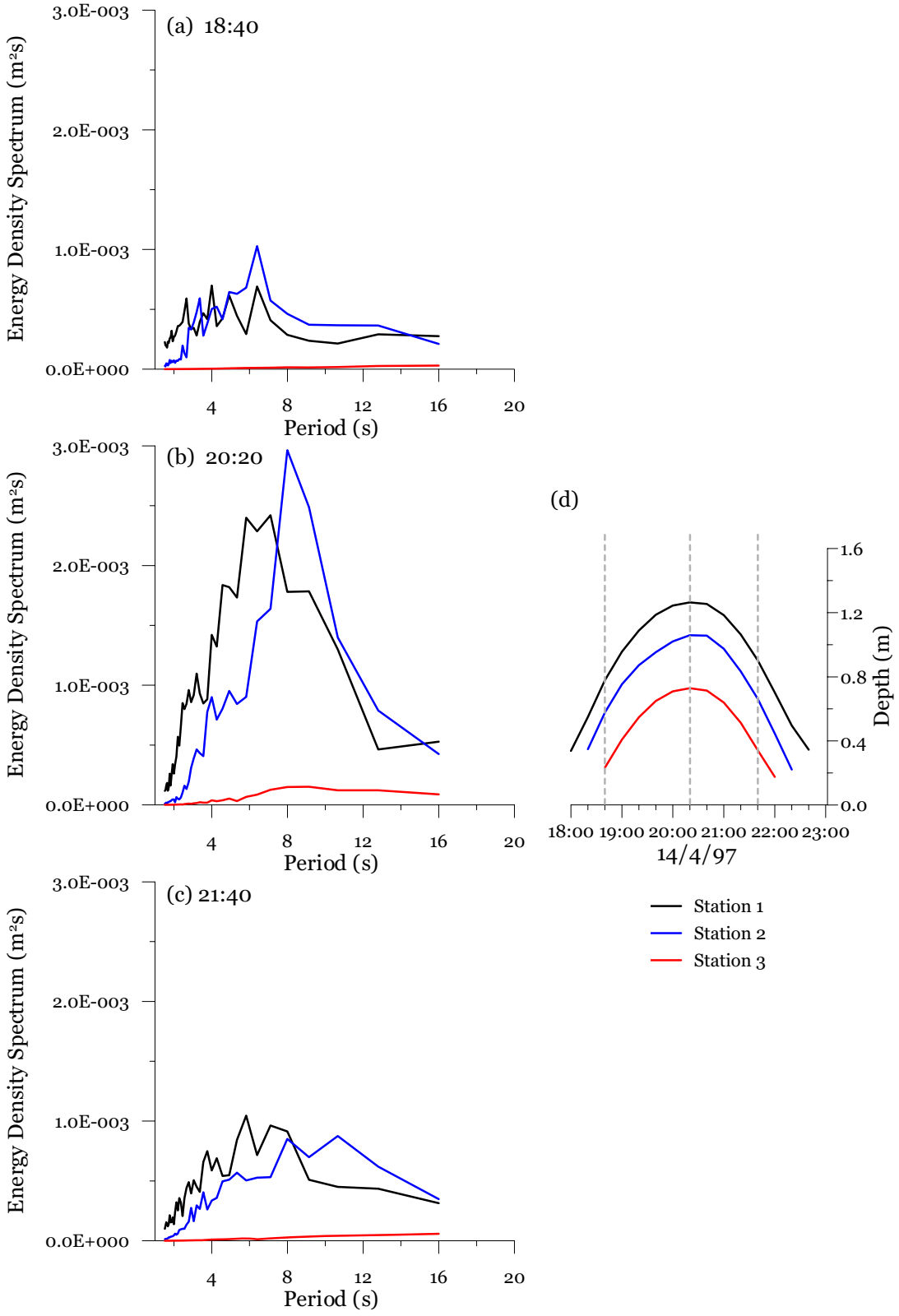

Figure 5.3 Wave energy density spectra at Oonoonba on April 14, 1999: (a).18:40, (b) 20:20 and (c) 21:40. Observed water depth is shown in (d), and vertical lines indicate the times of spectra shown in (a) – (c).

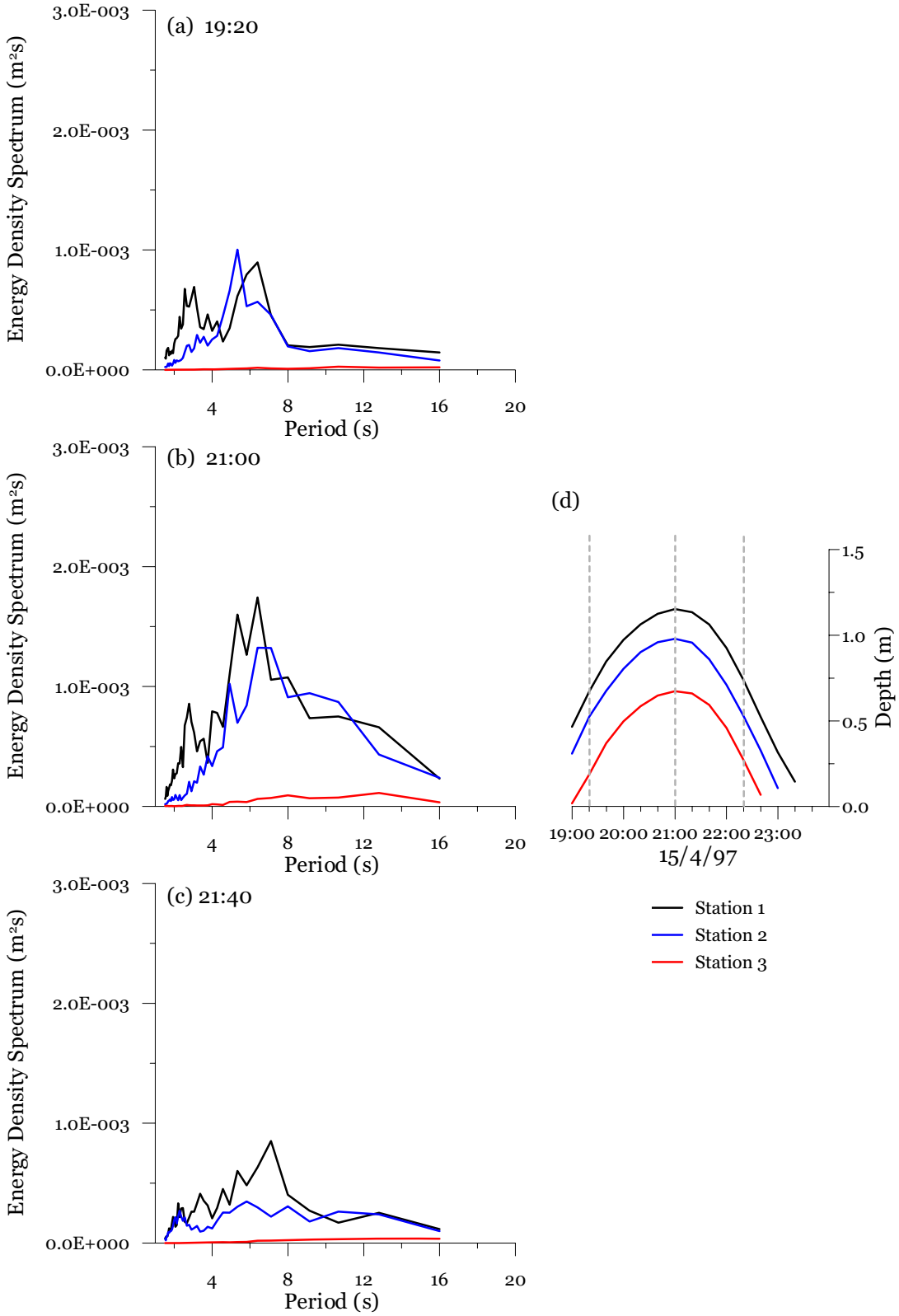

Figure 5.4 Wave energy density spectra at Oonoonba on April 15, 1999: (a).19:20, (b) 21:00 and (c) 21:40. Observed water depth is shown in (d), and vertical lines indicate the times of spectra shown in (a) – (c).

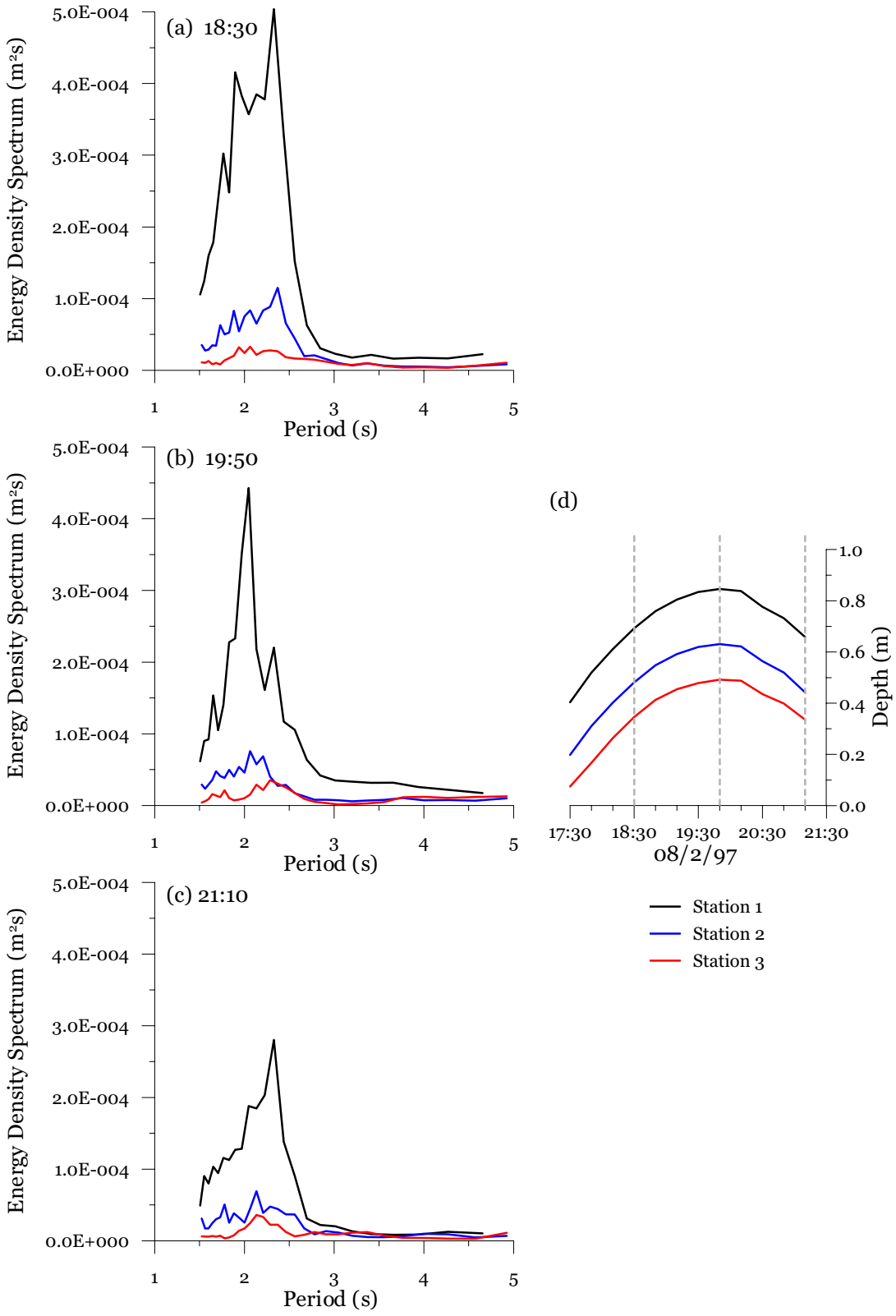

Figure 5.5 Wave energy density spectra at Iriomote on February 8, 1997: (a).18:30, (b) 19:50 and (c) 21:10. Observed water depth is shown in (d), and vertical lines indicate the times of spectra shown in (a) – (c).

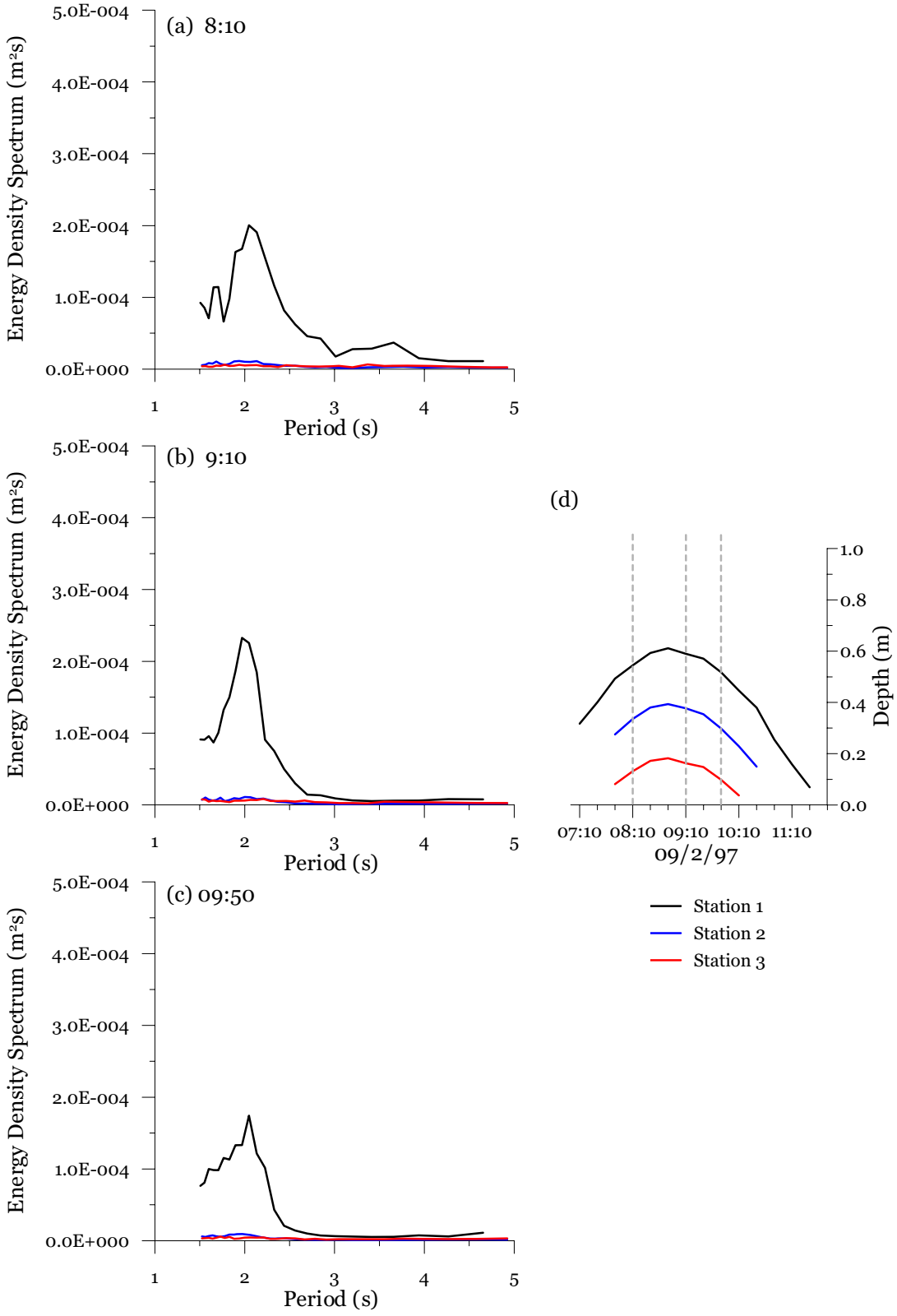

Figure 5.6 Wave energy density spectra at Iriomote on February 9, 1997: (a).08:10, (b) 09:10 and (c) 09:50. Observed water depth is shown in (d), and vertical lines indicate the times of spectra shown in (a) – (c).

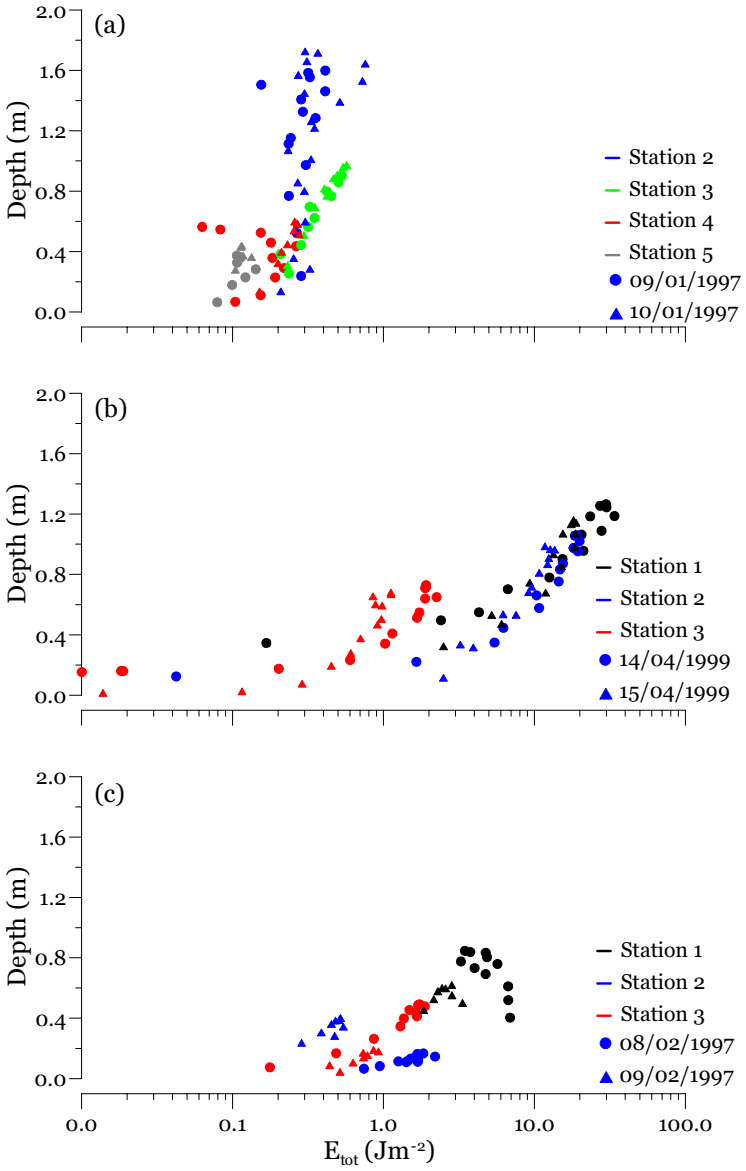

Figure 5.7 Variation of total wave energy, E_{tot}, with water depth for all wave bursts during inundation events at (a) Cocoa Creek, (b) Oonoonba and (c) Iriomote study sites.

Figure 5.8 illustrates the attenuation of total wave energy with distance into the forest at the three study sites. It is evident that the reduction in total energy is not uniform with distance, or even positive in all cases, with increases in wave energy clearly apparent in the first 80 m of the Cocoa Creek study site. Increase in wave energy was only apparent during times of initial inundation of the forest. This increase in wave energy may be explained by a more complex process in which the interaction between wave energy reflection of the dense, near bed roots, wave shoaling (i.e. an increase in wave height due to a sudden decrease in water depths),

play important roles. However, taking all data into account, there is a general trend that as distance into the forest increases, the rates of attenuation become more uniformly positive. This is particularly true for the Oonoonba study site. These observations are confirmed by summary statistics of all data on wave transformation over the different sections of the three observation transects, documented in Table 5.1, Table 5.2 and Table 5.3 for the Cocoa Creek, Oonoonba and Iriomote Island Study sites, respectively.

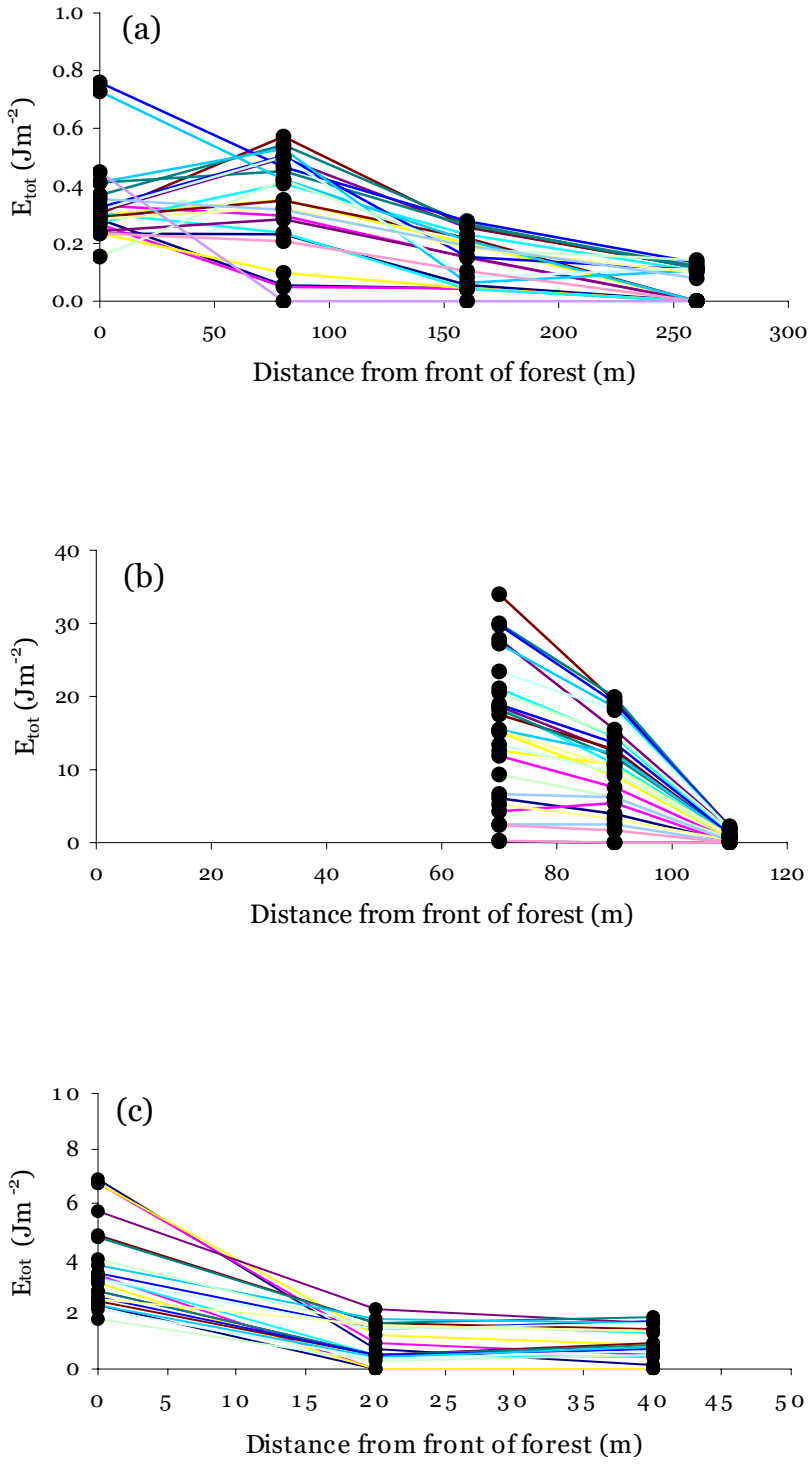

Figure 5.8 Attenuation of total wave energy, E_{tot}, with distance into the forest for all wave bursts during inundation events at (a) Cocoa Creek, (b) Oonoonba and (c) Iriomote study sites. Coloured lines join data from simultaneous wave bursts.

At the Cocoa creek study site, the total wave energy, E_{tot}, decreased on average by 64% through the mangrove forest, or ~0.24% m^{-1}. Significant wave height, H_s, also decreased over the same distance by an average of 50% (0.19% m^{-1}). As mentioned above, there were occasions where both total energy and significant wave height did not attenuate with distance into the forest, but instead increased. Similarly, total wave energy decreased by averages of 95% and 71% at the Oonoonba and Iriomote study sites, respectively. Given that the Oonoonba array spanned only the most landward 80m of the forest, actual overall attenuation rates (of both E_{tot} and H_s) are likely to be higher than reported here. For all three sites there was a consistent decrease in wave energy between the most seaward and most landward instruments. Mean rates of reduction in significant wave height per metre of vegetation were 0.24% m^{-1}, 2.4% m^{-1} and 1.8% m^{-1} for the Cocoa Creek, Oonoonba and Iriomote study sites, respectively. These observations are comparable to the rates of wave reduction of up to .20% m^{-1} of vegetation reported by Mazda *et al*. (1997a) from observations in a reforested mangrove area.

Table 5.1 Statistics of total wave energy and significant wave height characteristics and attenuation at Cocoa Creek.

	E_{tot} (Jm-2)					Attenuation of E_{tot} (%)				
Station	1	2	3	4	5	1-2	2-3	3-4	4-5	Overall*
Mean	0.37	0.33	0.36	0.16	0.11	2.33	-13.06	51.17	31.42	63.66
Std. Dev	0.15	0.13	0.15	0.08	0.02	31.03	57.99	19.44	41.75	18.72
Min.	0.20	0.15	0.05	0.04	0.08	-60.77	-171.37	8.30	-69.70	7.97
Max.	0.69	0.76	0.57	0.28	0.14	46.11	81.83	88.11	58.69	82.38
	H_s (m)					Attenuation of H_s (%)				
Mean	0.04	0.04	0.04	0.03	0.02	9.01	-5.56	30.84	19.79	49.93
Std. Dev	0.01	0.01	0.01	0.01	0.00	25.30	31.94	19.25	24.40	16.14
Min.	0.01	0.03	0.01	0.01	0.01	-58.17	-62.17	-6.56	0.09	7.87
Max.	0.07	0.05	0.05	0.04	0.02	54.29	70.35	58.63	53.64	76.84

* Overall attenuation of E_{tot} and H_s are calculated between the most landward station (#5) and the front of the mangrove forest (station #2)

Table 5.2 Statistics of total wave energy and significant wave height characteristics and attenuation at Oonoonba.

	E_{tot} (Jm-2)			Attenuation of E_{tot} (%)		
Station	1	2	3	1-2	2-3	Overall
Mean	15.78	10.74	0.94	29.67	91.08	94.67
Std. Dev	9.28	5.77	0.69	17.42	7.85	2.44
Min.	0.17	0.04	0.01	-26.67	55.45	88.74
Max.	33.94	19.92	2.25	74.72	99.82	99.76
	H_s (m)			Attenuation of H_s (%)		
Mean	0.18	0.15	0.05	16.08	69.12	75.38
Std. Dev	0.05	0.05	0.02	18.46	12.56	8.80
Min.	0.04	0.01	0.01	-26.99	38.52	60.27
Max.	0.25	0.20	0.09	69.95	95.86	95.51

Table 5.3 Statistics of total wave energy and significant wave height characteristics and attenuation at Iriomote.

	E_{tot} (Jm-2)			Attenuation of E_{tot} (%)		
Station	1	2	3	1-2	2-3	Overall
Mean	3.96	1.06	1.05	73.48	-13.59	70.74
Std. Dev	1.62	0.61	0.52	11.99	46.23	13.14
Min.	1.85	0.29	0.18	51.20	-81.85	49.54
Max.	6.89	2.20	1.88	89.23	76.22	97.44
	H_s (m)			Attenuation of H_s (%)		
Mean	0.11	0.06	0.05	40.79	18.94	53.64
Std. Dev	0.02	0.02	0.01	17.66	23.81	13.23
Min.	0.08	0.03	0.02	13.22	-25.00	32.69
Max.	0.15	0.10	0.07	68.25	66.06	87.14

The variation of significant wave height, maximum wave height, mean period and mean wavelength with water depth over an inundation event are shown in Figure 5.9. These data confirm many of the observations described so far: (i) attenuation of wave energy and wave height with distance into the forest; and (ii) increased energy transmission with increased water depth. However, these data also demonstrate subtle variations in wave period and wavelength with observation of marginally larger mean wavelengths and mean periods at stations further into the forest. Such an increase in mean period and wavelength indicates attenuation of shorter period (higher frequency) waves, and there is some evidence of this in the wave energy spectra, particularly from the more energetic data from Oonoonba.

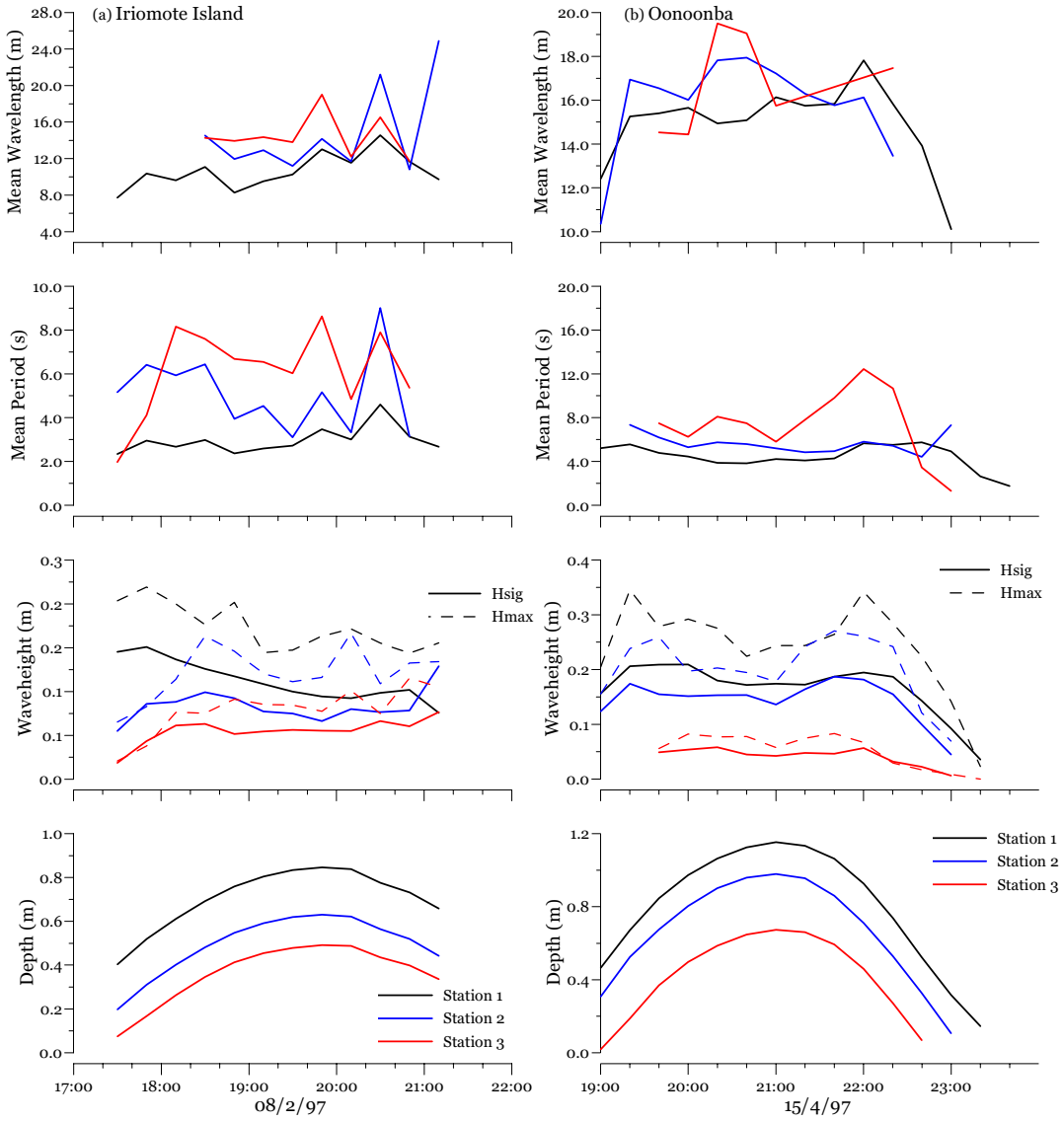

Figure 5.9 Variation of wave parameters over an inundation event at (a) the Iriomote study site on 8/2/1997, and (b) the Oonoonba study site on 15/4/1999.

5.2.2 Summary of key observations from the field data

The field data presented above demonstrate a number of key effects of mangrove vegetation on the propagation of random wind-induced gravity waves through mangroves, common to all study sites: Firstly, there is strong attenuation of wave energy with distance into the forest. Secondly, it is evident that energy transmission into the forest increases with an increase in water depth, due in part to the vertical structure of the mangrove trunks and roots and their obstruction to water flow, which decreases with distance above the sea bottom (see Figure 3.2). Thirdly, there

is evidence of an increase in the mean period with distance into the forest, suggesting preferential attenuation of shorter period (higher frequency) waves within mangrove forests.

5.3 Model Results

5.3.1 Model for uniform horizontal bathymetry

The theoretical approach and computational model presented in Chapter 3 were developed for the case of a mangrove forest with a uniform horizontal bathymetry. Due to the limitations of this model to represent realistic, non-uniform bathymetry profiles, it is not intended to show in this section comparisons of the numerical model with field observation. Instead, examples of numerical calculations are presented to qualitatively demonstrate the model's performance against the key features of wave propagation through mangroves as determined from the field data.

Field data presented earlier in this Chapter suggest that each of the study sites was exposed to wind-induced waves typically characterised by a narrow spectrum. Therefore, for the purposes of evaluating the model, the incident wave spectra were described by a Gaussian shaped spectrum of the form

$$S(\omega) = \frac{\sigma_\varsigma^2}{\omega_p} \exp\left[-a \left(\frac{\omega}{\omega_p} - 1 \right)^2 \right] \tag{5.1}$$

where σ_ς is the standard deviation of the frequency spectrum of the sea surface displacement, defined as $\sigma_\varsigma = \frac{H_s}{4}$, and H_s and ω_p are as previously defined. The variance of the incident wave spectrum is σ_ς^2. Peak frequency, ω_p, is related to the peak period, T_p, by the relationship $\omega_p = \frac{2\pi}{T_p}$. Shape parameter, a, controls the total energy of the spectrum and is found from the relation

$$\int_0^\infty S(\omega)\, d\omega = \sigma_\varsigma^2 \tag{5.2}$$

Estimates of both peak period and significant wave height were available from the field data, as were parameters describing the vegetation characteristics.

In order evaluate the model's sensitivity to the spectral characteristics of the incident waves and vegetation density, a number of numerical calculations were performed using model input parameters (which define wave spectra and vegetation characteristics) as determined from field observations. For example, observations of the spatial density and structure of the vegetation, and its variability at the three study sites defined the vegetation parameters used to represent sparse, medium and densely vegetated forests. Descriptions of the vegetation parameters are given in detail in Section 3. However, it is practical to recall that in the model the mangrove structure is represented by an idealized structure of two layers of vertical cylindrical elements with different diameters and number of elements in each layer, as displayed in Figure 3.1. Within the bottom layer, $-h \le z \le -(h - h_l)$, there are N_l trunks, each of the mean diameter D_l. Above the bottom layer, beginning at z = -(h-h_l) and extending up to and beyond the sea surface at z = 0, there are N_u trunks, each of the mean diameter D_u. Vegetation and wave spectral parameters used in the sensitivity analysis are given in Table 5.4.

Table 5.4 Vegetation, wave spectra and depth parameters used for model sensitivity analysis and comparison.

Vegetation Parameters						Wave Spectral Parameters		Total Water Depth
Vegetation Density	Upper Layer		Lower Layer					
	N_u (-/m^2)	D_u (m)	N_l (-/m^2)	D_l (m)	h_l (m)	T_p (s)	H_s (m)	h (m)
Sparse	1	0.08	9	0.02	0.75	2,4 & 6	0.2	1.0
Medium	4	0.08	25	0.02	0.75	2,4 & 6	0.2	1.0
High	16	0.08	49	0.02	0.75	2,4 & 6	0.2	1.0

Computed wave spectra at three locations within a mangrove forest of width = 50 m and uniform horizontal bathymetry are shown in Figure 5.10 for sparse, medium and high vegetation densities, and with incident wave spectra with peak periods of 2, 4 and 6 seconds. It is clear that wave energy attenuates with distance into the forest, and that the rate of attenuation is proportional to the vegetation density. Also, in all cases, there is no significant shifting of the period of peak of wave energy for spectra calculated at various distances into the forest, which is as expected as the model formulation neglected non-linear processes (such as wave breaking) that may cause a redistribution of wave energy among frequencies.

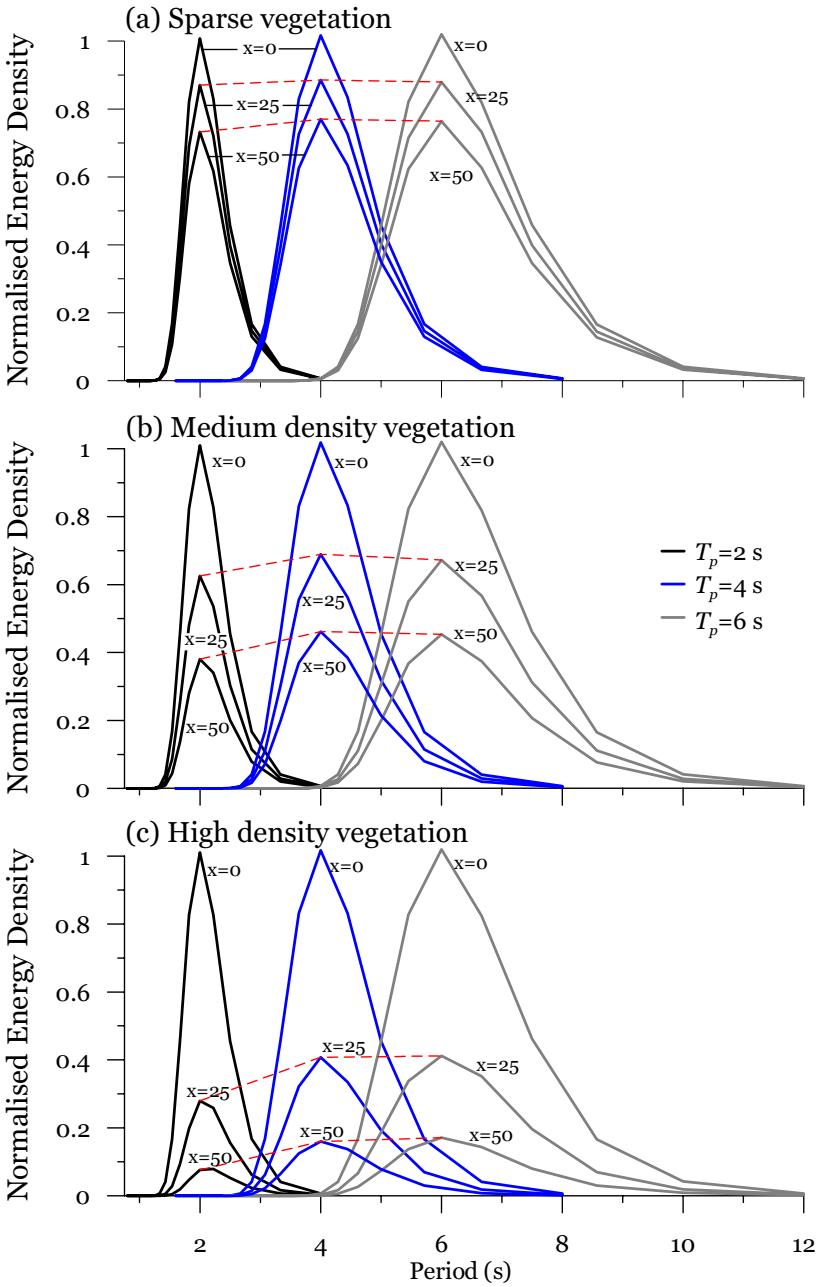

Figure 5.10 Computed wave spectra at three locations within a mangrove forest with uniform horizontal bathymetry, for sparse, medium and high vegetation densities, and for incident wave spectra with peak periods of 2, 4 and 6 seconds. The red dashed line is a visual guide to show increased attenuation of spectra with lower peak periods, and numbers above spectra indicate distance in metres from front of forest.

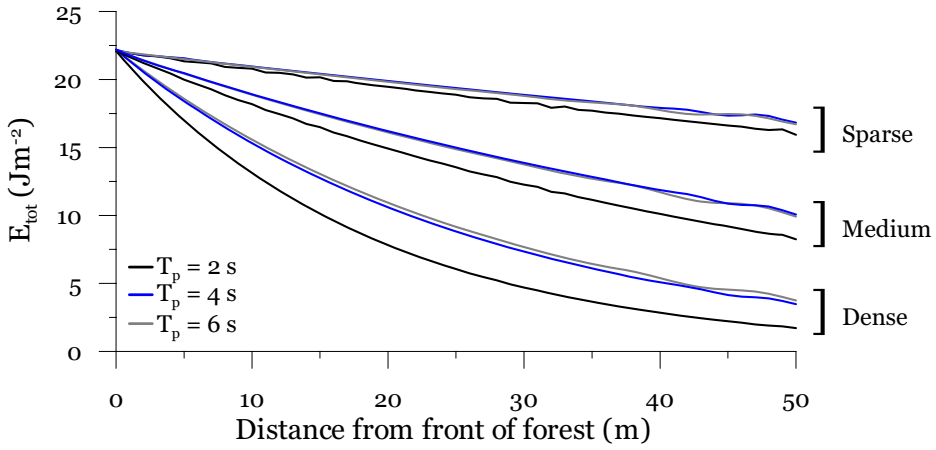

Figure 5.11 Predicted attenuation of total wave energy, E_{tot}, with distance into the forest for sparse, medium density and dense vegetation, and uniform horizontal bathymetry.

Predicted rates of attenuation of total wave energy, E_{tot}, with distance into the forest are presented in Figure 5.11. These results suggest that there is little difference in the predicted attenuation rates for wave spectra with peak periods of 4 and 6 seconds, for each of the three vegetation densities. However, in all cases (sparse, medium density and dense) there is enhanced attenuation of the spectra with a peak period of 2 seconds.

In order to more rigorously assess the amount of wave energy predicted to be transmitted through, reflected by and dissipated by the mangroves, it is useful to determine coefficients of transmission, reflection and dissipation. The energy balance in the vicinity of the mangroves is

$$E_r + E_t + E_{dis} = E_i \quad \text{or} \quad \frac{E_r}{E_i} + \frac{E_t}{E_i} + \frac{E_{dis}}{E_i} = 1 \tag{5.3}$$

where E_r ,E_t, E_{dis} and E_i denote reflected, transmitted, dissipated and incident energy, respectively. As energy is proportional to the square of the wave height, Equation (5.3) can be represented as

$$\left(\frac{H_r}{H_i}\right)^2 + \left(\frac{H_i}{H_i}\right)^2 + \left(\frac{H_{dis}}{H_i}\right)^2 = 1 \tag{5.4}$$

or

$$K_r^2 + K_i^2 + K_{dis}^2 = 1 \tag{5.5}$$

where K_t, K_r and K_{dis} are transmission, reflection and dissipation coefficients, respectively. These coefficients can be expressed in terms of the standard deviations of the wave spectra as follows

$$K_t = \frac{\sigma_t}{\sigma_i} \quad \text{and} \quad K_r = \frac{\sigma_r}{\sigma_i} \tag{5.6}$$

where σ_T, σ_R and σ_i are standard deviations of the transmitted, reflected and incident waves.

Values of computed coefficients of reflection, transmission and dissipation, given in Table 5.1, confirm the attenuation of wave energy as shown by the computed spectra in Figure 5.10. Computed coefficients also demonstrate that there is little difference between the energy balance for calculations with peak periods of 4 and 6 seconds. However, it is evident that more energy is dissipated for the lower period (higher frequency) spectrum with a peak period of 2 seconds, confirming the data presented in Figure 5.11.

Table 5.5 Computed coefficients of reflection, transmission and dissipation and linearisation coefficient.

Veg.	T_p = 2 s				T_p = 4 s				T_p = 6 s			
density	K_t	K_r	K_{dis}	f_e	K_t	K_r	K_{dis}	f_e	K_t	K_r	K_{dis}	f_e
Sparse	0.80	0.01	0.59	0.005	0.82	0.01	0.57	0.012	0.82	0.01	0.57	0.019
Medium	0.57	0.01	0.82	0.014	0.63	0.01	0.77	0.033	0.63	0.01	0.77	0.051
Dense	0.26	0.01	0.97	0.032	0.37	0.02	0.93	0.068	0.39	0.02	0.92	0.104

The linearisation coefficients, f_e, presented in Table 5.5 demonstrate the dependence of this coefficient on both the vegetation density and on the statistical characteristics of the wave field. For example, for a given peak period, f_e increases with vegetation

density, and for a given vegetation density, f_e increases with peak period. This is as expected, as f_e is a function of the drag force on the vegetation which is in turn dependent on both the wave-induced orbital velocities and the vegetation characteristics itself.

Wave-induced velocities in mangrove forests are of special interest, as water kinematics control the exchange of water, fluxes of nutrients and sediments. Both vertical and horizontal components of wave-induced velocity change their direction during a wave period. However, for practical applications, the most useful characteristics of wave-induced velocity is the mean amplitude. Under the assumption that both components of the wave-induced velocity are random quantities with a normal probability density, the mean amplitudes of the horizontal (u) and vertical (w) velocity components are

$$\overline{u}(x,z) = \sqrt{\frac{\pi}{2}}\sigma_{u(x,z)} \quad \text{and} \quad \overline{w}(x,z) = \sqrt{\frac{\pi}{2}}\sigma_{w(x,z)} \tag{5.7}$$

where $\sigma_{u(x,z)}$ and $\sigma_{w(x,z)}$ are the standard deviations of the horizontal and vertical velocity components, respectively, at point (x,z) in the fluid domain. The vertical profiles of mean amplitudes $\overline{u}$ and $\overline{w}$ at three locations in a mangrove forest are shown in Figure 5.12. It is clear that in all cases presented, the magnitudes of the velocity components attenuate very quickly, and profiles of both components become more vertically uniform with distance from the mangrove front.

Field data presented earlier in this Chapter showed that energy transmission into the forest at each study site was a function of inundation depth. This is primarily due to the vertically non-uniform structure of the mangrove vegetation, which changes dramatically with distance above the forest floor. As water inundates the forest, the lower layer of dense trunks and roots occupies the entire water column until the water depth is equal to the thickness of the lower layer, h_l. As the water depth increases further, the upper layer of the vegetation becomes inundated. Various stages of tidal inundation can be simulated with the model by varying the total depth and vegetation structure, such that the thickness of the lower layer, h_l, is set equal to

the total water depth if the water depth is less than a threshold value of h_l. Table 5.6 documents parameters used to simulate wave propagation for various stages of tidal inundation.

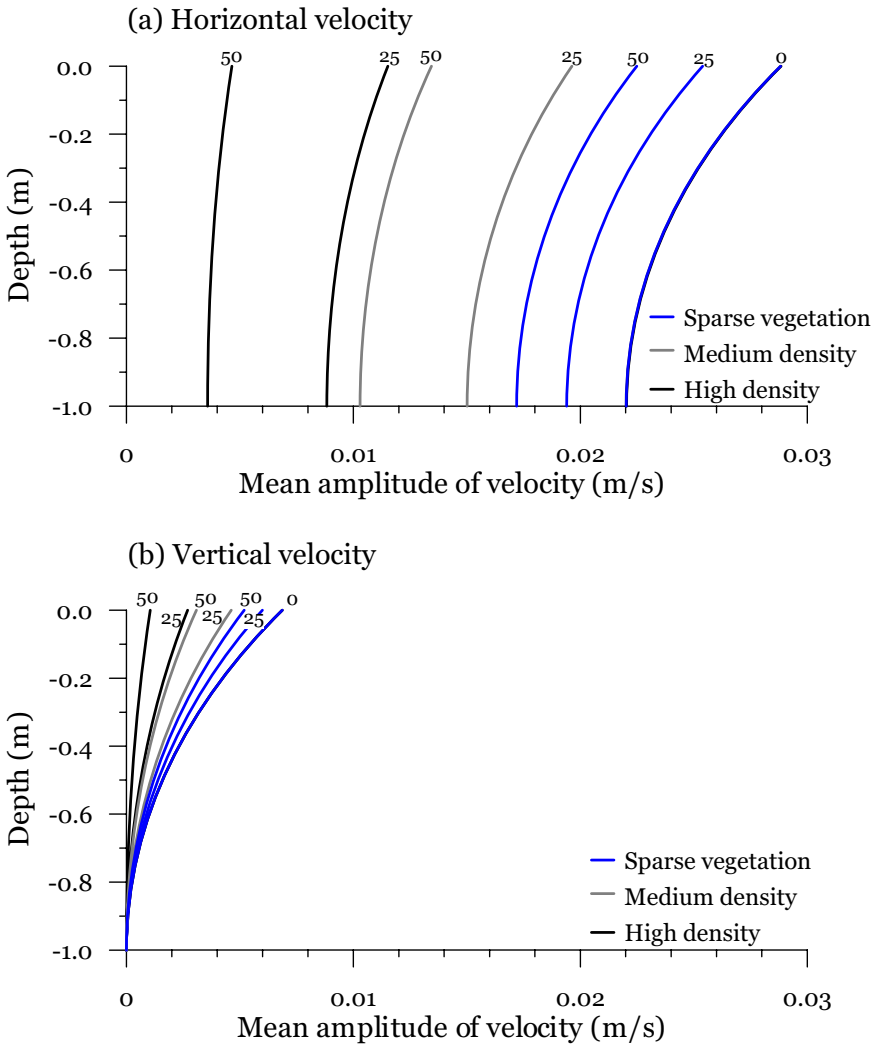

Figure 5.12 Computed vertical profiles of the mean amplitudes of horizontal and vertical components of wave-induced orbital velocity at three locations within a mangrove forest with uniform horizontal bathymetry, for sparse, medium and high vegetation densities. Numbers above each profile indicate distance in metres from the front of the forest.

Figure 5.13 illustrates the variations in predicted attenuation of total energy with both depth and distance into the forest, and these data support the field observations (shown in Figure 5.7 and Figure 5.8) of the dependence of energy transmission on water depth. Also shown for comparison in Figure 5.13 is the predicted attenuation of wave energy over a seabed with no vegetation. It should be recalled that in the

development of the model it was assumed that energy dissipation was dominated by fluid-vegetation interactions and thus bottom friction was neglected. Whilst not absolutely justifying this assumption, Figure 5.13 does demonstrate that the strong energy dissipation can be predominantly attributed to the vegetation.

Table 5.6 Vegetation, wave spectra and depth parameters used to simulate wave propagation for various stages of tidal inundation.

Vegetation Parameters						Wave Spectra Parameters		Total Water Depth
Vegetation Density	Upper Layer		Lower Layer					
	N_u (-/m^2)	D_u (m)	N_l (-/m^2)	D_l (m)	h_l (m)	T_p (s)	H_s (m)	h (m)
Medium	4	0.08	25	0.02	0.25	4	0.2	0.25
Medium	4	0.08	25	0.02	0.50	4	0.2	0.50
Medium	4	0.08	25	0.02	0.75	4	0.2	0.75
Medium	4	0.08	25	0.02	0.75	4	0.2	1.00
Zero	0	0	0	0	0	4	0.2	0.25

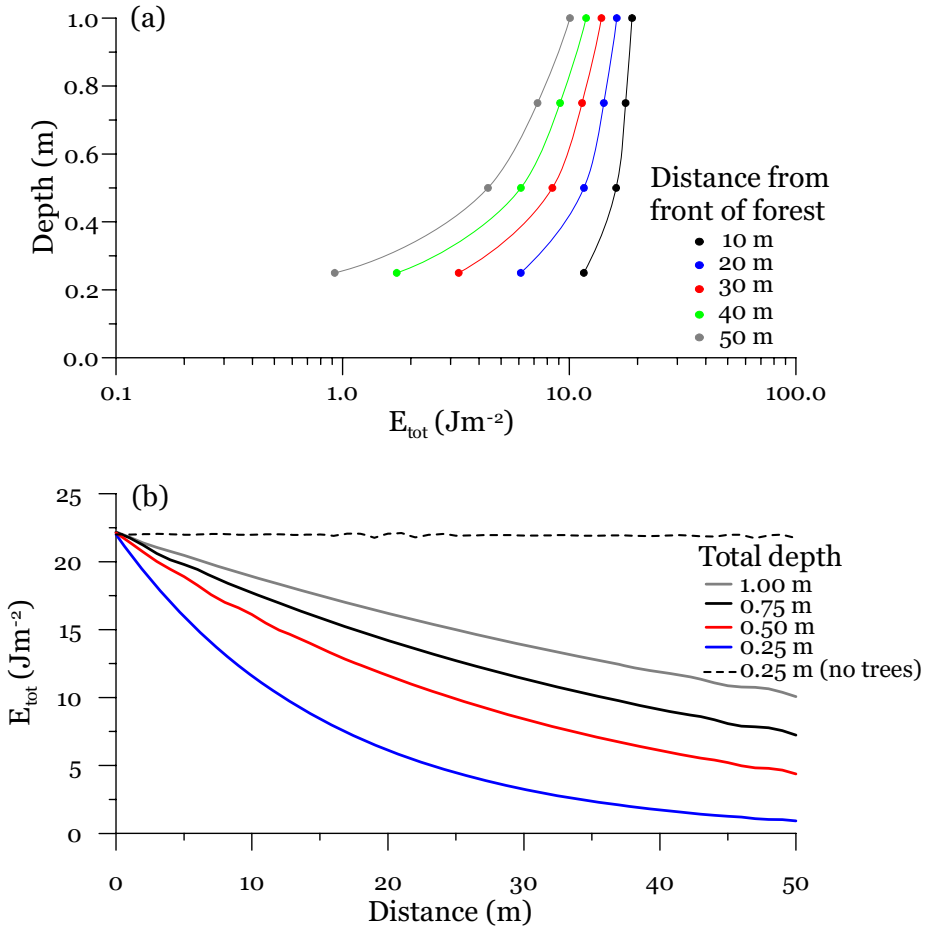

Figure 5.13 Predicted variations of total spectral wave energy, E_{tot}, with (a) water depth and (b) distance into the forest. Coloured lines in (a) indicate predicted changes in E_{tot} with depth at each of 4 locations within the forest, and in (b) show attenuation of E_{tot} with distance for different total water depths. The dashed line shows attenuation predicted by the model with not vegetation present.

5.3.2 Model for arbitrary bathymetry

Chapter 4 of this thesis described a theoretical approach and computational model developed for wave propagation through a mangrove forest of arbitrary bathymetry. The approach adopted was to describe the wave motion in the vicinity of the forest by a complex wave amplitude which is a solution to the mild-slope equation with dissipation due to the wave/vegetation interaction. The solution differs from that presented in Chapter 3, where wave motion in the vicinity of the forest is described by a set of amplification factors. Whilst the model for arbitrary bathymetry effectively supercedes the model presented in Chapter 3, it does so via a very different theoretical approach. Thus a comparison of the two models performance

for the case of a horizontal bathymetry is a good evaluation of the robustness of the theory underpinning each model. Numerical calculations were performed for a forest with horizontal bathymetry and various vegetation and wave spectral parameters given in Table 5.4. Incident waves conformed to a Gaussian shaped spectrum as described by Equations (5.1) and (5.2).

A comparison of predicted wave spectra from the two models, shown in Figure 5.14, indicates that computations using incident spectra with peak periods of 4 and 6 seconds show very good agreement. For these cases, differences in peak normalised energy were at most 15% and 8%, for waves with peak periods of 4 and 6 seconds, respectively. However results from the two models diverge for computations using a peak period of 2 seconds, with a maximum error of 31% predicted at $x = 0$ m. It should be recalled from the development of the models that each follows a different approach to represent the wave field within the forest. The model for horizontal bathymetry represents the wave field by a series of coefficients of transmission and refelction. At the seaward margin of the forest, these coefficients are in balance with the similar coefficients outside of the forest. In contrast, the model for arbitrary bathymetry represents the wave field by a modified mild slope equation. Boundary conditions for this equation at the seaward edge of the forest are established through balancing incident wave energy. Because of this approach, simulation from the two models of the first few metres of the forest may differ slightly, as the predictions from the model with arbitrary bathymetry will show increased reflections that are not fully represented in the prescription of the boundary condition. The amount of reflection in the initial few metres of the forest is dependent of wave frequency.

In general, there is good agreement between the results of both models for wind-induced waves with peak periods in the range 2 – 6 seconds, which is typical of medium to low wave-energy environments where mangroves commonly grow (Mazda *et al*., 1997a).

The conformity of the calculated wave spectra from the two models indicates a good level of confidence in their accuracy, because the theory underlying each model is different. Such agreement gives confidence not only to the results from each model,

but also indicates that the two disparate approaches are fundamentally sound and capture the relevant processes of energy dissipation.

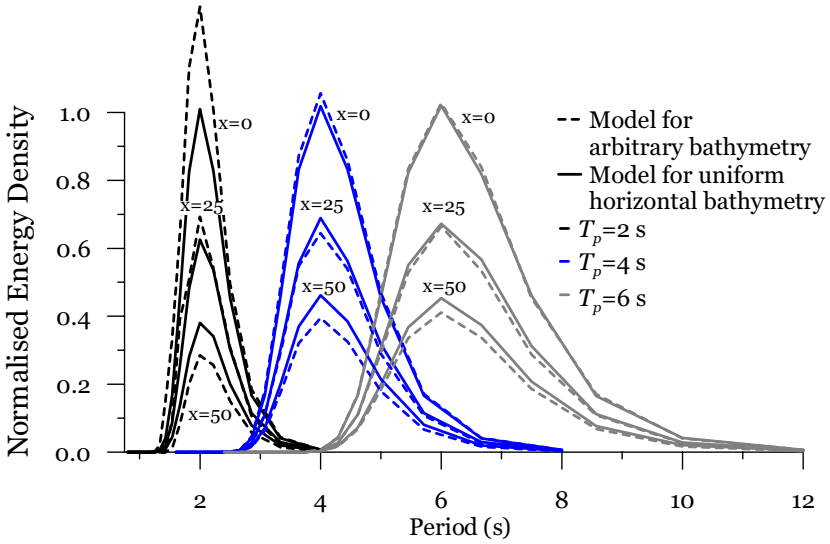

Figure 5.14 Comparison of computed wave spectra at three locations within a mangrove forest with uniform horizontal bathymetry as determined by the models for arbitrary (dashed lines) and horizontal (solid lines) bathymetry. Shown are the computed spectra for medium vegetation density and incident wave spectra with peak periods of 2, 4 and 6 seconds. Numbers above spectra indicate distance in metres from front of forest.

Predicted attenuation of total wave energy for the two models using various vegetation densities is shown in Figure 5.15. As in the above case there is good agreement between the two models, and for the given set of input parameters, both approaches predicted comparable levels of attenuation. This is confirmed by computed coefficients of reflection, transmission and dissipation, presented in Table 5.7. The similarity of the linearisation coefficients computed by both models is also noteworthy, as this indicates that for a particular vegetation density, both models are calculating equivalent levels of energy dissipation.

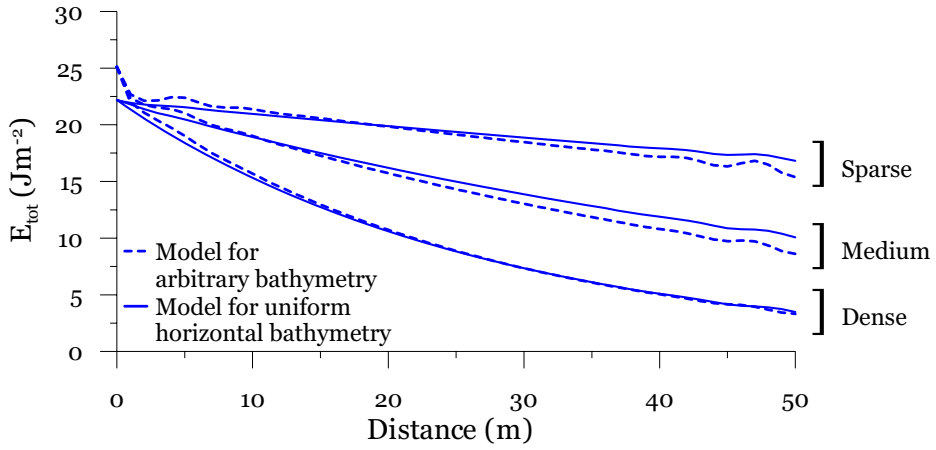

Figure 5.15 Comparison of predicted attenuation of total wave energy, E_{tot}, with distance into the forest for sparse, medium density and dense vegetation, as determined by the models for arbitrary (dashed lines) and horizontal (solid lines) bathymetry. Incident wave spectra has a peak period of 4 seconds.

Table 5.7 Computed coefficients of reflection, transmission and dissipation and linearisation coefficient.

	Uniform bathymetry model				Arbitrary bathymetry model			
Veg. density	T_p = 4 s				T_p = 4 s			
	K_t	K_r	K_{dis}	f_e	K_t	K_r	K_{dis}	f_e
Sparse	0.82	0.01	0.57	0.012	0.78	0.03	0.62	0.013
Medium	0.63	0.01	0.77	0.033	0.58	0.03	0.81	0.036
Dense	0.37	0.02	0.93	0.068	0.36	0.03	0.93	0.073

Predictions of wave parameters using the theoretical approach developed for the case of an arbitrary bathymetry profile incorporate the effects of both the vegetation density and non-uniform bathymetry, via the mild slope equation with dissipation. As both bathymetry and vegetation have an effect on wave propagation, a number of computations were performed to elucidate each effect, and determine the sensitivity of the model to bottom slope. Observations from the present study and data from the literature suggest that, in general, the bottom slopes within mangrove forests are between 1/100 and 1/500 (Mazda *et al*., 1997a). As such, computations were restricted to this range of bottom slopes. Parameters used for these computations are presented in Table 5.8. It should be noted that the convention used in Table 5.8 to describe bottom slope is such that a positive slope indicates a decrease in depth with distance into the forest.

Table 5.8 Vegetation, wave spectra and depth parameters used for analysis of sensitivity of the computational model to bottom slope.

Vegetation Parameters						Wave Spectra		Bathymetry Parameters	
Vegetation Density	Upper Layer		Lower Layer					Water depth at $x = 0$	Slope
	N_u (-/m^2)	D_u (m)	N_l (-/m^2)	D_l (m)	h_l (m)	T_p (s)	H_s (m)	h (m)	
Medium	4	0.08	25	0.02	0.25	4	0.2	0.25	0
Medium	4	0.08	25	0.02	0.25	4	0.2	0.25	1/500
Medium	4	0.08	25	0.02	0.25	4	0.2	0.25	1/200
Medium	4	0.08	25	0.02	0.25	4	0.2	0.25	1/100

Figure 5.16 illustrates the effects of both bottom slope and vegetation on wave propagation through a mangrove forest, and indicates that the effects of vegetation density dominates any wave transformations due to water depth. Results from computations for a number bottom slopes but with vegetation density held constant show equivalent levels of energy attenuation, suggesting that it is vegetation density that plays a dominant role in controlling changes in total wave energy. When there is no vegetation, total spectral wave energy is predicted to increase within the forest for cases of decreasing depth. It should be recalled that total energy, E_{tot}, is the total wave energy contained in the wave spectrum, defined as

$$E_{tot} = \int_0^\infty S(\omega)\, d\omega \rho_w g = \sigma_\varsigma^2 \rho_w g \tag{5.8}$$

where, as defined previously, σ_ς^2 is the variance of the frequency spectrum of the sea surface displacement, and ρ_w and g are water density and acceleration due to gravity, respectively. In the case of the model results the limits of the integral are set by the extent of the modelled frequency range. Results of numerical calculations, which neglect bottom friction and wave breaking, show that for the case of a shoaling bottom and zero vegetation, there is an increase in total spectral wave energy (and therefore, by definition, an increase in wave height) with distance into the forest, which would be expected for a calculation that neglects all dissipative processes.

Results of numerical calculations undertaken to investigate the sensitivity of the model to water depth, performed to simulate various stages of tidal inundation, conformed to results described in Section 5.3.1 (see Figure 5.13), and are thus not repeated here. It is sufficient to mention that energy transmission increases with increasing water depth, due primarily to the vertically non-uniform structure of the mangrove vegetation which decreases in density with distance above the bottom.

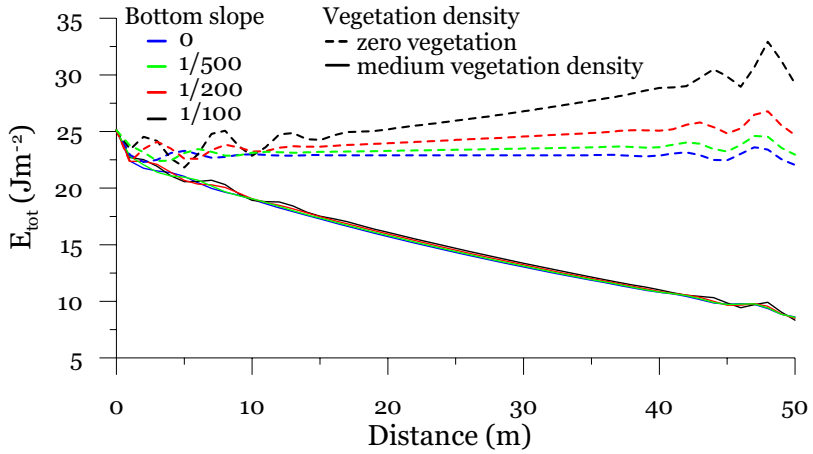

Figure 5.16 Changes in total wave energy with distance into the forest for various bottom slopes with no vegetation and medium vegetation density.

5.3.3 Summary of key observations from the computational models

Results from the computational models presented above demonstrate the qualitative performance of the model against a number of key observations of the propagation of random wind-induced gravity waves through mangroves. Firstly, the models reproduce the observed strong attenuation of wave energy with distance into the forest. This is confirmed by model predictions of: (i) wave energy spectra at locations within the forest; (ii) the reduction in total wave energy, E_{tot}, within the forest; and (iii) the coefficients of energy transmission and dissipation, K_t, and K_{dis}, respectively. Further, the rate of attenuation of incident wave energy was shown to be proportional to the density of the vegetation. Secondly, model results support the observation that energy transmission into the forest increases with water depth due

primarily to the structure of the vegetation. In order to understand the model's sensitivity to various input parameters, model runs were performed for a number of incident wave spectra with differing, but realistic, peak periods, as well as for a number of vegetation densities and bottom slopes. These results show that, for a given incident spectra, there is enhanced attenuation of spectra with lower peak periods (higher frequencies), supporting evidence from the field data of preferential attenuation of higher frequency waves.

There is strong agreement between the calculated wave spectra from the two models for the case of horizontal bathymetry, which gives confidence in the results from each model, and also indicates that the different approaches underlying each model are sound and capture the relevant processes of energy dissipation.

5.4 Comparison of Field and Model results

The development of the computational model for arbitrary bathymetry profiles facilitates making a direct comparison between observed and predicted wave processes within the mangrove forests. Numerical calculations were performed for each study site, with observations of peak period, significant wave height, vegetation density and dimensions, and forest bathymetry used as model input. In order to accurately set the correct water depth profile for each site at the time used for model/field comparison, forest bathymetry profiles were vertically offset based on observed water depth at station locations along the observational transect. Incident waves conformed to a Gaussian shaped spectrum as described by Equations (5.1) and (5.2). It should be recalled that due to an instrument malfunction, the Oonoonba instrument array covered only the most landward 80 m of the forest, and thus model calculations only spanned this section of the forest.

For each site, calculations were performed first using vegetation densities based on field estimates. Subsequent calculations were performed with reduced vegetation densities to evaluate the response of the model to these parameters. Model input parameters used in the simulation of wave processes at each study site are tabulated

in Table 5.9. As recalled from 3.4, the vegetation characteristics are used to determine a modification factor for the drag coefficient. In order to do this, vegetation is described in the discrete vortex model as the random placement in a set volume, of a number of cylinders of known diameter. Using this approach, it is not necessary to reproduce the exact vegetation structure (the 'network' of individual trunks, roots, limbs) as observed in the field, as only estimates based on observations are required. The extent to which the model is sensitive to these estimates is described later in the thesis.

Table 5.9 Vegetation, wave spectra and depth parameters used for numerical simulations of study sites.

Study site	Vegetation Parameters						Wave Spectra		Bathymetry Parameters
	Veg. Density	Upper Layer		Lower Layer					Water depth at $x = 0$
		N_u (-/m^2)	D_u (m)	N_l (-/m^2)	D_l (m)	h_l (m)	T_p (s)	H_s (m)	h (m)
Cocoa Creek	Dense[1]	16	0.1	49	0.05	0.75	2.2	0.05	1.73
	Medium	4	0.1	25	0.05	0.75	2.2	0.05	1.73
	Sparse	1	0.1	9	0.05	0.75	2.2	0.05	1.73
Oonoonba	Med./Dense[1]	1	0.15	49	0.05	0.40	6.0	0.17	0.25
	Medium	1	0.15	25	0.05	0.40	6.0	0.17	0.25
	Sparse	1	0.15	9	0.05	0.40	6.0	0.17	0.25
Iriomote	Dense[1]	16	0.15	49	0.05	0.40	2.05	0.085	0.66
	Medium	4	0.15	25	0.05	0.40	2.05	0.085	0.66
	Sparse	1	0.15	9	0.05	0.40	2.05	0.085	0.66

Calculated wave energy spectra at locations within the mangrove forests at the Cocoa Creek, Oonoonba and Iriomote study sites are shown in Figure 5.17, Figure 5.18 and Figure 5.19, respectively. In general, predicted wave energy spectra are in good agreement with field observations. In particular, the predicted spectra at the Cocoa creek and Iriomote study sites exhibit extremely good qualitative and quantitative agreement with the field data. The predicted incident spectra is a realistic representation of the observed spectra, and within the forest the predicted spectra demonstrate key features of the field data; namely, significant attenuation of energy with distance into the forest and little or no shifting of the period of peak wave energy. Results for the Oonoonba study site do not demonstrate the same level

of agreement with field data as found at the other two sites. Whilst the predicted and observed incident spectra are adequately equivalent, the model is unable to reproduce the observed spectra within the forest, over-predicting the dissipation of energy in the region $0 \le x \le 20$ (between observational stations 1 and 2), and under-predicting for the region $20 \le x \le 35$ (between observational stations 2 and 3). Such disagreement is due to inappropriate prescription of a single peaked incident wave spectra to describing the observed wave spectra (with it's double peak as described in Section 5.2). It is important to note at this stage that the model is only capable of utilizing relatively smoothed incident spectra (as described by Eq. 5.1). The discrepancy between the model and field data may also be due to an inadequate representation of the spatial density (in the horizontal plane) and structural dimensions of the vegetation within the forest, both of which are assumed to be uniform with distance into the forest.

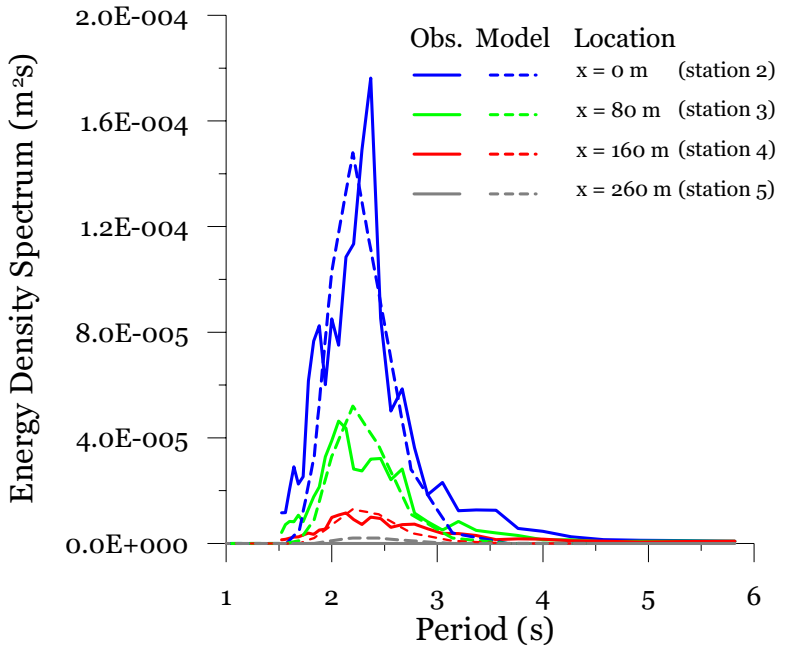

Figure 5.17 Observed and predicted wave energy density spectra: Cocoa Creek study site, at 10:40 January 10, 1997, using vegetation parameters determined from field data.

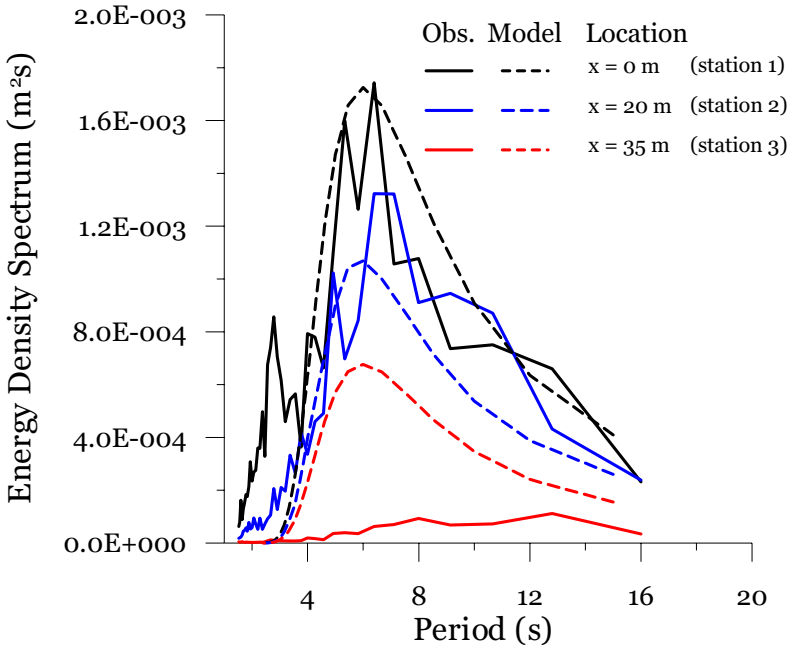

Figure 5.18 Observed and predicted wave energy density spectra: Oonoonba study site, at 21:00, April 15, 1999, using vegetation parameters determined from field data.

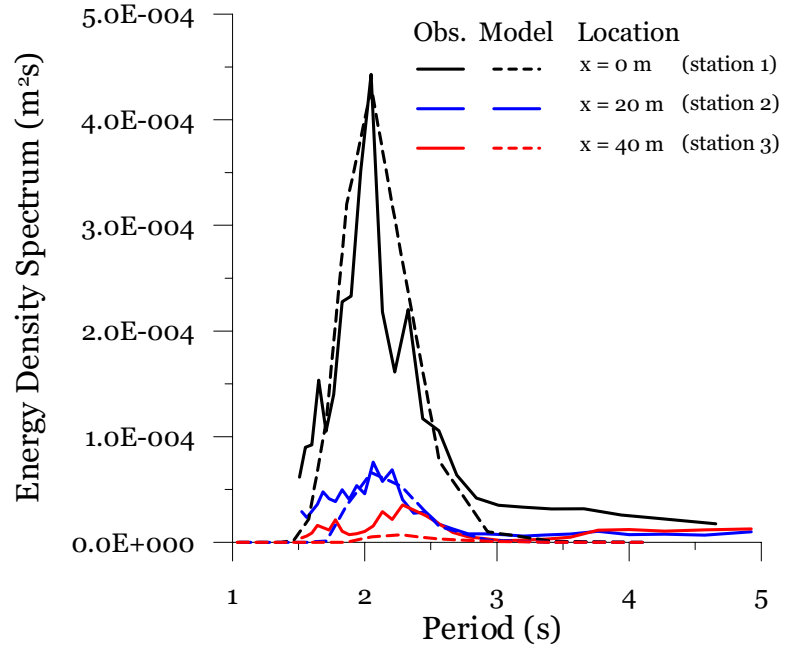

Figure 5.19 Observed and predicted wave energy density spectra: Iriomote study site, at 19:50, February 8, 1999, using vegetation parameters determined from field data.

Figure 5.20 contrasts predicted and observed attenuation of total wave energy, E_{tot}, at the three study sites for three spatial densities of vegetation. Predicted rates of attenuation at Cocoa Creek and Iriomote, using vegetation parameters estimated from field observations, are shown to fall within observed ranges of energy attenuation. With decreasing vegetation density predicted wave energy within the forest increases above the range of observations. Predicted data for Oonoonba do not display good agreement with field observations, and the under-prediction of energy dissipation over the last 40 m of the forest again suggest that the vegetation density at this study site may vary significantly (over short distances) from the 'general' vegetation characteristics observed for the majority of the forest.

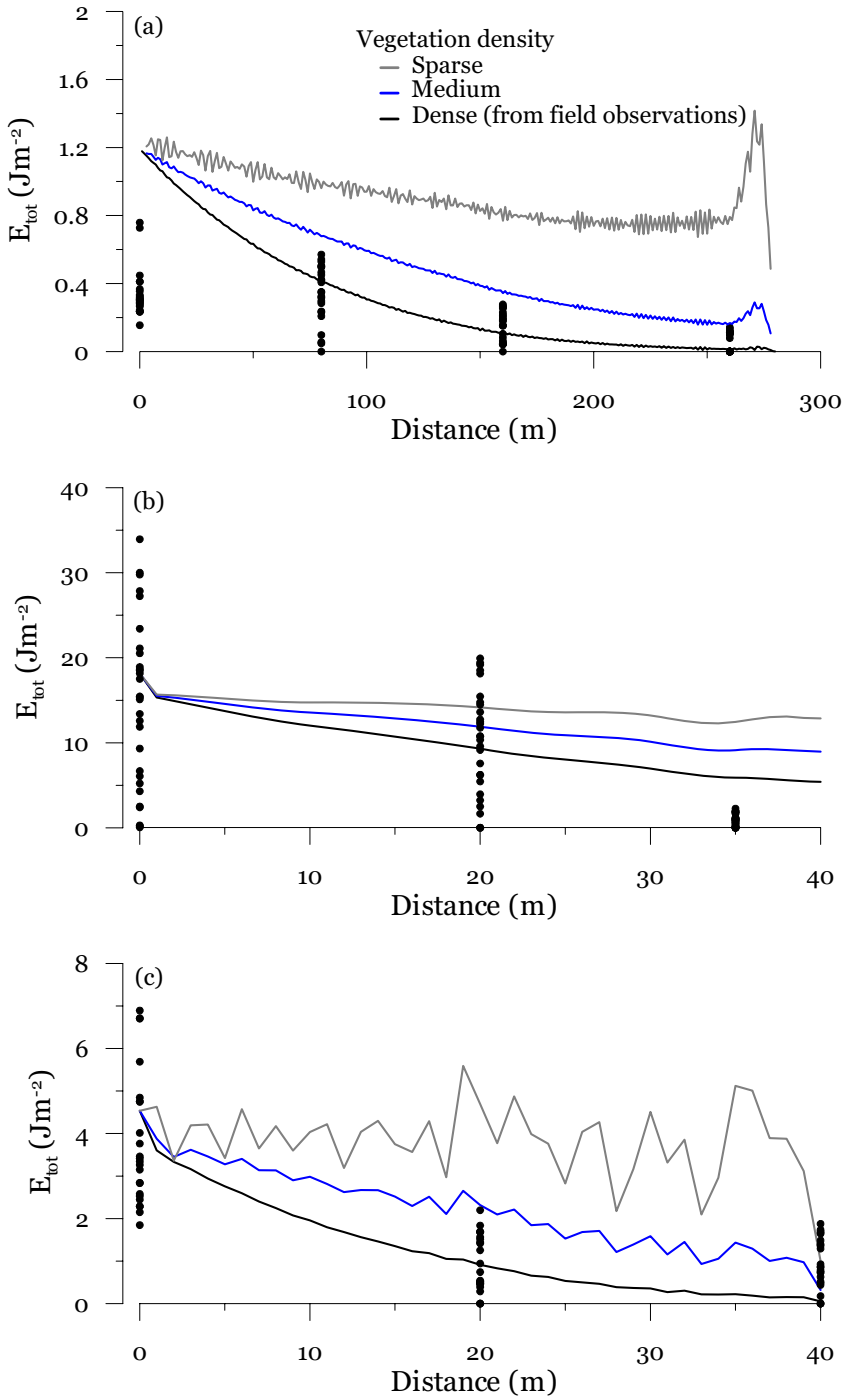

Figure 5.20 Predicted attenuation of total wave energy, E_{tot}, with distance into the forest at (a) Cocoa Creek at 10:40, 10/1/1997, (b) Oonoonba at 21:00, 15/4/1999 and (c) Iriomote at 19:50, 8/2/1997. Black circles (●) show observed attenuation of E_{tot}, for all wave bursts during inundation events at the particular study site.

5.5 Summary

This Chapter documents results from the field observations and modelling undertaken using the two theoretical approaches developed in Chapters 3 and 4.

The field data demonstrate a number of key effects of mangrove vegetation on the propagation of random wind-induced gravity waves through mangroves: (i) strong attenuation of wave energy with distance into the forest; (ii) increase in energy transmission into the forest with an increase in water depth; and (iii) an increase in the mean period with distance into the forest, suggesting preferential attenuation of shorter period (higher frequency) waves within mangrove forests. Both field data and model results show that as waves propagate through mangroves, there is a reduction in the total wave energy across all frequencies of the wave spectrum, with enhanced attenuation of shorter period waves. As such, the shape of the wave energy spectrum changes, and there is a corresponding shift in the mean period of the spectrum to longer period waves. As the shape of the spectrum evolves with propagation into the forest, the energy of the dominant period diminishes rapidly as the wave spectrum flattens.

These key findings were then used to assess the performance of the computational models developed in Chapters 3 and 4. Both models were able to qualitatively reproduce the key features described above as demonstrated by predictions of: (i) wave energy spectra at locations within the forest; (ii) the reduction in total wave energy, E_{tot}, within the forest; and (iii) the coefficients of energy transmission and dissipation, K_t, and K_{dis}, respectively.

Results for the two models were also inter-compared for the case of a horizontal bathymetry. Whilst the two models were each based on a different theoretical approach, there was strong agreement between the calculated wave spectra from the two models for this special case of horizontal bathymetry. Such conformity in the numerical results gives confidence in each model's performance, and also indicates that different approaches underlying each model are sound and capture the relevant processes of energy dissipation for waves propagating through mangrove forests.

Finally, the performance of the more general computational model developed for wave propagation through a mangrove forest of arbitrary bathymetry was verified directly against field data, with the model configured with input parameters (such as bathymetry, incident wave energy spectra and vegetation characteristics) determined from the field data. Results from these verification calculations demonstrated general qualitative and quantitative agreement with the field data and the model was able to reproduce the key features of wave propagation through mangroves. In situations where model results and field data did not display high levels of quantitative agreement, it should be noted that vegetation parameters within the model are applied over the whole forest; i.e. the vegetation structure is assumed constant throughout the whole forest. However, mangrove forests are typically comprised of more than one species of mangrove vegetation, and as such, vegetation density is not constant with distance into the forest. Through analysis of the model's sensitivity to vegetation characteristics and forest bathymetry, it was demonstrated that the interaction of the fluid with the mangrove vegetation is the dominant mechanism for energy dissipation. Given that the models use only a limited number of representative variables to describe the vegetation within the forest, the results are very encouraging.

6 APPLICATION TO COASTAL PROTECTION

6.1 Overview

The application of the theory presented in Chapter 4 to the design and evaluation of coastal protection measures was initiated after discussions with Dr Halide (pers comm.) regarding the need for a simple, cost effective means for protecting mangrove seedlings replanted along wave exposed coastlines as part of coastal rehabilitation efforts. The model developed in Chapter 4 found immediate application to this problem, due to the general approach used in the model formulation in regards to the description of the characteristic vegetation parameters and the bathymetry.

As described in Chapter 1, mangroves play a vital and complex role in sustaining coastal ecosystems by supporting estuarine and nearshore food-webs through providing habitats and nursery refuge for many marine and terrestrial organisms. Mangrove forests trap and stabilise sediments (Furukawa and Wolanski, 1996) and, as described in previous Chapters, mangroves attenuate significant amounts of incident surface wave energy. From a socio-economic perspective, mangroves are also important as a traditional and commercial resource for fuelwood, charcoal, timber, a variety of fisheries and the production of tannins for dying and leather production (Qureshi, 1990; Woodroffe, 1992; Siddiqi and Khan, 1990, Bandaranayake , 2002, Glaser, 2003).

In general, mangrove forests exist in areas of soft soil in the inter-tidal zone of sheltered coastal and riverine areas with medium to low wave energy climates. Such locations are prime sites for land based aquaculture developments for the production of prawns or shrimps, and as such, mangrove forests are also being increasingly exploited as sites for these developments due to the suitability of the sheltered, low wave energy environment, the proximity to clean salt water and the ease at which mangroves can be cleared and the land developed. For example, in the South Sulawesi province of Indonesia, 65 % of 112 000 ha of pristine mangrove forests

have been converted into ponds between 1950 and 1990 (ADB, 1993). Clearing of mangroves for aquaculture pond development has also occurred in Thailand, Malaysia, the Philippines, and Vietnam (Barbier, 2003; Ong, 1982; Primavera, 1995; De Graaf and Xuan, 1998). Even though ponds built on cleared mangroves produce 82 % of the world's shrimp products (Dierberg and Kiattisimkul, 1996), these developments have taken their toll on coastal systems, with mangrove ecosystems disappearing or being degraded world-wide at rates exceeding 1% per year (Ellison, 2000). On the east coast of India the loss of coastal protection provided by mangroves due to the construction of shrimp ponds resulted in the loss of life and severe property damage during a tropical cyclone (Pearce, 1999). The clearing of mangroves also results in other detrimental environmental effects including increased water pollution and eutrophication, and degradation of the health of the local ecosystem (Stevenson and Burbridge, 1997).

In order to rehabilitate cleared or disturbed areas, mangrove seedlings are often replanted along the coastlines (Mazda *et al*., 1997a). As the health and functioning of mangrove ecosystems is controlled by only a few key variables, notably hydrology and soil factors, restoration and recovery of disturbed mangroves can proceed fairly rapidly, given the appropriate physical conditions (Ellison, 2000). This approach, however, is hampered by the frequent failure of mangrove seedlings to established due to wave action (Teas, 1977). Therefore, a cost effective method is required to reduce wave energy incident on the seedlings for a period of time long enough to allow the seedlings to establish a sufficiently strong root system enabling them to withstand the locally expected wave action. As wave energy is only required to be reduced for a period of time, any structure developed is, therefore, only temporary.

There are many approaches used to attenuate ocean surface waves. Many of these involve the dissipation of wave energy through interactions between the wave motion and a structure. These methods include, but are not limited to, arrays of vertical cylinders, vegetation planted on the seabed and many varieties of floating breakwaters including scrap tyres (Kakuno *et al*., 1996; Kobayashi *et al*., 1993; McCartney, 1995). One such floating breakwater design, the Y-frame design (Mani, 1991) and its latest modification known as the cage system (Murali and Mani, 1997)

has proven to be efficient in terms of performance, cost, installation, and eco-friendliness. Other designs of floating tyre breakwaters cost as little as the cage system but can accumulate debris and litter (Nece *et al*., 1988). However, most floating breakwater designs operate in water depths of over 2 m and use a metal anchor and mooring system. Thus the problem of deterioration due to corrosion is inevitable, as is wear and tear due to the relentless wave action, which increases maintenance costs. In this Chapter, a method for temporarily attenuating wave energy is proposed which utilises the use of bamboo poles.

In many developing countries, such as Indonesia, people living near the coasts use bamboo for housing, furniture, bridges, and rafts. Bamboo has also found application in aquaculture ponds for construction and for caging mangrove seedlings in nursery areas. The extensive usage of bamboo in developing countries is mainly based on its strength, and its availability at all times at minimum cost. In recent times, bamboo and PVC pipes have been used in a method known as the "Riley encasement" for protecting mangrove seedlings planted along coasts with high wave energy (Kent and Lin, 1999). These tubular casings protect the seedlings from the harsh external environment, including wave attack, until the seedlings reach a stage where they become self-supportive (Riley and Kent, 1999). Even though the encasement stimulates plant growth by reducing UV light, the method creates dwarf plants due to the root systems being limited by the space available within the casing. Another problem that may be encountered is the collapse of the casings erected on an erosive shoreline due to wind and waves.

In this Chapter, the use of bamboo as a means for temporarily attenuating waves is presented. The degree of wave attenuation is computed with the numerical model developed in Chapter 4, and the attenuation performance of several bamboo densities and diameters are evaluated. The width of the bamboo barrier and the cost incurred for attenuating 50 % of incident wave energy are calculated. The performance and cost are then compared with those of conventional floating breakwaters. Finally, the depth of embedment of the bamboo required to avoid dislodging and scouring is discussed.

6.2 Material and Methods

Figure 6.1 shows the simple design of a bamboo wave attenuation method. A large number of bamboo poles are inserted into the sediment in a band offshore from the mangrove seedlings requiring protection. The wave-induced forces on individual poles are small, as is the attenuation due to individual poles. However, by using a dense matrix of bamboo poles, significant attenuation of wave energy can be achieved.

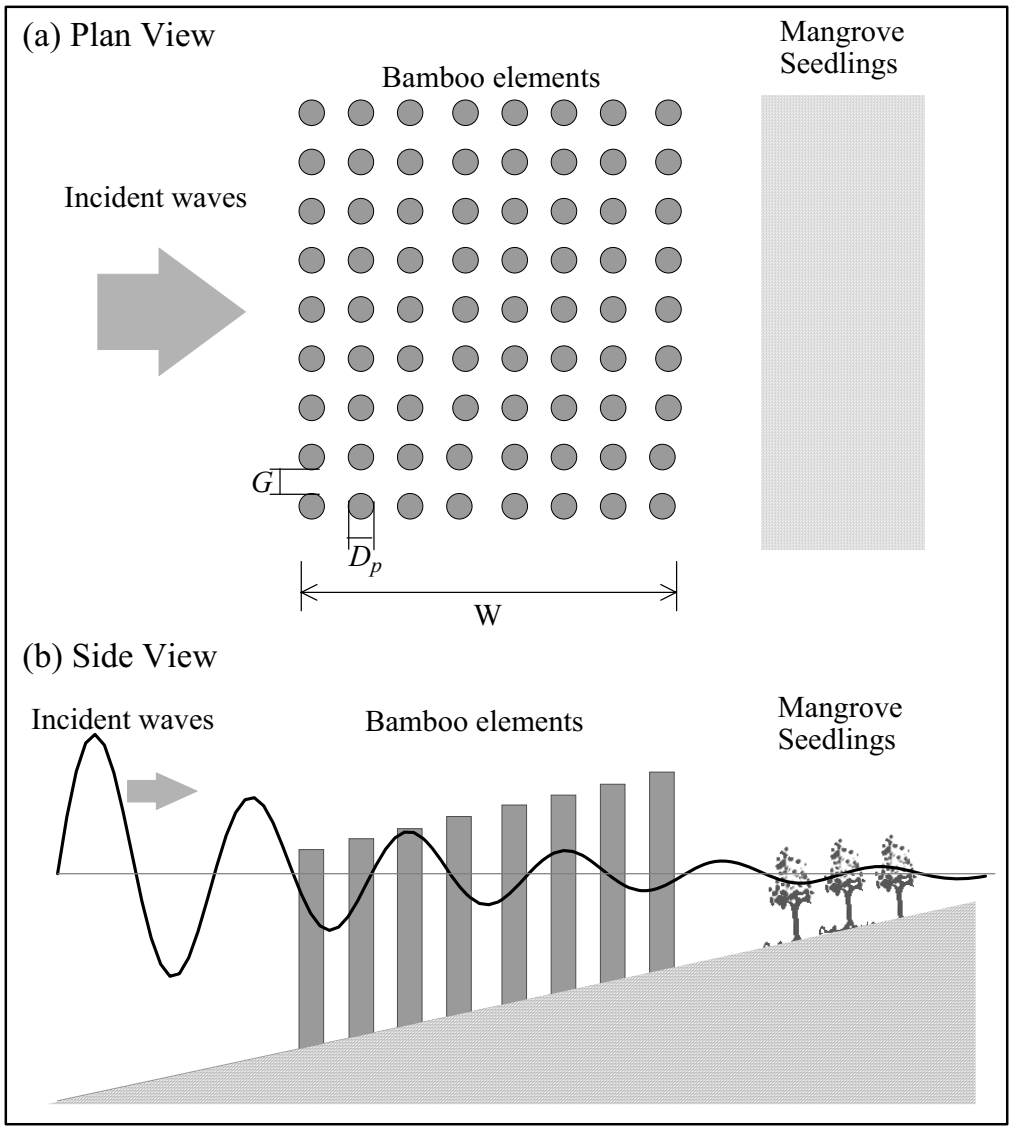

Figure 6.1 Outline of the bamboo wave attenuator design. The bamboo elements embedded on a sloping seabed occupy a band of width W along a given length of coastline. The bamboo diameter is D_p and the gap between adjacent elements is G.

6.2.1 Material

Bamboo was investigated as a suitable material for a low cost, efficient, temporary wave attenuator design because it possesses the following properties: it is flexible yet strong, abundant, renewable, ecologically harmless, and low cost. As an indication of the strength and flexibility of bamboo, bamboo homes were reported to have survived a 6.7 magnitude earthquake in Costa Rica (Stevens, 1994). Bamboo is also completely biodegradable and thus is safe to be used in any environment (Kent and Lin, 1999). Finally, bamboo is renewable, easily cultivated and the cost is very low. For example, a bamboo culm of 9 m length can be purchased for 6000 rupiahs (Indonesian currency), or approximately US$ 0.75 (Lidemar, personal comm.).

6.2.2 Methods

Modelling Wave attenuation

The theoretical performance of the proposed bamboo structure in its ability to attenuate wave energy was evaluated using the numerical model presented in Chapter 4. Whilst this model was initially developed to investigate the attenuation of waves propagating through mangrove forests, the model found immediate application to this problem, due to the general approach used in the description of both the bathymetry and the characteristic vegetation parameters. It is appropriate now to recall a number of features of the model relevant to its application to this specific problem. Firstly, that the model is formulated based on the number of vegetation elements in a known control volume and knowledge of exact positions of individual vegetations element is not necessary. Further, as a simplifying assumption, the model represents vegetation elements as vertical cylinders, much like the real structure of bamboo. Finally, drag force is assumed to be the dominant wave-induced force acting on the vegetation elements and inertial forces are assumed to be minimal and are neglected. It will be demonstrated later that this assumption is justified in this application of the model. Thus the model is ideally suited to test various scenarios of bamboo size and spatial density in the evaluation of the performance of the proposed design of a bamboo structure for the attenuation of wave energy.

Numerical calculations were performed for bamboo inserted such that each element extended a height of 1 m above the sea bed in a total water depth of 2 m. The bed was defined as having a slope of 0.01, shallowing towards the shoreline. This bed slope is typical of gently shoaling shorelines of tidal mudflats (pers. obs.). Calculations were made for spatial densities of: 1, 2, and 4 bamboo elements per m^2 and for bamboo diameters of: 2, 4, and 8 cm. The first two diameters can be obtained practically by splitting a bamboo culm of diameter 8 cm. The arrangements of bamboo were subjected to waves conforming to a typical spectrum for shallow water (Massel, 1996) with significant wave height, H_s, and peak period, T_p, of 1 m and 4 s respectively,

Depth of embedment

To determine the appropriate insertion depth of the bamboo into the bed, several factors must be considered. Firstly, the lateral force acting upon each bamboo with particular spatial density must not be too large otherwise the bamboo will be dislodged. The numerical model was used to estimate the magnitude of the force caused by waves of given characteristics on the bamboo poles. A field experiment was also conducted to determine the threshold magnitude of the force that will cause dislodgment of the bamboo. The experiment is described in Figure 6.2, and involved embedding a cylinder of diameter 7 cm into a highly unconsolidated mud-bank to a known depth. The mud bank was sufficiently soft that a person walking on the surface would sink 50 to 75 cm. A lateral force was applied to the cylinder by pulling horizontally back and forth a string attached to a spring-balance, itself attached to the pipe. The force that caused cracks on the mud surface was taken as the threshold force and was read from the spring balance scale. Several embedment depths and positions of the lateral force along the pipe were tried.

Secondly, scouring around the base of the bamboo may also lead to dislodgement. Scouring around groups of piles has been studied extensively, and it has been demonstrated that the scour depth depends on the Keulegan-Carpenter (*KC*) number and on the ratio between gap spacing of adjacent piles, *G,* and the pile diameter, D_p (Sumer and Fredsoe, 1998). The *KC* number is defined as

$$KC = \frac{U_m T_p}{D_p} \tag{6.1}$$

where U_m is the maximum horizontal water particle velocity and T_p is the wave period. Using linear Airy theory (Chakrabarti,1991) this velocity is

$$U_m = \frac{gH_s T_p}{L} \tag{6.2}$$

where g is the gravitational acceleration, L is the wavelength. Wavelength is calculated based on T_p, H_s, and water depth, d (Hallam *et al*., 1977). The larger the KC number and the smaller the ratio G/D, the greater the scour depth.

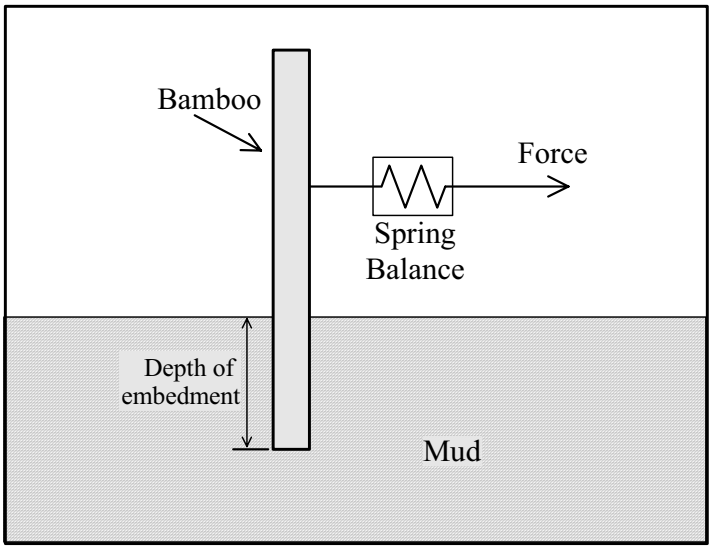

Figure 6.2 Experimental design for measuring the threshold lateral force on a length of bamboo embedded into a mud-bank. Parameters that are measured are (i) the amount of force that produces cracks on the mud surface, (ii) the height at which the force is applied, relative to the mud surface, and (iii) the embedment depth.

Drag force dominance

As described in Chapters 3 and 4 the numerical model assumed that drag force dominates over inertia force. The former force relates to the fluid velocity while the later relates to the fluid acceleration. It has been shown that if a KC number of the wave-structure system is greater than 30, then the drag force is dominant (Li and

and Ye, 1990). Another way of determining the dominant force is by calculating the ratio between bamboo diameter, *D,* and orbit width, *O,* of the water particle (Hallam *et al*., 1977). The orbit width is

$$O = \frac{H_s}{\tanh(kd)} \tag{6.3}$$

where k is the wave number ($= \frac{2\pi}{L}$). If the ratio D/O is less than 0.2, drag also dominates (Hallam *et al*., 1977).

6.3 Results and discussions

6.3.1 Wave attenuation and cost

Results of the wave attenuation for the three different spatial densities (1, 2, and 4 bamboo elements per m^2) and for the three different bamboo diameters (2, 4, and 8cm) are presented in Figure 6.3, which show the normalised energy, (*i.e.* ratio between transmitted and incoming wave energy) plotted against the width of the bamboo attenuator. Expectedly, numerical calculations predicted that the larger the diameter and the higher the spatial density of bamboo, the greater the wave attenuation. This is to be expected since energy dissipates more with increased obstructions to the flow and hence increased drag. Results also show that total wave attenuation increases with increasing width of bamboo band.

From Figure 6.3, the width needed to attenuate 50 % of the incident wave energy for a particular spatial density and bamboo diameter can be estimated. This criterion was also used when designing floating breakwaters (Murali and Mani, 1997). The results are shown in columns 1-3 of Table 6.1. For instance, 50 % attenuation is achieved by a width of 90 m of bamboo barrier for a spatial density of 1 bamboo stake per m^2 and a bamboo diameter of 4 cm.

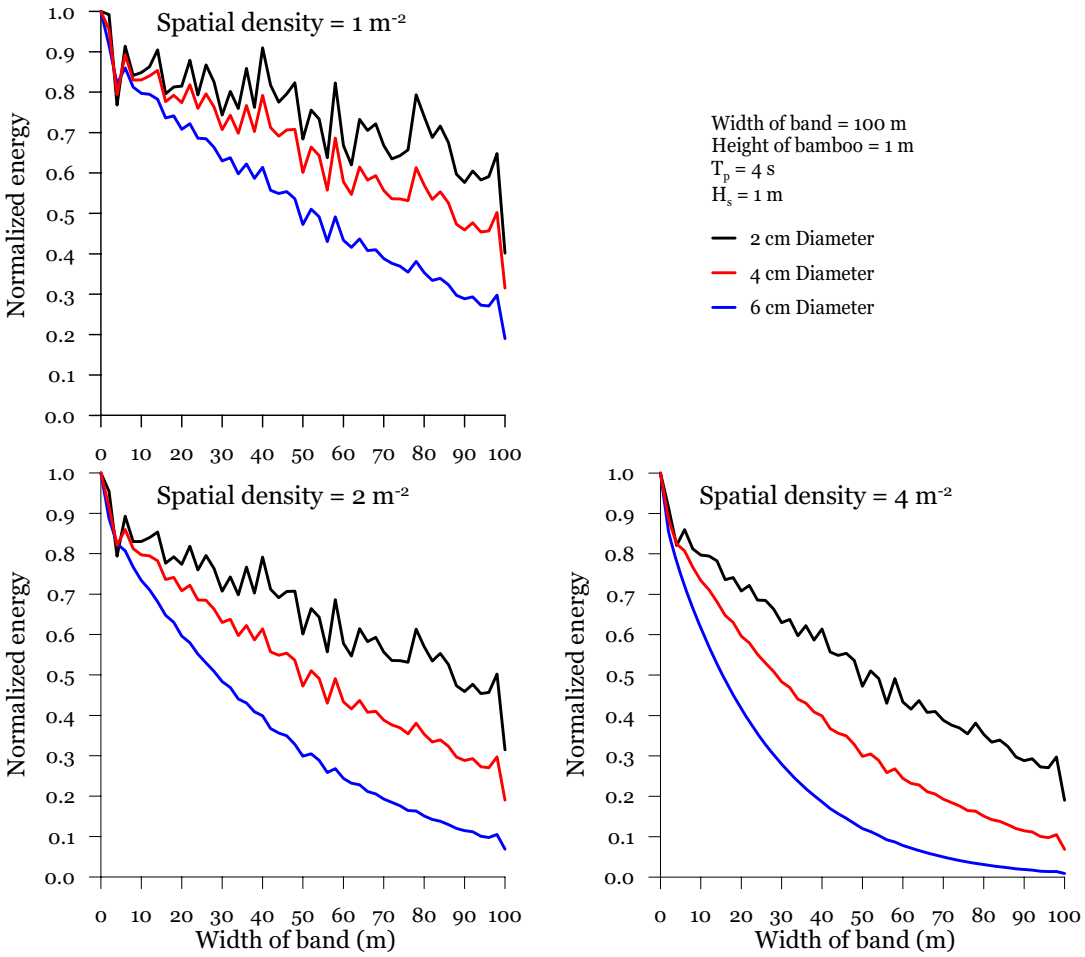

Figure 6.3 Computed normalized wave energy versus width of band for various spatial densities and bamboo diameters. Normalized energy is the ratio of local and incident wave energy.

Table 6.1 Width and cost needed to attenuate 50 % of incoming wave energy. Columns 4, 5 and 6 are based on a 100m-length of protected coastline.

Spatial density per m^2	Diameter (cm)	Width of band (m)	# bamboo stakes	Bamboo cost (US$)	Installation Cost (US$)	Total cost per m (US$)
Column 1	2	3	4	5	6	7
1	4	90	9 000	1 350	2 700	40.5
	8	50	5 000	750	1 500	22.5
2	2	90	18 000	2 700	5 400	81.0
	4	60	12 000	1 800	3 600	54.0
	8	30	6 000	900	1 800	27.0
4	2	50	20 000	3 000	6 000	90.0
	4	30	12 000	1 800	3 600	54.0
	8	15	6 000	900	1 800	27.0

Consider now a 100 m length of coastline to be protected. Having estimated the width (Table 6.1, column 3) and the amount of bamboo elements (Table 6.1, column 4) needed for 50 % wave attenuation, a cost is determined. This calculation is performed using the fact that 5 stakes are obtained from a 9-m long culm of bamboo, *i.e.* the minimum length of each stake is 1.5 m. Each culm costs 6000 Indonesian rupiahs or US$ 0.75. The cost of bamboo needed for each spatial density is shown in Table 6.1, column 5. An estimated installation cost for implanting the stakes is also computed (*i.e.* US$ 6 per 20 stakes in, column 6). The cost has been estimated by Dr H. Halide (pers. comm.) and covers renting a boat and 2 crew members, estimated at US$ 50 and US$ 10 per day, respectively. This is expected to allow planting 200 stakes per day. In this calculation, it is considered that 1 day is equal to 10 working hours. The total cost in US$ per m is given in Table 6.1, column 7. It is found that that for each density, the cheapest design is obtained by using a bamboo diameter of 8 cm.

The cost of the bamboo attenuator is found to be as low as US$ 22.5 per m, whilst scrap tyres (Bishop, 1982) and Y-frame structures (Mani, 1991) cost about US$ 1,300 and US$ 1,340 per m, respectively. The performance of these three designs is illustrated in Figure 6.4, where the transmission coefficient, K_t, defined as the ratio between the local and incident wave energy, is plotted against the design parameter

W/L (width of band divided by wavelength). For the bamboo design, a diameter of 8 cm is used. Note that results for each system were obtained for waves with different periods. Figure 6.4 shows that the bamboo design has a capability to attenuate more wave energy than the other two methods, which are limited by their size, due to high costs. The ability of each type of attenuator to withstand extreme weather associated with tropical depressions is not known, but should be considered when estimating cost effectiveness.

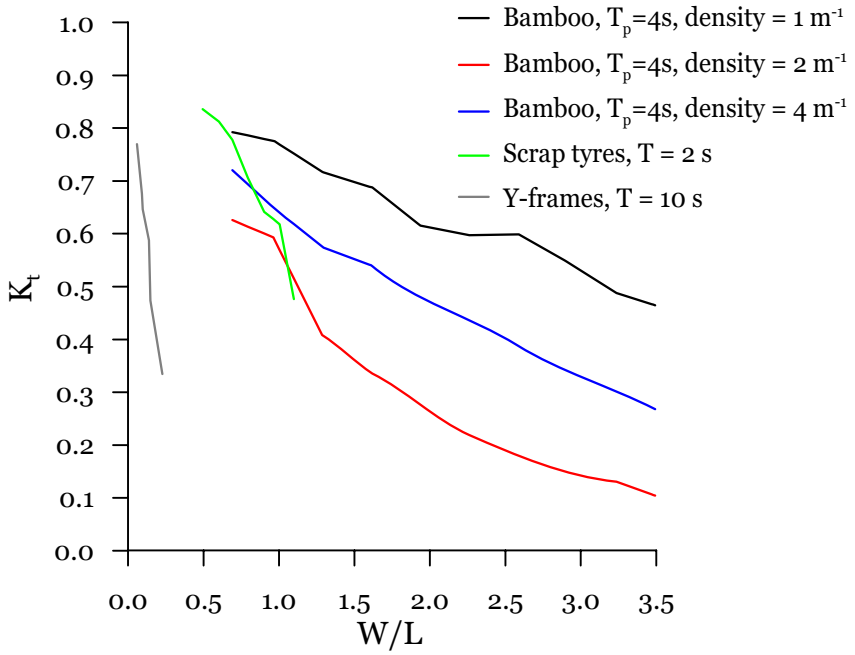

Figure 6.4 Illustration of the performance, in terms of the transmission coefficient, K_t, for several floating breakwaters and the bamboo design presented in the present study.

6.3.2 Embedment

Given a spatial density and diameter, the numerical model was used to estimate the magnitude of the horizontal forces acting on the bamboo. Before proceeding, it is appropriate to validate the assumption that drag force dominates over inertial force. Based on wave characteristics T_p and L of 4 s and 15.5 m, respectively, and using a significant wave height, H_s, of 1 m in Equation (6.2), the resulting KC number is 32.25. This value is greater than 30, which indicates that drag force dominates over

inertial force. Further, the *D/O* ratio in Equation (6.3) is 0.04, which also indicates that the drag force dominates.

Drag forces were estimated for a 50m wide band of bamboo, with a spatial density of 4 bamboo elements per m^2, and a bamboo diameter of 4 cm and 8 cm. The estimates of these forces resulting from a wave height of 1 m are presented in Table 6.2. Results from the field experiment carried out to define the lateral force required to dislodge a bamboo element are given in Table 6.3. From Table 6.2 and Table 6.3, it is suggested that in order to avoid dislodgment of bamboo elements by waves, depth of embedment should be no less than 60 cm.

Table 6.2 Estimated forces on lengths of bamboo of different diameters at several locations within the bamboo band. Position is given as distance from the seaward extent of the band: Seaward = 0 m, Middle = 25m and Landward = 50 m.

Diameter (cm)	Position	Force (N)
4	Seaward	9.3
	Middle	5.6
	Landward	4.7
8	Seaward	17.6
	Middle	7.3
	Landward	3.3

To investigate potential scouring around the bamboo elements, consider now the case of a spatial density of 4 bamboo elements per m^2 with a bamboo diameter of 8 cm. The ratio between scouring depth, *S*, and pile diameter, *D,* against the ratio between the gap and pile diameter *G/D*, has been studied for *KC* values of 13 and 37 (Sumer and Fredsoe, 1998). The ratio *S/D* for a *KC* number of 13 is less than that for *KC* = 37. For instance, for *KC* = 13 and 37, and ratio *G/D* of 1.5, the scouring depth over pile's diameter *S/D* is 0.3 and 0.67, respectively. For the present case, with a *KC* number of 32.25, this ratio should be a little less than 0.67. Using the ratio *S/D* = 0.67 implies that in order to avoid scouring, the depth embedment has to be much deeper than 0.67 × 8 cm, *i.e*. 5.36 cm. This depth is only one-tenth of that required to avoid dislodgment. Thus, in order to avoid both dislodging and scouring, the bamboo element should be implanted no less than 60 cm into the bed.

Table 6.3 Embedment depth of bamboo and the corresponding lateral threshold force for 4 cm and 8 cm diameter bamboo elements

Depth of embedment (cm)	Location of the applied force above the bed (cm)	Breaking force (N)	
		4 cm	8 cm
50	50	6.5	14.0
60	50	11.5	24.5
70	50	15.0	30.5

6.4 Summary

A low cost design for temporarily attenuating wave energy in shallow water is presented. The design uses bamboo elements driven into the seabed at various spatial densities. Bamboo is chosen for the design as it is strong, flexible, abundant, biodegradable and relatively inexpensive. The performance of the design in attenuating incoming wave energy was evaluated using the numerical model presented in Chapter 4. Various spatial densities of bamboo with a range of diameters were used in the model to evaluate the attenuation of incident wave energy. The cost of a design capable of attenuating up to 50% of the incident wave energy was estimated. For 50 % attenuation, the cost obtained can be as low as US$ 22 per metre for bamboo elements of diameter of 8 cm and spatial densities ranging from 1 to 4 bamboo elements per m^2. This cost per metre is much cheaper than that for floating breakwaters using scrap tyres (US$1,300 per m) and Y-frames (US$1,340 per m). The minimum depth of embedment of the bamboo element into the bed to avoid dislodging was determined to be 60 cm. The minimum depth of bamboo embedment to avoid scouring (5 cm) was found to be much smaller than the minimum depth for dislodging to occur. Hence to avoid dislodging and scouring in the lowest cost design mentioned earlier, the depth of embedment should be no less then 60 cm.

The practicality of a method utilizing bamboo as described here, using for example a 15 m wide strip with 4 bamboo elements per m^2, would be dependant on the site chosen. On the relatively sheltered western shoreline of South Sulawesi, for example, this method would prove logistically practical and easy to install due to

the availability of bamboo, suitable vessels and the micro tidal range. However, even for small (100 m) section of coast, the US$2200 cost is likely to prove prohibitive for general application.

To the author's knowledge the system described in this paper has not been evaluated experimentally. The analysis presented in this work would have to be modified to cater for the field conditions at a particular locality. This is because bed-slopes, and typical wave heights and periods are unlikely to correspond exactly with those used in the calculations presented here. Further, differing field areas will have different sediment properties and thus will require varying embedment depths. Nevertheless, the theoretical analysis presented here indicates that a field trial using this methodology is warranted.

7 SUMMARY AND CONCLUSIONS

7.1 Summary

Mangroves are inter-tidal wetland ecosystems composed primarily of woody halophytes living at the confluence of the marine and terrestrial environments, generally in sheltered coastal and riverine areas with medium to low wave energy climates favorable to the deposition of fine sediment. Mangroves have adapted to this environment of soft, saline, oxygen-deficient soils in a number of unique ways, one of which is the above-sediment root system exhibited by many mangrove species as a means of increasing their oxygen supply and providing structural stability. The above-sediment components of mangrove root system comprise the roots and pneumatophoras, which together with the tree trunk and buttresses form a complex tangled network of woody, rigid vegetation above the forest floor. These densely interwoven trunks and roots of mangrove vegetation influence and modify the local circulation and hydrodynamics processes, and other processes driven by the hydrodynamics.

Mangroves forests that are exposed to significant wave action act as an energy-reducing buffer by dissipating surface wave energy and reducing the risk of shoreline erosion. The dissipation of wave energy is due primarily to the interaction of the wave motion with the submerged vegetation elements, and the most obvious manifestation of the dissipation is in the reduction of the surface wave height. A reduction in wave energy is accompanied by a reduction in the risk of shoreline erosion, which has significance in the area of coastal protection and suggests that, in appropriate circumstances, reforested mangroves could be employed as a coastal protection measure. The ability of mangrove forests to dissipate surface wave energy has, however, received very limited research interest.

This thesis presents field and theoretical investigations of the attenuation of random, wind–induced surface wave energy in mangrove forests. Field observations of wave processes in mangrove forests were undertaken at three study sites in Northern Australian and at Iriomote Island, Japan. Field sites were chosen to span the low to

medium wave energy environments favoured by mangroves. At each of the three study sites, an instrumented observational array was established along a transect through the mangrove forest, with the direction of the transect aligned with the dominant direction of the incident waves, thus ensuring the observation of wave transformations in the direction of propagation of dominant wave energy.

Observations of wave processes in mangrove forest revealed a number of key effects of mangrove vegetation on the propagation of random wind-induced gravity waves through mangroves, common to all study sites: Firstly, there was substantial attenuation of wave energy with distance into the forest. Mean rates of the reduction in total wave energy at the study sites ranged from 63.7% to 94.7%. This translated to mean rates of reduction in significant wave height per metre of vegetation of between 0.24% m^{-1} and 2.37% m^{-1}. For comparison, Mazda *et al*. (1997a) observed rates of wave reduction of up to 20% per 100 m of vegetation in a reforested mangrove area. Secondly, energy transmission into the forest was shown to increase with an increase in water depth, due to the vertically non-uniform structure of the mangrove trunks and roots and their obstruction to water flow, which decreases with distance above the sea bottom. Thirdly, data suggest an increase in the mean period with distance into the forest, suggesting preferential attenuation of shorter period (higher frequency) waves within mangrove forests. The preferred attenuation of higher frequency waves has also been observed in wave transformations over vegetated salt marshes (Möller *et al*., 1999).

Two theoretical approaches were developed to investigate the propagation of random, wind–induced surface wave energy in mangrove forests. In both cases a spectral method was adopted to describe the evolution of the wave spectrum within the forest. Spectral methods provide sufficient information to describe the most relevant parameters of the wave field, whilst not explicitly describing the sea-surface as a function of space and time, which is computationally demanding.

The first of the theoretical approaches was, for simplicity, developed based on the assumption of uniform horizontal bathymetry within the forest. The approach adopted was to describe the wave motion in terms of spectral qualities by a defining set of amplification factors in front of, within and behind the forest. These

amplification factors describe spectral components propagating in the positive and negative directions and account for energy transmission, reflection and dissipation. Energy dissipation is controlled by the drag force imposed on the vegetation. The complex and random nature of mangroves makes it extremely difficult to represent this vegetation exactly in a theoretical model. Therefore the vegetation was parameterized based on a number of representative characteristics, and was represented in the model by an idealized structure of two layers of vertical cylindrical elements with different diameters and number of elements in each layer. The bottom and top layers are representative of the root and trunk dominant sections of the mangrove structure, respectively. The total drag force is calculated based on the vegetation characteristics of both the top and bottom layers of vegetation.

Due to the high spatial density of mangrove vegetation, a modified drag co-efficient was employed to introduce the dependence of the drag coefficient on the vegetation density. Interactions that affect the drag coefficient take place at the scale of the vegetation elements, and take the form of vortices that are created on the downstream side of the obstacle and form a wake that intercepts obstacles further downstream. As such, a discrete vortex method was used investigate the effects of vegetation density for a number of densities common to mangrove forests.

Non-linear governing equations were linearised through a process which seeks to substitute a linear term for the non-linear term, under the constraint that the mean error due to the substitution is minimized. Such a procedure is widely used in ocean engineering for the determination of forces on off-shore structures.

As the course of this study progressed, a second theoretical approach was developed for the case of wave propagation through a forest with an arbitrary bathymetry profile. In this case the wave motion in the vicinity of the forest was described by a complex wave amplitude that is a solution to the mild-slope equation which incorporates effects of both the vegetation and non-uniform bathymetry. As done in the first theoretical approach, drag force imposed on the vegetation controls energy dissipation, a modified drag coefficient is used, and the linearisation procedure is again employed. In contrast to the first theoretical approach, non-propagating evanescent modes are neglected and only progressive waves are taken into account.

This second approach effectively supercedes the initial theoretical approach that neglected variations in bathymetry. However the two approaches converge for the case of a uniform bathymetry profile. A computational model was constructed for each theoretical approach.

Key effects of mangrove vegetation on the propagation of random wind-induced gravity waves, as identified from the field data, were used to assess the performance of the two computational models. Both models were able to qualitatively reproduce the key features described above as demonstrated by predictions of: (i) wave energy spectra at locations within the forest; (ii) the reduction in total wave energy within the forest; and (iii) the coefficients of energy transmission and dissipation.

The performance of the more general computational model developed for a mangrove forest of arbitrary bathymetry was verified directly against field data, with the model configured with input parameters (such as bathymetry, incident wave energy spectra and vegetation characteristics) determined from the field data. Results from these verification calculations demonstrated general qualitative and quantitative agreement with the field data. In situations where model results and field data did not display high levels of quantitative agreement, it should be noted that vegetation parameters within the model are applied over the whole forest; i.e. the vegetation structure is assumed constant through out the whole forest. However, mangrove forests are typically comprised of more than one species of mangrove vegetation, and as such, vegetation density is not constant with distance into the forest.

Through analysis of the sensitivity of the models to vegetation characteristics and forest bathymetry, it was demonstrated that the interaction of the fluid with the mangrove vegetation is the dominant mechanism for energy dissipation. Given that the models use only a limited number of representative variables to describe the vegetation within the forest, the results are very encouraging.

The model was validated for incident waves of low to medium energy. The performance of the model to accurately predict the attenuation of incident wave

energy during extreme wave events outside of the normal wave energy envelope was not attempted due to insufficient validation data for such conditions. Such extreme events are likely to occur during tropical cyclones (typhoons) and observations from the literature suggest that under such conditions, extreme wave energy, coupled with storm surge, may greatly increase the inundation levels of exposed mangroves, such that the vegetaion canopy (assumed to remain above water in the present models) is also submerged. This increased inundation will effectively increase the overall density of the submerged vegetaion and as such wave energy will still be reduced. However, with increases in both incident wave energy and water level, wave energy would be expected to propagate greater distances into (or through) the forest, increasing the risk of shoreline erosion landward of the mangroves. Further, increased velocities associated with larger wave heights may exceed thresholds for re-suspension of the sediments within the mangrove forests, thus reducing the stability of the vegetation which may lead to structural collapse. As a suggestion for further research, parameters controlling the stability of mangroves could be investigated, and coupled with model predictions of wave height and wave-induced velocities in order to assess the risk posed to mangroves by storms of various magnitudes.

7.2 Conclusions

There is scope for the theoretical approach presented in this thesis to be improved through a more realistic representation of the mangrove vegetation. For example, mangrove roots are, in general, not vertical as simplified in the models. However, drag force is calculated based on the projected area of the vegetation presented to the flow, and thus increasing the sophistication of the vegetation parameterisation is unlikely to significantly alter the model calculations. Mangrove forests are structurally very complex, and any approach to predict wave process within this environment will need to make numerous assumptions, as done here, in order to parameterise the vegetation. However, given the performance of the models presented in this thesis, increasing the sophistication of the vegetation parameterisation may not necessarily be warranted. It would be advantageous, however, to extend the model to allow vegetation characteristics to vary with distance into the forest.

The advances in modelling wave propagation through emergent vegetation presented in this study found immediate application in the design and performance evaluation of a simple, temporary and cost effective means for protecting mangroves seedlings replanted along wave exposed coastlines as part of coastal rehabilitation efforts. The design utilises bamboo elements driven in to the seabed at various spatial densities. Computations of predicted attenuation of wave height were performed for various spatial densities of bamboo with a range of diameters in order to evaluate the attenuation of incident wave energy. The cost of a design capable of attenuating up to 50% of the incident wave energy was estimated to be as low as US$ 22 per metre, which is significantly cheaper than that for two accepted low-cost measures.

This thesis increases the understanding of smaller-scale physical processes in mangrove forests. This study builds on the limited understanding of wave processes in mangroves, through the first co-ordinated field and theoretical investigation of wave processes in naturally occurring mangrove forests. With increasing interest in the conservation and rehabilitation of the coastal zone and mangrove forests in particular, it is hoped that the progress made in modelling wave propagation through mangrove forests will find purpose and application in the preservation and rehabilitation of these ecosystems.

8 REFERENCES

Abramowitz, M. and Stegun, I.A. 1968. Handbook of mathematical functions with formulas, graphs and mathematical tables. *Dover Publ., New York*, 1046 pp.

ADB. 1993. ADB report, Proposed Sulawesi Mangrove Investment Project, vol. 1.

Alongi, D, M., 2002. Present state and future of the world's mangrove forests. *Environmental Conservation. Vol.* 29(3):331—349.

Asano, T., Deguchi, H. and Kobayashi, N. 1992. Interaction between water waves and vegetation. *Proceedings of the 23rd Coastal Engineering Conference,* Vol. 3: 2710–2723.

Bandaranayake, W. M. 2002. Bioactivities, bioactive compounds and chemical constituents of mangrove plants. *Wetlands Ecology and Management,* Vol 10: 421–452,

Barbier, E.B. 2003. Habitat-fishery linkages and mangrove loss in Thailand, *Contemporary Economic Policy*, Vol. 21: 59–77.

Berkhoff, J.C.W., 1972. Computation of combined refraction-diffraction. *Proceedings of the 13th Coastal Engineering Conference*, Vol1: 471–490

Bishop, C.T. 1982. Floating tire breakwater design comparison. Mangroves as land-builders, *Journal of Waterway, Port, Coastal and Ocean Engineering*, Vol. 108: 421–426.

Brinkman, R.M., Massel, S.R., Ridd, P.V. and Furukawa, K. 1997. Surface wave attenuation in mangrove forests. *Proceedings of the 13th Australasian Coastal and Ocean Engineering Conf.,* Vol. 2:941–946.

Chakrabarti, S.K. 1991. Wave forces on offshore structures. In: J.B. Herbich (Ed.) *Handbook of Coastal and Ocean Engineering,* Vol. 2:1–54.

Chorin, A.J. 1973. Numerical study of slightly viscous fluid, *Journal of Fluid Mechanics*, Vol.57:785–796.

Cohen, J.E. and Small, C. 1998. Hypsographic demography: The distribution of human population by altitude. *Proc. Natl. Acad. Sci. USA,* Vol. 95: 14009–14014.

Cohen, J.E., Small, C., Mellinger, A., Gallup, J. & Sachs, J. 1997. Estimates of coastal populations. *Science,* Vol 278: 1211–1212.

Conacher, C.A., O'Brien, C., Horrocks, J.L., and Kenyon, R.K. 1996. Litter production and accumulation in stressed mangrove communities in the Embley River Estuary, North-eastern Gulf of Carpentaria, Australia, *Journal of Marine and Freshwater Research,* Vol. 47:737–743.

Das, P., Basak, U. C. and Das, A. B. 1997. Restoration of the mangrove vegetation in the Mahanadi delta, Orissa, India. *Mangroves and Salt Marshes,* Vol 1: 155–161.

De Graaf, G.J., and Xuan, T.T. 1998. Extensive shrimp farming, mangrove clearance and marine fisheries in the southern provinces of Vietnam, *Mangroves and Salt Marshes*, Vol. 2:159–166.

Department of Environment 1997. Wave data recording program, Townsville region, 1975-1997.Conservation report No. W03.3, *Queensland Government*, 42 pp.

Dierberg, F.E., and Kiattisimkul, W. 1996. Issues, impacts, and implications of shrimp aquaculture in Thailand, *Environmental Management*, Vol. 20: 649–666.

Dingemans, W.M., 1985. Evaluation of Two-Dimensional Horizontal Wave Propagation Models. *Delft Hydraulics Laboratory Report.* W301, 117pp.

Dubi, A. and Torum, A. 1994. Wave damping by kelp vegetation. *Proceedings of the 24th Coastal Engineering Conference, Kobe,* Vol. 1: 142–156.

Edwards, M. S. 1998. Effects of long-term kelp canopy exclusion on the abundance of the annual alga *Desmarestia ligulata* (Light F). *Journal of Experimental Marine Biology and Ecology,* Vol 228: 309–326.

Ellison, A.M. 2000. Restoration of Mangrove Ecosystems. *Restoration Ecology,* Vol 8(3): 217–218.

Elwany, M.H.S., O'Reilly, W.C., Guza, R.T. and Flick, R.E. 1995. Effects of southern Californian Kelp beds on waves. *Journal of Waterway, Port Coastal and Ocean Engineering,* Vol 121(2): 143–150.

Fonseca, M.S. and Cahalan, J.A., 1992. A preliminary evaluation of wave attenuation by four species of seagrass. *Estuarine, Coastal and Shelf Science,* Vol 35: 565 –576.

Furukawa, K. and Hosokawa, Y. 1996. Parameter fitting on a discrete vortex method with wake simulation behind an inclined flat plate. *Computational Fluid Dynamics Journal,* Vol. 5(1): 89–105.

Furukawa, K. and Wolanski, E. 1996. Sedimentation in mangrove forests. *Mangroves and Salt Marshes,* Vol. 1: 3–10.

Furukawa, K., Wolanski, E. and Mueller, H. 1997. Currents and sediment transport in mangrove forests. *Estuarine, Coastal and Shelf Science,* Vol. 44: 301–310.

Glaser, M. 2003. Interrelations between mangrove ecosystem, local economy and social sustainability in Caet´e Estuary, North Brazil. *Wetlands Ecology and Management,* Vol 12: 265–272.

Gudmestad, O.T. and Connor, J.J. 1983. Linearization methods and the influence of the nonlinear hydrodynamic drag force. *Applied Ocean Research,* Vol. 5: 184-194.

Hallam, M. G., Heaf, N. J., and Wootton, L. R. 1977. Dynamics of Marine structures. Report UR 8, *CIRIA UEG, London*, 319pp.

Hansen, E.A. and Arneborg, L. 1997. The use of a discrete vortex model for shallow water flow around islands and coastal structures. *Coastal Engineering,* Vol. 32: 223–246.

IPCC. 1995. Climate Change 1995, Impacts Adaptations and Mitigation of Climate Change: Scientific-Technical Analysis. *Cambridge University Press*, 878pp.

Jackson, G.A. 1984. Internal wave attenuation by coastal kelp stands. *Journal of Physical Oceanography,* Vol. 14:1300–1306.

Jackson, G.A. and Winant, C.D. 1983. Effect of a kelp forest on coastal currents. *Continental Shelf Research,* Vol. 2(1): 75–80.

Kakuno, S., Nakata, Y., and Liu, P. F-L. 1996. Wave forces on an array of vertical cylinders, *Journal of Waterway, Port Coastal and Ocean Engineering,* Vol.122: 147–149.

Kawahara, K. 1978. Study of flow past a circular by an invisid model. *Journal of the Physics Society of Japan,* Vol. 45 (1): 292–297.

Kent, C.P.S., and Lin, J. 1999. A comparison of Riley encased methodology and traditional techniques for planting red mangroves (Rhizopora mangle*), Mangroves and Salt Marshes*, Vol. 3:215–225.

Kirkman, H. 1997. Seagrasses of Australia, Australia: State of the Environment Technical Paper Series (Estuaries and the Sea), *Department of the Environment, Canberra*. 36pp.

Knudson, P.L., Brochu, R.A., Seelig, W.N. and Inskeep, M., 1982. Wave damping in *Spartina alterniflora* marshes. *Wetlands* 2: 87–104.

Kobayashi, N., Raichle, A.W. and Asano, T. 1991. Prediction of wave attenuation by vegetation and seaweed. Research Report CACR-91-07, *Centre for applied Coastal Research, University of Delaware, Newark*. 55pp.

Kobayashi, N., Raichle, A.W. and Asano, T. 1993. Wave attenuation by vegetation *Journal of Waterway, Port Coastal and Ocean Engineering,* Vol. 119(1): 30–48.

Laird, A.D.K. 1962. Water forces on flexible oscillating cylinders. *Journal.of Waterways and Harbors Division, ASCE,* Vol. 88(3): 125–137.

Laird, A.D.K. and Warren, R.P. 1963. Groups of vertical cylinders oscillating in water. *Journal of Engineering, Mechanichal Division, ASCE,* Vol. 89(1): 25–35.

Larcombe, P. and Ridd, P.V. 1994. Data interpretation. In: Benson LJ, PM Goldsworthy, IR Butler& J Olivern (eds). Townsville Port Authority Capital Dredging Works 1993: Environmental Monitoring Program. *Townsville Port Authority, Townsville*. 165–194.

Larcombe, P., Ridd, P.V., Prytz, A. and Wilson, B. 1995. Factors controlling suspended sediment on inner-shelf coral reefs, Townsville, Australia, *Coral Reefs*, Vol 14:163-171.

Leonard, A, (1980). Vortex method for flow simulation, *Journal of Computational Physics*, Vol.37:289–335.

Li, Y., and Ye, Z. 1990. Random wave and current force on vertical cylinder, *Applied Ocean Research*, Vol.12: 126–133.

Losada I.J., Silva R. and Losada, M.A. 1996. Interaction of non-breaking directional random waves with submerged breakwaters. *Coastal Engineering,* Vol 28(4): 229–248.

Losada I.J., Silva R. and Losada, M.A. 1997. Effects of reflective vertical structures permeability on random wave kinematics. *Journal of Waterway, Port, Coastal and Ocean Engineering*, Vol. 123: 338–346.

Lou, J. and Ridd, P. V. 1996 Wave-current bottom shear stress and sediment resuspension in Cleveland Bay, Australia. *Coastal Engineering,* Vol 29:169–186.

Lovas, S.M. 2000. Hydro-physical conditions in kelp forests and effect on wave damping and dune erosion: a case study on *Laminaria Hyperborea*. PhD Thesis. The Norwegian University of Science and Technology. Trondheim, Norway. 183 pp.

Lovelock, C. 1993. Field guide to the mangroves of Queensland, *Australian Institute of Marine Science*, pp 72.

Mani, J.S. 1991. Design of Y-frame floating breakwater, *Journal of Waterway, Port Coastal and Ocean Engineering,* Vol. 117: 105–119.

Massel, S.R. 1996. Ocean Surface Waves: their Physics and Prediction, *World Scientifc Pubishing, Singapore*, 491p.

Massel, S.R. and Butowski, P. 1980. Transmission of wind waves through porous breakwater. *Proceedings of the 17th Coastal Engineering Conference,* Vol. 3:333–346.

Massel, S.R. 1996. "*Wave motion in vegetated and non-vegetated coastal zones*", In *Coastal Dynamics '95: Proceedings of the International Conference on Coastal Research in Terms of Large Scale Experiments,* Gdansk, Poland, September 4-8, 1995. American Society of Civil Engineers, New York, 1-12.

Massel, S.R., Furukawa, K. and Brinkman, R.M. 1999. Surface wave propagation in mangrove forests. *Fluid Dynamics Research,* Vol 24, 219–249.

Mazda, Y., Magi, M., Kogo, M. and Hong, P. N. 1997a. Mangroves as a coastal protection from waves in the Tong King Delta, Vietnam. *Mangrove and Salt Marches,* Vol. 1(2):127–135.

Mazda, Y., Wolanski, E., King, B., Sase, A. and Ohtsuka, D. 1997b. Drag force due to vegetation in mangrove swamps. *Mangroves and Salt Marches,* Vol. 1(3): 193–199.

McCartney, B. L. 1995. Floating breakwater design, 111: 304–318.

Mendez, J.F. and Losada I.J. 1999. Hydrodynamics induced by wind waves in a vegetation field. *Journal of Geophysical Research,* Vol 104(C8): 18,383–18,396.

Möller, I. and Spencer, T. 2002. Wave dissipation over macro-tidal saltmarshes: Effects of marsh edge typology and vegetation change. *Journal of Coastal Research,* Vol 36:506–521.

Möller, I., Spencer, T. and French, J.R. 1996. Wind wave attenuation over salt marsh surfaces: Preliminary results Norfolk, England. *Journal of Coastal Research*.12, 1009–1016.

Möller, I., Spencer, T. French, J.R., Leggett, D.J. and Dixon, M., 1999. Wave transformation over salt marshes: a field and numerical modelling study from North Norfolk, England. *Estuarine, Coastal and Shelf Science, Vol*. 49: 411–426.

Morison, J.R.M., O'Brien, M.P., Johnson, J.W. and Schaaf, S.A., 1950. The force exerted by surface waves on piles. *Petroleum Transactions, AWME,* Vol. 189.

Murali, K., and Mani, J.S. 1997. Performance of cage floating breakwater, *Journal of Waterway, Port Coastal and Ocean Engineering,* Vol. 123: 172–179.

Nece, R.E., Nelso, E.E., and Bishop, C.T. 1988. Some North American experiences with floating breakwaters. *Proceedings of the conference Breakwaters '88, Inst. Civil Engineers, Eastbourne, 4-6 May 1998. Thomas Telford, London*: 299–312.

Ong, J.E. 1982. Mangroves and aquaculture in Malaysia, *Ambio,* Vol. 11: 252-257.

Pearce, F. 1999. An unnatural disaster, *New Scientist,* Vol. 6:12–12.

Petryk, S. and Bosmanjian III, G. 1975. Analysis of flow through vegetation. *Journal of Hydraulics Division,* ASCE, Vol. 101(7):871–884.

Press, W.H., Flannery, B.P., Teukolsky, S.A. and Vetterling, W.T. 1986. Numerical Recipes. *The Art of Scientific Computing. Cambridge University Press, Cambridge*, 818 pp.

Primavera, J.H. 1995 Mangroves and brackishwater pond culture in the Philippines, *Hydrobiologia,* Vol. 295:303–309.

Qureshi, T.M. 1990. Experimental plantation of rehabilitation of mangrove forests in Pakistan. *Mangrove Ecosystems Occasional Papers , UNESCO,* Vol. 4, 37 pp.

Riley, R.W., Jr., and Kent, C.P.S. 1999. Riley encased methodology: principles and processes of mangrove habitat creation and restoration, *Mangroves and Salt Marshes*, Vol. 3: 207–213.

Siddigi, N.A. and Khan, M.A.S. 1990. Two papers on mangrove plantations in Bangladesh. *Mangrove Ecosystems Occasional Papers , UNESCO,* Vol. 8, 19 pp.

SPM (Shore Protection Manual). 1984. *Coastal Engineering Research Center, U.S. Army Corps of Engineers, Washington*, Vol. I.

Stevens, J. 1994. Building with bamboo, *Technological Review*, Vol. 97: 17–19.

Stevenson, N.J., and Burbridge, P. R. 1997. Abandoned shrimp ponds: options for mangrove rehabilitation. Intercoast Network, March 1997: 13–16.

Sumer, B.M., and Fredsoe, J. 1998. Wave scour around a group of vertical piles, *Journal of Waterway, Port, Coastal and Ocean Engineering*, Vol. 124: 248–256.

Teas, H.J. 1977. Ecology and restoration of mangrove shorelines in Florida, *Environmental Conservation,* Vol. 4: 51–58.

Wolanski, E. 1994. Physical Oceanographic Processes of the Great Barrier Reef, *CRC Press, Boca Raton*, 194pp.

Wolanski, E., Jones, M. and Bunt, J.S. (1980). Hydrodynamics of a Tidal Creek-Mangrove Swamp System, *Australian Journal of Marine and Freshwater Research*, Vol. 31: 431-450.

Woodroffe, C. 1992. Mangrove sediments and geomorphology. In: Robertson, A.I. and Alongi, D.M.(*eds*.) *Tropical Mangrove Ecosystems*.*: American Geophysical Union, Washington DC, USA*. 7–41

APPENDIX A: SYMBOLS AND NOTATION

a	Wave amplitude
a_0	Incident wave amplitude
A	Wave amplitude
A	Projected area of submerged cylinder
A_i	Amplitude of components of sea surface displacement spectra
C	Phase velocity
C_g	Group velocity
C_d	Drag coefficient
$C_d^{(m)}$	Modified drag coefficient
C_m	Coefficient of Inertial
D	Diameter of cylinder
D_l	Diameter of mangrove trunks in lower layer
D_p	Diameter of bamboo cylinder
D_u	Diameter of mangrove trunks in upper layer
$E[x]$	Average of the variable x
E_{dis}	Dissipated wave energy
E_i	Incident wave energy
E_r	Reflected wave energy
E_t	Transmitted wave energy
E_{tot}	Total wave energy contained in the wave spectrum (J m^{-2})
f_e	linearisation coefficient
$\vec{F}$	Force vector
F_d	Drag force
F_i	Inertial force
$\vec{F}_l$	Total force per unit volume in lower layer

$\vec{F}_u$	Total force per unit volume in upper layer
g	Acceleration due to gravity
G	Function to describe variation in wave number due to water depth
h	Water depth
h_1	Water depth in front of mangrove forest
h_2	Water depth in mangrove forest
h_3	Water depth behind mangrove forest
H	Wave height
H_{max}	Maximum wave height
H_s	Significant wave height
i	Imaginary unit, $i = \sqrt{-1}$
I_0	modified Bessel function of the zero order
k	Wave number
k_i	Wave number in region i of fluid domain, i = 1,2,3
K	Drag modification factor
K_d	Coefficient of wave energy dissipation
K_{diss}	Coefficient of wave energy dissipation
K_h	Horizontal eddy viscosity
K_r	Coefficient of reflection of waves off the ocean/mangrove interface
K_t	Coefficient of transmission of wave energy through mangroves
KC	Keulegan-Carpenter Number
l	Width of mangrove forest
L	wavelength
L_m	Mean wavelength
M_α	Amplification factors of particular spectral components for wave numbers α

n_v	Volume porosity
n_p	Surface porosity
N	Number of vegetation per unit area
N_u	Number of mangrove trunks in upper layer
N_l	Number of mangrove trunks in lower layer
p	Dynamic pressure
p_i	Dynamic pressure in region i of fluid domain, i = 1,2,3
p_a	Atmospheric pressure
p	Dynamic pressure
P_ψ	Amplification factors of particular spectral components propagating in the positive direction for wave numbers ψ
Q_ψ	Amplification factors of particular spectral components propagating in the negative direction for wave numbers ψ
r	Distance from centre of vortex
Re	Reynolds number
S_i	Incident frequency spectrum
S_2	Frequency spectrum in the mangrove region.
t	Time
T_α	Amplification factors of particular spectral components for wave numbers α
T_m	Mean wave period
T_p	Peak wave period
u	Wave-induced velocity
$\vec{u_i}$	Wave-induced velocity vector $\vec{u_i} = (u_i, w_i)$ in region i of fluid domain, i = 1,2,3
$\boldsymbol{U}$	Depth averaged velocity vector

$\tilde{U}_2$	Amplitude of the particular spectral components of the horizontal velocity spectra
U_m	Maximum horizontal water velocity
u_i, v_i, w_i	Velocity components along x-axis, y-axis and z-axis in region i of fluid domain, i = 1,2,3
$\vec{u}_{n,j}(x,z)$	water velocity, normal to the longitudinal axis of the particular trunk j induced by wave orbital velocity $\vec{u}(x,z)$.
v	kinematic viscosity
V	Volume of cylinder
V_t	Volume of vegetation
V_0	Total control volume
W	Linearization coefficient for bottom friction
x, z	Co-ordinates of a right handed Cartesion co-ordinate system with the x-axis pointing in the direction of wave propagation, and the positive z-axis pointing upwards.
α	Complex wave number α = - ik
γ	Energy dissipation factor
Γ	Circulation
δ	Dirac's delta function
ε	Error of linearization approximation
$\boldsymbol{\varepsilon}$	Radius of core of vortex
$\varepsilon_1, \varepsilon_2$	Functions of wave number and bottom slope in mangrove forest
ε	Error of linearization approximation
ζ_i	Displacement of the free sea surface in region i of fluid domain, i = 1,2,3
ρ	Fluid density
ρ_w	Water density

σ_x	Standard deviation of parameter x
$\Phi_i(x,y,z,t)$	Velocity potential in region i of fluid domain, i = 1,2,3
φ	Complex wave amplitude in mangrove region
ψ	Complex wave number within the mangrove region of the fluid domain
Υ	Amplification factor for sea surface displacement spectra in mangrove region
ω	Angular frequency
ω_p	Peak frequency
$\boldsymbol{\omega}$	Vorticity
∂	Partial differential operator
∇	Gradient operator
∇^2	Laplace operator
$\Im$	Imaginary part of a complex number
$\Re$	Real part of a complex number